INTERNATIONAL DOCTORAL
SCHOOL OF THE USC

Khodor
Nasser

PhD Thesis

Synergistic Effects of Nanoparticles and Ionic Liquids as Hybrid Lubricant Additives

Santiago de Compostela, 2022

Doctoral Programme in Fluid Thermodynamics Engineering

DOCTORAL THESIS

Synergistic Effects of Nanoparticles and Ionic Liquids as Hybrid Lubricant Additives

Khodor Nasser

INTERNATIONAL PHD SCHOOL OF THE UNIVERSITY OF SANTIAGO DE COMPOSTELA

PHD PROGRAM IN FLUID THERMODYNAMICS ENGINEERING

SANTIAGO DE COMPOSTELA

2022

DECLARACIÓN DEL AUTOR DE LA TESIS

D. **Khodor Nasser**

Título de la tesis: **Synergistic Effects of Nanoparticles and Ionic Liquids as Hybrid Lubricant Additives**

Presento mi tesis, siguiendo el procedimiento adecuado al Reglamento y declaro que:

1) La tesis abarca los resultados de la elaboración de mi trabajo.
2) De ser el caso, en la tesis se hace referencia a las colaboraciones que tuvo este trabajo.
3) Confirmo que la tesis no incurre en ningún tipo de plagio de otros autores ni de trabajos presentados por mí para la obtención de otros títulos.
4) La tesis es la versión definitiva presentada para su defensa y coincide la versión impresa con la presentada en formato electrónico.

Y me comprometo a presentar el Compromiso Documental de Supervisión en el caso que el original no esté depositado en la Escuela.

En **Santiago de Compostela** , **02 de marzo de 2022.**

Firma electrónica

AUTORIZACIÓN DE LAS DIRECTORAS DE LA TESIS

Synergistic Effects of Nanoparticles and Ionic Liquids as Hybrid Lubricant Additives

Dª. Josefa Fernández Pérez
y
Dª. Enriqueta López Iglesias

INFORMAN:

Que la presente tesis, se corresponde con el trabajo realizado por D Khodor Nasser, bajo nuestra dirección, y autorizamos su presentación, considerando que reúne los requisitos exigidos en el Reglamento de Estudios de Doctorado de la USC, y que como directoras de esta no incurren en las causas de abstención establecidas en la Ley 40/2015.

De acuerdo con lo indicado en el Reglamento de Estudios de Doctorado, declaramos también que la presente tesis doctoral es idónea para ser defendida en base a la modalidad de COMPENDIO DE PUBLICACIONES con reproducción de publicaciones en los que la participación del doctorando fue decisiva para su elaboración y las publicaciones se ajustan al Plan de Investigación.

En Santiago de Compostela, 2 de marzo de 2022.

ABSTRACT

In this Doctoral Thesis, the performance of several lubricant additives as friction and wear reducers was analyzed. For this purpose, some nanomaterials and ionic liquids (ILs) were used as single or combined additives to design new nanolubricants based on polyalphaolefin oils (PAO32 and PAO10). The selected additives were: hexagonal boron nitride (h-BN) nanoparticles (NPs), graphene nanoplatelets (GnP) and iron oxide NPs as nanomaterials, and trihexyltetradecylphosphonium bis(2-ethylhexyl)phosphate ([$P_{6,6,6,14}$][DEHP]), tributyl-ethylphosphonium diethylphosphate ([$P_{2,4,4,4}$][DEP]) and trihexyltetradecylphosphonium bis(2,4,4-trimethylpentyl)phosphinate ([$P_{6,6,6,14}$][$(iC8)_2PO_2$]) as phosphonium ILs. The base oils were kindly provided by two lubricant companies (Repsol and Tehnosint), h-BN and GnP nanoadditives as well as the ILs were supplied by Iolitec. Moreover, iron oxide nanomaterials were synthetized from the sludge of an iron mine located at Omarska (Bosnia and Herzegovina). Different techniques were used to characterize the base oils, nanoadditives and ionic liquids including Raman, FTIR and XRD spectroscopies as well as HRTEM. Corrosion tests of smooth steel discs wet with the pure ILs were carried out. The presence of synergistic effects between nanomaterials and ionic liquids as hybrid additives into lubricant oils was studied. A three-stages strategy was followed to analyze the synergies: in the first only one additive was used and leads to single nanodispersions (PAO/NPs) or mixtures (PAO/IL), in the second two additives were combined and lead to hybrid nanodispersions (PAO/IL/NPs or PAO/NP1/NP2) and in the third three additives were used giving rise to double hybrid nanodispersions (PAO/IL/NP1/NP2). The stability of formulated lubricants was carried out visually by taking photos of the samples from time to another as well as using a UV-VIS spectroscopy for the nanolubricants containing iron oxide NPs. PAO32/0.05 wt% GnP, PAO32/0.1 wt% GnP and eight PAO32 nanodispersions containing IL1 or IL3 were stable for the overall analyzed time (150 or 240 days). The nanodispersions based on PAO32 or PAO10 and iron oxide NPs with three different concentrations, 0.1, 0.25 and 0.5 wt%, showed stability lower than five-days. Thermophysical properties (viscosity, viscosity index and density) and tribological behavior (friction and wear) of the designed nanolubricants were also investigated. The thermophysical properties of the base oil (PAO32), mixtures and nanolubricants were measured using a Stabinger SVM 3000 viscometer in order to identify the effect of the additives on the thermophysical behavior of PAO32. Thus, respect to the corresponding properties of PAO32, the maximum average relative change in density is 0.44 %, that of viscosity 7.6 % whereas the viscosity index barely varies. The tribological performance of the samples was studied by means of an CSM standard tribometer with ball-on-disc configuration, an MCR 302 rheometer from Anton Paar equipped with a tribology cell T-PTD200 a with ball-on-three-pins configuration, and a 3D optical profiler for surface analysis of the specimens. Results showed that although in terms of the tribological characterizations IL2, [$P_{2,4,4,4}$][DEP], as additive led to the lowest friction coefficient and wear among the three ILs, it produced corrosion on the steel discs and did not improve the time stability of the nanodispersions. The effect of the concentration of the NPs and the ILs as well as their hybrid combination on the tribological properties was analyzed finding friction reductions up to 40 % and wear reductions up to 99 %. In addition, the additives on the worn surface and the tribological mechanisms were analyzed with a confocal Raman microscope, among others, finding that the main tribological mechanisms are film formation due to ILs and surface repairing effect due to NPs.

Keywords: Tribology, Lubricants, Nanoadditives, Synergy, Hybrid, Thermophysical Properties, Graphene, Hexagonal Boron Nitride, Iron Oxide, Ionic Liquids

RESUMEN

En esta Tesis Doctoral se analizó el desempeño de varios aditivos de lubricantes como reductores de fricción y desgaste. Para ello, se utilizaron algunos nanomateriales y líquidos iónicos (LIs) como aditivos únicos o combinados para diseñar nuevos nanolubricantes basados en polialfaolefinas (PAO32 y PAO10). Los aditivos seleccionados fueron: nanopartículas (NPs) de nitruro de boro hexagonal (h-BN), nanoplaquetas de grafeno (GnP) y NPs de óxido de hierro como nanomateriales, y trihexiltetradecilfosfonio bis(2-etilhexil)fosfato ([$P_{6,6,6,14}$] [DEHP]), dietilfosfato de tributil-etilfosfonio ([$P_{2,4,4,4}$][DEP]) y trihexiltetradecilfosfonio bis(2,4,4-trimetilpentil)fosfinato ([$P_{6,6,6,14}$][$(iC8)_2PO_2$]) como ILs de fosfonio. Los aceites base fueron proporcionados por dos empresas de lubricantes (Repsol y Tehnosint), los nanoaditivos h-BN y GnP, así como los ILs fueron suministrados por Iolitec. Además, se sintetizaron nanomateriales de óxido de hierro a partir de lodos de una mina de hierro ubicada en Omarska (Bosnia y Herzegovina). Se utilizaron diferentes técnicas para caracterizar los aceites base, los nanoaditivos y los ILs, incluidas espectroscopias Raman, FTIR y XRD, así como HRTEM. Se llevaron a cabo pruebas de corrosión de discos de acero lisos en los que se depositaron los IL puros. Se estudió la presencia de efectos sinérgicos entre nanomateriales y ILs como aditivos híbridos en aceites lubricantes. Se siguió una estrategia de tres etapas para analizar las sinergias: en la primera se utilizó un solo aditivo y se obtuvieron nanodispersiones simples (PAO/NPs) o mezclas (PAO/IL), en la segunda se combinaron dos aditivos y se obtuvieron nanodispersiones híbridas (PAO/IL/NPs o PAO/NP1/NP2) y en la tercera se utilizaron tres aditivos dando lugar a nanodispersiones doblemente híbridas (PAO/IL/NP1/NP2). El análisis de la estabilidad de los lubricantes formulados se llevó a cabo visualmente tomando periódicamente fotografías de las muestras y utilizando espectroscopia UV-VIS para los nanolubricantes que contienen NPs de óxido de hierro. PAO32/0,05 wt% de GnP, PAO32/0,1 wt% de GnP y ocho nanodispersiones de PAO32 conteniendo IL1 o IL3 fueron estables durante el tiempo total que duró el estudio de estabilidad (150 o 240 días). Todas las nanodispersiones basadas en PAO32 o PAO10 y NPs de óxido de hierro mostraron una estabilidad inferior a cinco días. También se investigaron las propiedades termofísicas (viscosidad, índice de viscosidad y densidad) y el comportamiento tribológico (fricción y desgaste) de los nanolubricantes diseñados. Las propiedades termofísicas del aceite base (PAO32), las mezclas y los nanolubricantes se midieron con un viscosímetro Stabinger SVM 3000 con el fin de identificar el efecto de los aditivos en el comportamiento termofísico de PAO32. Así, respecto a las propiedades correspondientes de PAO32, el máximo cambio relativo promedio de la densidad es 0,44 %, el de la viscosidad 7,6 % mientras que el índice de viscosidad apenas varía. El comportamiento tribológico de las muestras se estudió mediante un tribómetro estándar CSM con configuración bola sobre disco, un reómetro MCR 302 de Anton Paar equipado con una celda tribológica T-PTD200 con configuración de bola sobre tres pines, y un perfilómetro óptico 3D para el análisis superficial de las probetas. Los resultados mostraron que si bien en términos tribológicos IL2, [$P_{2,4,4,4}$][DEP] condujo al menor coeficiente de fricción y desgaste entre los tres ILs, desafortunadamente produjo corrosión en los discos de acero y no mejoró la estabilidad temporal de las nanodispersiones. Finalmente, se encontraron reducciones de fricción de hasta 40 % y reducciones de desgaste de hasta 99 %. Además, se analizó la presencia de aditivos en la superficie desgastada y los mecanismos tribológicos con un microscopio confocal Raman, entre otros, encontrando que los principales mecanismos tribológicos son la formación de películas debido a los IL y el efecto reparador de la superficie debido a las NPs.

Palabras clave: Tribología, Lubricantes, Nanoaditivos, Sinergia, Híbrido, Propiedades Termofísicas, Grafeno, Nitruro de Boro Hexagonal, Óxido de Hierro, Líquidos Iónicos

RESUMO

Nesta Tese Doutoral analizouse o rendemento de varios aditivos lubricantes como redutores de fricción e desgaste. Para iso utilizáronse algúns nanomateriais e líquidos iónicos (IL) como aditivos únicos ou combinados para deseñar novos nanolubricantes a base de polialfaolefinas (PAO32 e PAO10). Os aditivos seleccionados foron: nanopartículas (NP) de nitruro de boro hexagonal (h-BN), nanoplaquetas de grafeno (GnP) e NPs de óxido de ferro como nanomateriais e fosfato de bis(2-etilhexil) de trihexiltetradecilfosfonio ([$P_{6,6,6,14}$][DEHP]), dietilfosfato de tributil-etilfosfonio ([$P_{2,4,4,4}$][DEP]) e bis(2,4,4-trimetilpentil)fosfinato de trihexiltetradecilfosfonio ([$P_{6,6,6,14}$][$(iC8)_2PO_2$]) como IL de fosfonio. Os aceites base foron proporcionados por dúas empresas de lubricantes (Repsol e Tehnosint), os nanoaditivos h-BN e GnP, así como os IL foron subministrados por Iolitec. Ademais, sintetizáronse nanomateriais de óxido de ferro a partir de lodos dunha mina de ferro situada en Omarska (Bosnia e Hercegovina). Utilizáronse diferentes técnicas para caracterizar os aceites base, nanoaditivos e IL, incluíndo espectroscopia Raman, FTIR e XRD, así como HRTEM. Realizáronse ensaios de corrosión en discos de aceiro lisos nos que se depositaron IL puros. Estudouse a presenza de efectos sinérxicos entre nanomateriais e IL como aditivos híbridos en aceites lubricantes. Seguiuse unha estratexia de tres etapas para analizar as sinerxías: na primeira utilizouse un só aditivo e obtivéronse nanodispersións simples (PAO/NPs) ou mesturas (PAO/IL), na segunda combináronse dous aditivos e obtivéronse nanodispersións híbridas. (PAO/IL/NPs ou PAO/NP1/NP2) e no terceiro utilizáronse tres aditivos, dando lugar a nanodispersións dobremente híbridas (PAO/IL/NP1/NP2). A análise da estabilidade dos lubricantes formulados realizouse visualmente tomando periodicamente fotografías das mostras e utilizando espectroscopía UV-VIS para os nanolubricantes que conteñen NPs de óxido de ferro. PAO32/0,05% en peso de GnP, PAO32/0,1% en peso de GnP e oito nanodispersións de PAO32 que conteñen IL1 ou IL3 foron estables durante toda a duración do estudo de estabilidade (150 ou 240 días). Todas as nanodispersións baseadas en PAO32 ou PAO10 e NPs de óxido de ferro mostraron unha estabilidade de menos de cinco días. Tamén se investigaron as propiedades termofísicas (viscosidade, índice de viscosidade e densidade) e o comportamento tribolóxico (fricción e desgaste) dos nanolubricantes deseñados. As propiedades termofísicas do aceite base (PAO32), mesturas e nanolubricantes medíronse cun viscosímetro Stabinger SVM 3000 para identificar o efecto dos aditivos no comportamento termofísico do PAO32. Así, con respecto ás propiedades correspondentes do PAO32, o cambio relativo medio máximo na densidade é do 0,44%, o da viscosidade é do 7,6%, mentres que o índice de viscosidade apenas varía. O comportamento tribolóxico das mostras estudouse mediante un tribómetro CSM estándar con configuración de bola sobre disco, un reómetro Anton Paar MCR 302 equipado cunha célula tribolóxica T-PTD200 con configuración de bola en tres pins e un perfilómetro óptico 3D. para a análise da superficie das probetas. Os resultados mostraron que aínda que en termos tribolóxicos o IL2, [$P_{2,4,4,4}$][DEP] conduciu ao menor coeficiente de rozamento e desgaste entre os tres IL, desafortunadamente produciu corrosión nos discos de aceiro e non mellorou a estabilidade temporal das nanodispersións. En definitiva, atopáronse reducións do rozamento de ata un 40% e reducións de desgaste de ata o 99%. Ademais, analizouse a presenza de aditivos na superficie desgastada e os mecanismos tribolóxicos cun microscopio confocal Raman, entre outros, concluíndo que os principais mecanismos tribolóxicos son a formación de películas debido ás IL e o efecto reparador da superficie debido ás NPs.

Palabras chave: Triboloxía, Lubricantes, Nanoaditivos, Sinerxía, Híbrido, Propiedades Termofísicas, Grafeno, Nitruro de Boro Hexagonal, Óxido de Ferro, Líquidos Iónicos

ACKNOWLEDGMENTS

I would like to thank without exception everyone and those who have contributed directly or indirectly to the finalization of this work. Special thanks for my supervisors, *Prof. Josefa Fernández Pérez* and *Dr. Enriqueta López Iglesias*, for their great support and extensive knowledge for accomplishing what has been achieved in this Doctoral Thesis.

I appreciate *Dr. José Manuel Liñeira del Río, Dr. María Jesús García Guimarey* and *Ph.D. candidate Fátima Mariño* for their assistance and guidance and their company during the studies. To the rest of the people in the NaFomat Group: *Dr. María José Pérez Comuñas, Dr. Josefa Salgado Carballo, Dr. María Villanueva Lopez, Dr. Juan José Parajó Vieito* and *Ph.D. candidate Pablo Vallet Moreno.* To the staff of the research and technological development support infrastructures network (RIAIDT) at the University of Santiago de Compostela for their capacity, dedication and assistance for characterizing the samples. From this division, special thanks for *Mr. Ezequiel Vázquez*, and *Mrs. Raquel Antón* for their great work and patience. To *Mrs. María Herrero* for her wise understanding and help with the profilometer.

Special thanks for *Assist. Prof. Dr. Suzana Gotovac Atlagić* my supervisor during my research stay at the University of Banja Luka from the Department of Chemistry. In addition, I would like to thank, *Prof. Milica Balaban, Prof. Saša Zeljković, Prof. Biljana Davidović-Plavšić, Mrs. Sunčica Sukur, Mrs. Sanja Pržulj, Mrs. Dejana Savić, Mrs. Mirela Boroja, Mrs. Olga Bulović* and *Mr. Drago Kopren* for their support in my research stay at their lab. Moreover, I do appreciate *Prof. Peter Gevero* from the department of mechanical engineering for his wise advices and recommendations. It was a pleasure to do a research stay at the University of Banja Luka in Bosnia and Herzegovina funded by Erasmus group whom are quietly thankful as well. In addition, I would like to thank the vice rector for international and interuniversity cooperation of the University of Banja Luka *Prof. Biljana Antunović* for her great welcome.

I am thankful for the *Erasmus group* in the University of Santiago to Compostela and in the University of Banja Luka for offering this research stay. And I would like to thank, *Mrs. Ana Guerra, Mrs. Fátima Fernández* and *Mr. Đorđe Kenjalo* for their support during the stay.

In addition, I would like to thank Prof. Yoshiyuki Hattori form the Shinshu University (Japan) for providing the HRTEM images and the XRD analyses. Thank Repsol for providing a PAO32 sample and to Tehnosint for PAO32 and PAO10 samples.

This PhD Thesis was developed in the framework of the ENE2017-86425-C2-2-R project funded by the Ministry of Science, Innovation and Universities of Spain and the European Regional Development Fund (ERDF) and of the ED431C 2016/001 and ED431C 2020/10 projects of Xunta de Galicia.

To my family, to my supportive mother *Fatima*, my wise father *Ismail*, my helpful brother *Mohamed*, my three lovely sisters *Nahida, Nadine,* and *Nojod*, for my nieces and nephews *Rama, Ana, Maria, Ali and Noah* to my brothers in law *Ahmad, Hilal and Abdullah* for everything they did, do and still doing for me. I fully trust that without my faith in God I would not have been able to accomplish what I have achieved, thanks God.

INDEX

1 INTRODUCTION

1.1 MOTIVATION

Economic and technical developments around the world have led to significant increase in energy demand. The energy need is growing in all activities, industrial activities, transportation, residential use and raw materials consuming 29 %, 28 %, 34 % and 9 % of the worldwide energy, respectively. The impact of friction and wear on worldwide total energy consumption was recently calculated, revealing that tribological contacts are the origin of 23 % of this consumption, using 20 % to overcome friction and the remaining 3 % to remanufacturing of worn parts and replacing equipment damaged due to wear related failures [1]. It is further estimated that, if new materials, surfaces, and lubrication technologies are used, energy losses due to friction and wear could be reduced by 40 % in 15 years (long term) and by 18 % in 8 years (short term), where potential economic savings from the promotion and implementation of new tribological solutions are around 74 % from friction reduction and 26 % from better wear protection. In general, wear is more critical than friction because it can cause operational breakdowns, or even catastrophic failures, and negatively affect productivity and therefore costs. The greatest expected short term energy savings are 25 % in transportation and 20 % in power generation (such as wind turbines) [2]. The development of lubricants for gearboxes of wind turbines is one of the focus of the present Doctoral Thesis.

Part of this Doctoral Thesis addressed the use of nanoparticles obtained from mining waste. Such recycling of the secondary raw materials should help reduce net global anthropogenic CO_2 emissions, which must be reduced to zero by 2060-2075 to achieve the above goal [3]. This reduction should come from the lower energy consumption in recycling of mining tailings, than in the classical mining, which is the most energy demanding industry [4,5]. The climate change is an issue of world interest, and the objective proposed in 1996 by the European Union (EU) of keeping the global warming below 2 °C, has been for more than two decades a key focus of the international climate debate [6-9]. To reduce these emissions, the renewable energy generation must be strongly increased [9-11]. Renewable energy sources such as wind, hydropower, biomass, geothermal, solar, wave and tide are optimal for environmental pollution control [12]. Other targets proposed by the EU for 2030 are at least: 40 % reductions in greenhouse gas emissions (from 1990 levels), 32 % share for renewable energies, and 32.5 % improvement in energy efficiency [13].

In all energy demand reduction scenarios, tribology has emerged as the multidisciplinary engineering science underpinning friction and wear losses, durability, and sustainability in mechanical system main components as means for contributing in reduction of global carbon emissions [14]. This includes different sectors that consume energy such as transportation, manufacturing, power generation, and residential [2]. Tribology and sustainability are closely related. Thus, among the benefits of applying tribological practices, we can highlight the longer service lifespan, the lower wear, the energy savings due to the reduction of friction losses or the selection of efficient and environmentally friendly lubricants. Friction and wear can be controlled by proper selection of the lubricant that is embedded between the contact surfaces [15]. In selecting the optimal lubricant for a specific application, many factors should be considered such as the operational temperature range, load, speed, materials, and general design factors of the machine [16] .

An unsuitable lubricant selection would lead to higher operating costs and lower production efficiency. Consequently, to select the appropriate lubricant, it is imperative to improve the tribological performance of the currently available commercialized oils. In this regard, additives are needed in the formulation of the final product to better fit the requirements of the machinery and to improve the efficiency. Based on that, nanotechnology is considered to play a leading role in technological advances of the 21st century. Nanoadditives should be able to reduce friction and/or wear in mechanical systems by their dispersion in lubricants. Thus, small amounts of solid particles at the nano-scale can improve the antifriction and wear reduction properties of the base oil [17,18]. Several methods are used to homogenize these nanoparticles (NPs) into the base oil, but even so the stability of the dispersions during prolonged time can be limited [17]. From now on, lubricants with additives will be referred to as nanolubricants.

Ionic liquids (ILs) are organic salts that have low melting points, often below room temperature, which consist of combinations of an anion and a cation and lead to promising results when used as neat lubricants [19-21], but their high production price, in comparison to both mineral and synthetic oils, limits their use to key applications. Nevertheless, small amounts of ILs (1–5 wt%) could be enough to improve the tribological performance of the base oils. For this reason, ILs are being investigated as antifriction and antiwear additives [22-25].

To solve the problems of using NPs additives to base oils, their use with ILs as hybrid additives has been proposed [26-28]. These hybrid combinations can have synergistic effects that can lead to better lubricant performance than using NPs and ILs separately. From cost perspectives, a minimum added quantity of NPs and ILs can be preferable to achieve high nanolubricant performance and long stability. These new hybrid potential additives can affect the thermophysical properties of the base oil, such as density, viscosity or viscosity index, which can also alter the performance of the final lubricant.

1.2 LUBRICANTS

Although the use of lubricants is as old as human history, studies on lubrication, friction and wear are relatively new [29]. Reducing both friction and wear, or even avoiding the latter, by using lubricants and lubrication technologies, results in energy conservation, emission reduction, and environmental protection [29,30], important benefits from both economical as well as ecological points of view. Nevertheless, lubricants were not considered functional elements in engineering until recently, increasingly attracting the attention of engineers [29].

When two surfaces are in relative motion, friction and wear are generated, which also implies energy losses, risks associated with machine failures and costly maintenance operations. The simplest method of trying to control friction and wear is interposing a lubricant between the rubbing surfaces. The main functions of the lubricant are to reduce the tribological effects, while lowering both heat generation and energy losses, as well as smoothing the mechanical motion. Moreover, lubrication can attenuate noise and vibrations [31].

Friction is usually evaluated in terms of the friction coefficient, which for lubricated contacts, depends on the conditions under which the interaction between the rubbing surfaces occurs, the lubricant viscosity (η), the normal load (N), and the sliding speed (v). The Stribeck curve relates the friction coefficient to the Hersey number, which is a dimensionless parameter involving these relevant physical parameters, $H=\eta v/N$, or to the lambda ratio, Λ (Fig. 1.1). This ratio can be determined as:

$$\Lambda = \frac{h_{min}}{\sigma} \qquad (1.1)$$

being h_{min} the minimum film thickness and σ the equivalent roughness of the surfaces given by:

$$\sigma = \sqrt{\sigma_1^2 + \sigma_2^2} \qquad (1.2)$$

Where σ_1 and σ_2 are the RMS roughness of each surface, i.e., the mean root square average of the profile height deviations from the mean line. Several authors [32] use in the above equation central-film thickness instead minimum film thickness [33] although qualitatively there is hardly any difference, quantitatively there is.

There are three main lubrication regimes: boundary (BL, when most of the asperities are in contact), mixed (ML, when certain amount of asperities is in contact), and full film elastohydrodynamics lubrication, EHD (there are no asperities in contact and the contact surfaces are separated due to the contact pressures are high and the surfaces elastically deformed).Most researchers [34] indicate that when Λ <1, BL takes place, when 1<Λ <3 implies ML, and being Λ>3 for full film EHD lubrication [35]. Nevertheless, there is a controversy on Λ ratio for the mixed regime. From the results of different authors [36-40], the mixed lubrication could span the Λ range from 0.05 to 3 [38].

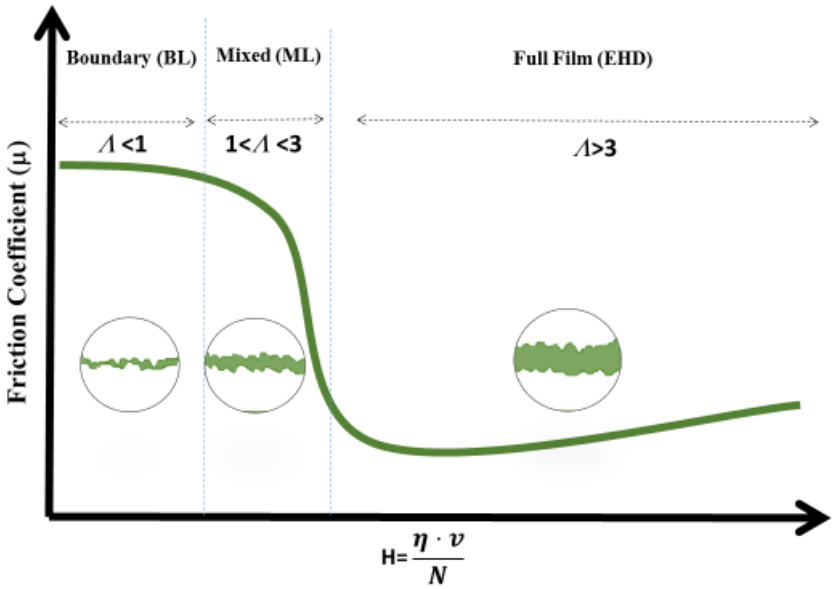

Fig. 1.1. Stribeck curve: dependence of the friction coefficient with the lambda ratio and Hersey number for the lubrication regimes; This graph is adapted from Robinson et al. [41]

In terms of the Hersey number (Fig. 1.1), the highest load, and/or lowest speed (or viscosity) produce the BL which leads to high contact between surfaces resulting in high friction and wear values. If the speed (or the viscosity) increases and/or the load decreases, there is a greater surface-to-surface separation (ML). If the load decreases more, there would be no direct physical contact between the asperities of the contact, leading to full film EHD, for which friction is very low.

The wide range of use of lubricants in important applications such as engines, vehicles, compressors, turbines and hydraulic systems, among others, led to the productions of different forms of lubricating materials such as oils and greases. Formulated lubricants, which account for around 90 % of lubrication consumption, consist of approximately 93 % of base oil and 7 % of chemical additives [29]. Mineral, synthetic, and natural oils are the three main categories of base oils. Mineral oils are manufactured by refining crude petroleum, which is a complex mixture of many compounds (mainly organic chemicals) of different molecular sizes and different hydrocarbon types [42-44]. The properties of the mineral oils are an average of those of their components: those of the most appropriate and those of the least appropriate. Separating the best components is uneconomical. On the other hand, with synthetic oils, the most suitable components can be selected for each application (planned and predictable properties). Synthetic

oils are obtained by chemical reactions. Compared to mineral oils, synthetic oils have better characteristics and perform better with temperature, having a much lower pour point, which makes them favorable for low temperature applications, being some of them ecofriendly [44,45]. Based on their chemical structure, synthetic lubricants can be classified as polyalphaolefins, esters, polyalkylene glycols, alkylated aromatics, among others [44]. Natural oils are mainly obtained from plant sources, including vegetable oils, or lignocellulose, among others [46].

Since the 1980s, the development of the automotive sector led to an increase in the use of polyalphaolefins (PAOs) in many applications. PAOs, are usually obtained by a two-step process from linear alphaolefins. PAOs have a wide operational temperature range, high thermal, hydrolytic, oxidative and shear stabilities, high viscosity index, low corrosiveness and are compatible with mineral oils and common materials [47,48]. In addition, PAOs are not toxic or irritating and are expected to be also nontoxic to sea organisms. PAOs are named by their kinematic viscosity, in cSt, at 373.15 K. In certain applications such as hydraulic fluids, they show improvements over mineral oils due to their unique combination of physical, chemical, and environmental properties [49]. PAOs of low molecular masses show Newtonian behavior, but for higher molecular masses shear thinning occurs which affects film thickness and traction in elastohydrodynamic lubrication contacts [50,51].

Additives are needed in the formulation of the final lubricant to improve some base oil performance properties and to fulfill with machinery specific requirements. These additives are classified according to the role they play in the tribological system [52]. *Antioxidant* additives are used in the formulation of lubrication oils aiming to minimize the oxidation rate. These chemicals are categorized into primary antioxidants, secondary and metal deactivators depending on the mechanism of action of the antioxidant [53,54]. Corrosion is attenuated by *corrosion inhibitors,* additives that minimize the corrosion rate, these additives are used in the presence of water since it is considered a metal corrosion accelerator, that include several applications such as in industrial and automobile sectors [55,56]. *Dispersants and detergents* keep the particles well dispersed in the lubricant and help in the elimination of deposits caused by sedimentation of other additives [57]. *Viscosity index improvers* are polymers that act to decrease the loss of viscosity when temperatures increase. These additives are mainly used in multi-grade engine oils, which need to be low viscous at low temperatures, assisting the engine in cold starting and, on the contrary, sufficiently highly viscous at high temperatures keeping the load-bearing features [58]. *Antifriction and antiwear additives* are used mainly in boundary and mixed lubrication regimes, the tribological performance at the boundary one being controlled mainly by the tribo-film formation on the contact surfaces [59-61]. Carboxylic acids with a linear hydrocarbon chain were the first additives used to improve lubricity of mineral oils [62]. The *antiwear additives* commonly used are organic compounds: Zinc dialkyldithiophosphates (ZDDP), Molybdenum dialkyldithiophosphate (MoDTP), Dibutyl phthalate (DBP), molybdenum dithiocarbamate (MoDTC), among others. These last additives and *friction modifiers* are typically the main two types used for lubricants [59,63-65]. Generally, these additives can react with surfaces forming reaction films that provide good surface protection, but due to the use of active elements such as phosphorus, sulfur, chlorine or polar groups for better adsorption of the additives, they cause harmful environmental effects as well as corrosion of certain metal surfaces [66]. A recent way to solve this drawback is the use of nanoparticles, which leads to notable improvements in the lubricant behavior, such as resistance to oxidation or improvements in both tribological characteristics and thermal properties [67]. Therefore, the addition of nanoadditives showed enhancements in the tribological performance of base oils, as they can activate additional lubrication surface mechanisms. Moreover,

nanoadditives (1 to 100 nm) can play an important role as friction and wear reducers [68] showing improved tribological properties than traditional solid lubricant additives [69]. One more current line of research in additives for lubricants involves ionic liquids (ILs), which have shown good performance as antifriction and antiwear lubricant additives, either individually or in combination with nanoparticles [22-24,26,27,70].

1.3 NANOPARTICLES AS ADDITIVES

Nanotechnology is spreading widely today due to its applications in many fields, its ability to optimize systems for better performance, and its relevance in positive environmental benefits [71,72]. Nanomaterials are materials, for which one or more external dimensions is in the size range 1 nm to 100 nm for 50 % or more of its particles in the number size distribution [73]. Nanomaterials are in continuous improvement, because they have functional properties that enable their useful implementation in engineering and design applications [74-76]. From the point of view of tribological applications, the use of nanomaterials as lubricant additives has demonstrated, in the boundary lubrication region, friction and wear enhancements to the base oil behavior [18,77]. For instance, friction reduction up to 70 % was achieved for a blend of PAO4 and PAO40 [78], and wear reduction up to 67 % for a ester oil [79]. Nanomaterials may form films on many different types of surfaces and do not need to be more chemically reactive being more durable with less probability of reacting with other additives [65]. As friction modifiers, nanoadditives can act through different mechanisms [64,80], categorized into two groups. The first includes the mechanisms due to the direct effects of nanoparticles in lubrication enhancement, which are the rolling mechanism [81,82] and the formation of a protective tribofilm [83]. The second group includes the mechanisms that involve surface enhancement: mending [84] and polishing [85] effects. Fig. 1.2 summarizes the mechanisms of the nanoparticles as additives [17,77,86].

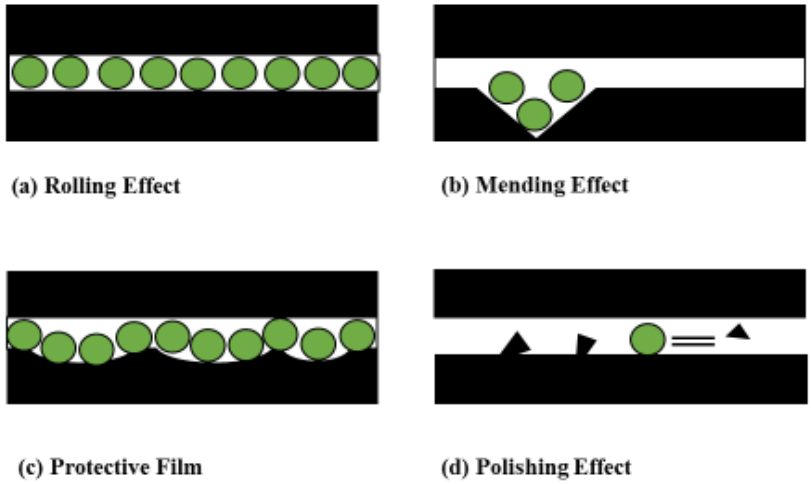

Fig. 1.2. Lubrication mechanisms of nanoparticles as additives

Considering their chemical structure, nanomaterials as lubricant additives are mainly classified into several categories: metals, metal oxides, carbon-based nanomaterials, ceramics, rare earth compounds, or composites, among others [77,87]. Nanomaterials can present 0, 1, 2 or 3 dimensions. Among them, two dimensional (2D) materials are 1 atom thick sheets which are free standing layers and do not need a substrate to exist. Frequently, layers with up to 10 atoms thick are also considered as 2D sheets [88]. 2D nanomaterials present excellent friction behavior, have a high specific surface area, high in-plane resistance, low resistance to interlaminar shear and good surface chemical stability [89]. For these reasons, it is expected

that nanoadditives will create opportunities for different applications in diverse engineering fields [90]. The 2D materials selected in this Doctoral Thesis as nanoadditives are graphene nanoplatelets (GnP) and hexagonal boron nitride (h-BN) nanoparticles.

1.3.1 Carbon Nanomaterials

Carbon nanomaterials such as fullerenes, carbon nanotubes (CNTs), graphene or nanodiamonds attracted much interest in tribology since they show high chemical stability and effective thermal, mechanical, chemical and electrical properties [91]. Graphene shows many advantages in various applications including tribological systems such as its extreme strength, high chemical inertness, easy shear capability, among others [92]. Graphene nanoplatelets (GnP) are carbon nanostructures containing small stacks of graphene sheets that have a thickness ranging from 1 nm to a few tens of nanometers, and lateral dimensions which vary from a few micrometers up to hundreds of micrometers [93]. Kiu et al. [94] used graphene nanoplatelets as lubricant additives for a palm oil based vegetable oil, finding friction coefficient and wear scar diameter reductions of 13.5 and 9.6 % respectively, at an optimum concentration of 50 ppm. Eswaraiah et al. [95] studied the tribological influence of ultrathin graphene additives to an engine oil, achieving 80 % friction reduction and 33 % wear reduction. Zheng et al. [96] evaluated the tribological properties of graphene nanosheets dispersed in PAO4 base oil as additives on textured alloy cast iron surface and achieved 70 % and 50 % reduction in friction and wear, respectively. Radhika et al. [97] studied the tribological effects of carbon spheres (FCS) with GnP as hybrid additives into CASTROL-20 W 40 engine oil. These authors found that the hybrid dispersion containing 0.275 wt% of FCS/GnP showed stability for 30 days with no addition of any surfactant and led to friction reductions up to 18 % compared to the neat oil. Liñeira del Río et al. [98] studied the tribological behavior of trimethylolpropane trioleate oil (TMPTO) using GnP as nanoadditives. Different concentrations were selected (0.05, 0.10, 0.25 and 0.50 wt%). The best antifriction capability was obtained when 0.5 wt% of GnP was used leading to 36 % reduction, whereas 0.25 wt% was the optimal antiwear concentration leading to 3.3 % reduction. Moreover, Liñeira del Río et al. [99] investigated the antifriction and antiwear abilities of GnP as additives for PAO40 oil, achieving best reduction with 0.5 wt% GnP concentration being the reductions 21 % and 22 % for friction and wear, respectively, when compared to the base oil. Guimarey et al. [100] studied the tribological performance of two different 2D nanomaterials, GnPs and molybdenum disulfide nanoplatelets (MSNP) as lubricant additives for a commercial engine oil, 5W30. Steel-to-steel contact in two configurations, pure sliding and rolling/sliding were used. Three mass concentrations of the NPs were used 0.05, 0.1 and 0.2 wt%. The results showed that low concentration (0.05 wt%) of additives into 5W30 led to best friction and wear reductions in the sliding test, whereas, in the rolling/sliding mode 0.2 wt% of MSNP into 5W-30 was the best nanolubricant for friction and wear reductions. Liñeira del Río et al. [101] investigated the antifriction and antiwear capacities of two pristine GnPs, identified as GnP7 and GnP40 as additives for a biodegradable ester. Four mass concentrations of the additives were selected, 0.015, 0.035, 0.055 and 0.075 wt%. Their tribological studies showed that the optimum concentration that led to better tribological performance is 0.055 wt% for both nanoadditives. The best antifriction behavior was achieved by the addition of GnP40 leading to 26 % reduction, whereas the best antiwear capability was achieved by the addition of GnP7 reducing wear by 56 %.

1.3.2 Hexagonal Boron Nitride Nanomaterials

h-BN is one of the five different crystalline forms of boron nitride (BN) [102]. h-BN is the softest and most lubricious polymorph of BN being its structure lamellar crystalline. There are van der Waals forces between its sheets, like those of molybdenum disulfide or graphite, being

the last three compounds excellent solid lubricants [103,104]. h-BN is an interesting material used in many industrial applications. It is efficient, clean and a non-harmful source for the atmosphere being environmentally friendly. Other features include softness, high thermal stability and great thermal conductivity [105]. h-BN is strongly used in tribological applications [106]. BN nanostructures can present different morphologies such as nanosheets or spherical nanoparticles [107]. The use of h-BN as nanoadditive in different base oils, has been studied by several authors [99,108-110], concluding, in general, its positive influence as antifriction and antiwear enhancer of the base oil behavior. For instance, Ramteke et al. [111] studied h-BN NPs as additives to a 20W40 base oil for diesel engines, finding by UV spectroscopy and SEM analysis that the nanolubricant containing 1 wt% h-BN is more stable and well dispersed than nanofluids with other concentrations, as well as being the optimum concentration improving the antifriction and antiwear properties of the base oil. Wang et al. [112] investigated friction and wear mechanisms of castor oil upon the addition of h-BN nanoparticles and concluded that 5 wt% h-BN additive increases the friction coefficient by 22 % and reduces the wear area by 55 % at low load and high speed. At high load and low speed, the major improvements were achieved by 1 wt% h-BN addition, the friction coefficient decreasing 30 % and being the wear area improvement 52 %. Liñeira del Río et al. [103] studied the influence of h-BN NPs when added to trimethylolpropane trioleate ester-based oil and the results have shown reductions up to 25 % in the friction coefficient and 22 % on the transversal wear area using the nanolubricant with 0.75 wt% of h-BN. Çelik et al. [110] concluded that the addition of h-BN NPs to an engine oil, SAE 10W, improved the friction coefficient up to 14 %, and reduced wear by 65 % in AISI 4140 steel disks.

1.3.3 Iron Oxide Nanoparticles

Different metal oxides NPs were studied as lubricant additives, such as CuO, TiO_2, Fe_2O_3, Fe_3O_4, Al_2O_3 and ZnO. The lubrication mechanisms due to these NPs are tribofilm formation, rolling effect or repairing/mending effect [30,77,113]. Fe_2O_3 NPs were selected in this Doctoral Thesis as nanoadditives because there is a big interest to use the waste of the iron mines to synthetize NPs. Iron oxide Fe_2O_3 is the most known oxide of iron, being the most frequent polymorphic structures found in nature, hematite (α-Fe_2O_3, rhombohedral-hexagonal and prototype corundum structures) and maghemite (γ-Fe_2O_3, cubic spinel structure) [114]. Scientists showed interests in Fe_2O_3 since its potential practical applications including covering magnetic storage devices as well as magnetic resonance imaging contrast agents [115]. Also, very importantly, these two oxides are not toxic, they are even biocompatible and therefore environmentally friendly choice. Fe_2O_3 NPs can be used as additives for lubricants performing different tasks such as improving their thermal conductivity [116]. Fe_2O_3 NPs have also been used as antifriction and antiwear enhancers. Majeed et al. [117] used a four-ball tribometer (steel balls) to measure the friction and wear of iron oxide nanoparticles (Fe_2O_3) as additives for paraffin base oil. Three different concentrations, 0.4, 0.8 and 1.2 wt% of Fe_2O_3 were studied. At 0.8 wt% concentration the nanolubricant showed the highest wear scar diameter reduction, 24.5 %, compared to the base paraffin oil. Sathishkumar et al. [118] studied the tribological performance of Fe_2O_3 with pearlite as additives to low cost heavy engine oil (15w 40). Two different mass concentrations were selected, 0.3 and 0.5 wt%. The tests were carried out in aluminum and steel contacts using pin-on-disc configuration. Results showed that nanoadditives with 0.5 % of concentration are more efficient in reducing wear rather than friction reduction.

In this Doctoral Thesis, iron oxide nanoparticles were synthesized from the collected sludge of iron mines in Omarska (Bosnia and Herzegovina). The mining waste contains several metals, such as copper, cobalt and more expensive metals, some of them are toxic, thus their

accumulation in the environment carries health hazards. Conversely, iron oxides are considered non-toxic and safe materials. Thus, it would be optimal to remediate wasted iron and other metals from sludge, while producing valuable nanomaterials [4].

In this regard, currently management of mining sludge is a main issue in mines, such as those in Sulcis-Iglesiente (Sardinia, Italy) and in Balkans area. The objective of the EU project BloW-uP, *Balkans Waste to Products: transfer of NoI model to Balkan area: de-siloing new waste-derived raw materials and developing new applications – RIS* was to transform waste from mining and metallurgical activities into major value products (additives for lubricants, carbon based materials for fuel cells/electrolyzers and metal-sir batteries, as well as materials for cleantech and eco industry) within a circular economy perspective. The project resulted in a published patent on synthesis of highly crystalline hematite nanoparticles based exclusively on mining sludge [5]. Sludge remaining after mining (called also "tailing") is mainly rich in materials, such as metal oxides that could be recycled and reused. Their recovery mostly goes via acid digestion to ionic solutions, and thus synthesis of nanoparticles is the most convenient way for valorization. Compared with their bulk counterparts, NPs of metal oxides display unique chemical, physical, optical and electronic properties reasoned by the quantum confinement and the greater availability of atoms on the surface compared to interior atoms to participate in any reaction [119]. Metal oxides nanoparticles have potential applications in different fields regarding their different properties including conductivity, shape, size and stability, among others [120]. Their applications include battery storage systems, gas sensors, solar cells, antennas, optoelectronic and electronics and tribology [115,121]. This project has been followed by a National Project from Bosnia and Herzegovina LubriCAD, *Nanochemistry Solutions in Technical Lubricants Additive Improvements*, which aims to develop a line of iron oxide based lubricant additives [122].

However, an issue in the development of lubricants containing nanoadditives is the poor dispersion stability owing to the non-polar nature of most oils. Several methods are used for dispersion of these nanoadditives in base oils trying to improve their stability that depends on both the nanomaterials and the base fluid properties. The techniques to enhance the stability of nanolubricants can be categorized in three groups: physical treatments, surfactant use and NPs surface modification [123].

1.4 IONIC LIQUIDS AS ADDITIVES

The term ionic liquids (ILs) replaced the old "molten salts" because this last suggested corrosive and viscous media at high-temperature, where ILs refers to compounds formed entirely of ions (cations and anions) that are liquids around or below 373.15 K, which fundamentally, show great potential benefit for sustainable chemistry [124,125]. They have unique thermal, physical, chemical, and biological properties, which results in significant advantages, which is why they have emerged as a clean, efficient, and a more environmentally friendly option of volatile organic solvents [126]. ILs have been used as effective solvents and catalysts for clean chemical reactions [127], and their use as lubricants or additives for lubricants has been proposed in many applications depending on certain properties (solubility, thermal and mechanical properties or combinations) [21,128], their first use as lubricants being reported in 2001 by Ye et. al. [129]. In fact, ILs possess extremely important properties such as high thermal stability, good thermal conductivity, low volatility, and low flammability that make them excellent candidates as lubricants and lubricant additives [130]. In addition, the highly tunable nature of ILs, by changing cation, anion, or both, allows for adapting of these properties, as well as viscosity, to specific applications. However, ILs are used as lubricants only in critical applications because of their high cost compared to traditional base oils [131,132]. Nevertheless, the reliability and

efficiency of the use of ILs as additives in different types of base oils for various tribological applications has been demonstrated in numerous articles recently analyzed in two reviews [23,24]. Imidazolium, alkyl-ammonium, pyridinium, and phosphonium are the main four categories in which ILs are classified based on their cation structure. The first ILs used in tribology were formed of imidazolium-based cations and fluorine-based anions. Indeed, ILs with imidazolium cations showed immiscibility in non-polar base oils whereas fluorine had caused corrosion [25,133,134]. Undoubtedly, ILs with fluorine in their anions show good antifriction and antiwear capabilities [135,136], but in addition to promote corrosion in the components, fluorine is a toxic halogen, making it necessary to find and use other less toxic alternatives [137]. A key factor that is considered essential in industrial applications for the development of lubricants containing IL additives is their miscibility in the base oils. Among the different types of ILs investigated in the literature as lubricant additives, those based on phosphonium cations, ammonium cations, or organophosphate anions were shown to be, in general, more miscible with most of the common nonpolar mineral-based or synthetic hydrocarbon oils [22]. Phosphonium based ILs reveal better miscibility and tribological performance when used as lubricant additives compared to most ILs [22,138,139], demonstrating effective anti-scuffing/antiwear functionality as additives of mineral or polyalphaolefins (PAOs) base oils [140]. For instance, Qu et al. [141] and González et al. [139] had studied the tribological behavior of trihexyltetradecylphosphonium bis(2-ethylhexyl)phosphate and trihexyltetradecylphosphonium bis(2,4,4-trimethylpentyl)phosphinate in lubricating oils in different contact surfaces such as steel to steel, steel to aluminum or steel to cast iron, showing that both phosphonium ILs are miscible in several synthetic and mineral oils, resulting in favorable tribological characteristics. Cigno et al. [137] evaluated the tribological performance of a bio-oil (BO), suitable for gearboxes of wind turbines, additivated with halogen-free phosphonium ILs, (trihexyltetradecylphosphonium bis(trifluoromethylsulfonyl) amide $[P_{6,6,6,14}][NTf_2]$, or trihexyltetradecylphosphonium bis(2,4,4-trimethylpentyl)phosphinate $[P_{6,6,6,14}][(iC8)_2PO_2]$, . The authors performed tribological tests in a tribometer operating in pin on disc configuration (steel on steel contact). Both ILs were miscible in BO. The results showed that the addition of $[P_{6,6,6,14}][NTf_2]$ or $[P_{6,6,6,14}][(iC8)_2PO_2]$ to BO led to wear reductions up to 74 and 68 %, respectively.

In general, the concentration of ILs added into oils ranges between 1 and 5 wt% and can effectively lead to high improvements of the base oils tribological performance [22,142,143]. Other advantages of phosphonium ILs are their commercial availability in the market. Given that they are manufactured on a scale of several tons, their synthesis is not expensive, they show low impact on the environment and help reducing waste while inhibiting corrosion and relatively good stability, features which make them attractive alternatives for wide synthetic applications [144-146].

1.5 IONIC LIQUIDS AND NANOMATERIALS AS HYBRID ADDITIVES

The combination of ILs and NPs as hybrid lubricant additives can lead to possible synergistic effects, not only tribologically such as antiwear and antifriction enhancements, but also to achieve better stability of the hybrid nanolubricant (which has two additives of different nature, the IL and the NPs, in this case) than that of the nanolubricant without ILs. Thus, ILs can lead to the formation of cationic-anionic ion layers that around NPs provide electrostatic forces which prevent them from aggregation [147]. Liñeira del Río et al. [26] studied the synergies of tri(butyl)ethylphosphonium diethylphosphate $[P_{4,4,4,2}][C_2C_2PO_4]$ IL and h-BN NPs or GnP in triisotridecyltrimellitate (TTM) achieving a 33 % reduction in friction and a 44 % in wear when

using the hybrid additive IL/GnP. Subsequently, Liñeira del Río et al. [28] have measured the full Stribek curves and bearing friction torque finding that the best friction behavior and the lowest friction torque (maximum reduction of 45% at 500 rpm) correspond to the TTM + 2 wt% IL + 0.1 wt% GnP nanolubricant. Murthy et al. [142] investigated the addition of GnP and a phosphonium-phosphate-based IL as a double additive for a rotorcraft gearbox oil aiming to enhance the scuffing resistance under starved lubricated conditions. The hybrid combination of IL/NPs led to an increase in time before the scuffing initiation in high-speed components of the tribological contacts, which helps to extend the gearbox operation during lubricant loss. Amiril et al. [148] investigated the tribological behavior of a chemically modified palm olein trimethylolpropane ester with the addition of h-BN NPs and $[P_{6,6,6,14}][(iC8)_2PO_2]$ IL finding a small increase in antiwear and antifriction properties in comparison to base oil. Upendra et al. [149] studied the synergistic effects between the latter IL and Al_2O_3, CuO, or SiO_2 NPs as additives to a mineral oil. The results show excellent synergy between IL and both Al_2O_3, CuO NPs, showing improvements in friction of 19 % and 24 %, and in wear of 32 % and 36 %, respectively. Nevertheless, the authors did not find clear evidence of any synergy between the IL and SiO_2 NPs. Recently, Bondarev et al. [150] studied the addition of h-BN nanosheets and/or spherical W nanoparticles to PAO6 base synthetic oil and their effect on the base oil tribological behavior for a 100Cr6 steel-steel tribo-pair. Synergistic effects were found upon the combination h-BN and W achieving better results than their individual addition as additives to the lubricating oil

1.6 THESIS FRAMEWORK

This Doctoral Thesis was carried out in the Laboratory of Thermophysical and Tribological Properties (LTTP) of the Department of Applied Physics, a laboratory integrated in the NaFoMat research group of the Universidade de Santiago de Compostela, within the framework of the national coordinated project "Development of hybrid nanofluids, nanolubricants and nano-enhanced Phase Change Materials for the transfer, storage and production of energy" (AdLuTer, 2018-30/9/2021, call "RETOS 2017"), in particular into the subproject 2, "Advanced nanoadditive based lubricants for gears and motors" (ENE2017-86425-C2-2-R), supported by the Spanish Ministry of Science, Innovation and Universities and the European Regional Development Fund (ERDF, FEDER in Spanish). The AdLuTer coordinated project aims to propose new advanced and specialized materials in the field of lubrication, and the storage and transfer of thermal energy focused on the field of renewable energies (solar, wind, hydraulic and geothermal) and in engines and transmissions. In the case of the subproject 2 the specific objective is to propose advanced lubricants based on nanoparticle dispersions and other carbon nanostructures for gears and motors in the field of wind, hydraulic and automotive transmissions. Attention is focused on the level of aggregation of nanoadditives and on the control of temporal stability. The selection is being made from the thermophysical and tribological characterization (friction and wear) to achieve a balance between the different parameters that affect the performance of the final lubricant. The NaFoMat group has been selected by Xunta de Galicia as competitive reference group through the 2016 and 2020 calls (ED431C 2016/001 and ED431C 2020/10, respectively). The LTTP group belonged to the AeMAT Strategic Grouping of Materials which was also funded by "Xunta de Galicia" (ED431E 2018/08). In addition, this group was also integrated in the 3rd edition of the Galician Ionic Liquid Network (ED431C 2017/22). This network has also received funding from "Xunta de Galicia". On the other hand, the three LTTP permanent staff and most of the NaFoMat researchers are currently integrated into the new Materials Institute (iMATUS) of the Universidade de Santiago de Compostela. The part of this Doctoral Thesis dedicated to iron

oxide NPs synthesis was carried out in the group of Prof. Gotovac Atlagić of the Department of Chemistry (Faculty of Natural Sciences and Mathematics) from the University of Banja Luka. The research stay was supported by Erasmus+ ICM [KA107] during the academic year 2020/2021. The research line was previously co-financed (04/2017 to 03/2019) by the EU through the coordinated BloW-uP project (grant number 16320 by EIT RM) and by the Ministry of Scientific-Research Development, Higher Education and Information Society of Republika Srpska in Bosnia and Herzegovina, in the framework of the LubriCAD project (grant number 19.032/961-151/19).

1.7 RESEARCH OBJECTIVES

The main goal of this Doctoral Thesis is to study the tribological performance of potential lubricants with hybrid additives for the field of renewable energies, such as in wind turbine gearboxes. In addition, a preliminary study on nanoadditives synthesized from mining sludge was also conducted. To achieve these aims, the following specified objectives are envisaged:

1. Selection of nanoadditives to design new potential nanolubricants and synthesis and characterization of iron oxide NPs from mining sludge;
2. Selection and characterization of ionic liquids (ILs) as lubricant additives of a polyalphaolefin (PAO32);
3. Evaluation of possible corrosion produced by selected ionic liquids on AISI 52100 steel;
4. Obtaining long-time stable dispersions of nanoadditives in lubricant base oils (PAO32 and PAO10);
5. Thermophysical characterization (density, viscosity, viscosity index) of PAO32, some of its mixtures with ILs, several of its dispersions with hybrid additives (ILs+nanoadditive), and with double hybrid additives (ILs+nanoadditive1+nanoadditive2);
6. Evaluation of the tribological behavior of steel/steel contacts lubricated with PAO32, several of its mixtures with ILs, and of its nanolubricants with hybrid additives and lubricants with double hybrid additives.

1.8 PHD DISSERTATION STRUCTURE

To deal with the proposed research objectives, this Doctoral Thesis is organized in five chapters and an annex, as follows:

- Chapter 1 provides a general introduction of the studies related to the proposed research;
- Chapter 2 describes the methodology followed, the work strategies and the different experimental techniques used;
- Chapter 3 reports the results obtained in the framework of this Doctoral Thesis;
- Chapter 4 includes a complete description and discussion of the results: stability analysis, thermophysical characterization and tribological investigation of the designed nanolubricants;
- Chapter 5 reports the Doctoral Thesis conclusions and proposed future work;
- An annex presents a summary of this Doctoral Thesis in Galician.

2 MATERIALS AND METHODS

This chapter describes the selection and characteristics of the materials involved in this investigation, including base oils, nanomaterials, and ionic liquids. The samples preparation methods, as well as the experimental techniques and strategies used to determine the thermophysical properties and the tribological behavior of the designed nanolubricants. In addition, the setup, methodologies and the experimental conditions for the characterization of the lubricants are presented. The flow diagram of the methodology of this Doctoral Thesis is shown in Fig. 2.1.

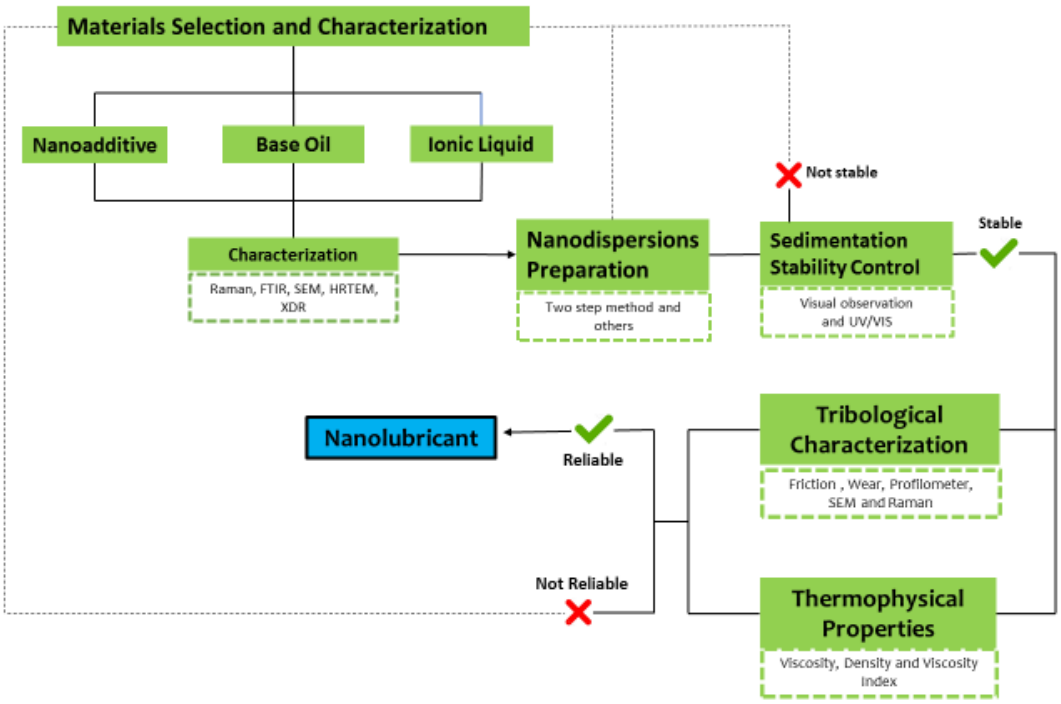

Fig. 2.1. Flow diagram of the experimental procedures followed in this Doctoral Thesis

2.1 MATERIALS SELECTION

The materials selection in this Doctoral Thesis was based mainly on:

1) The *application* of the prepared hybrid lubricants; which led to the selection of PAO32 as the based oil since it is used in the gearbox lubricants of wind turbines.
2) *Eco-friendly material*; which was the reason to choose the h-BN NPs to be used as PAO32 additives in addition to other characteristics such as their ability to reduce friction and wear.
3) The *availability* and *low cost* that led to the selection of GnP nanoplatelets to be used as additives, in addition to their *excellent properties* as friction and wear reducers.

4) *Better miscibility* and *performance as friction and wear reducers*; which ended in selecting three phosphonium-based ILs to be used as PAO32 base oil additives instead of other types of ILs for their additional advantages, also considering that the selected ILs are available commercially.
5) *Environmental-friendly process, availability and relatively nontoxic NPs*; which led to the synthesis of iron oxides NPs used as lubricants additives recycling mining sludge.

Table 2.1, 2.2 and 2.3 show all the lubricants and additives used in this Doctoral Thesis. One of the lubricants used is a synthetic oil, polyalphaolefin 32 (PAO32), which was provided by Repsol. PAOs are classified in group IV of the API (G-IV). The PAO32 sample was obtained at REPSOL by mixing PAO40 and PAO6 in a proportion ratio of 89 wt%/11 wt%, respectively. In this Doctoral Thesis PAO10 and another PAO32 samples provided by Tehnosint were also used. The second sample of PAO32 was prepared in Tehnosint by mixing PAO100 (79 wt%) and PAO6 (21 wt%). In a similar way, the PAO10 sample was prepared, by mixing 35.2 wt% of PAO100 and 64.8 wt% of PAO6. As already indicated, PAOs have better thermal stability, higher viscosity indexes (VI) and lower pour points than mineral oils (MOs), properties that makes them more attractive for operators and manufacturers than MOs [151]. In addition, PAOs can get better efficiency and oil cleanliness compared to MOs [152]. PAO32 are currently used as base oils of the formulated lubricants for wind turbine gearboxes [153,154].

Graphene nanoplatelets (GnP), hexagonal boron nitride (h-BN) nanoparticles and iron oxide, synthesized from the sludge of an iron mine, are the nanomaterials selected to be studied as lubricant nanoadditives in this Doctoral Thesis. In this Thesis, PAO32 supplied by Repsol was used to prepare the mixtures with ILs and the nanolubricants containing h-BN NPs or GnPs, with or without ILs. Furthermore, the PAO32 and PAO10 supplied by Tehnosint were used to prepare the nanodispersions of iron oxide NPs whose stability was studied. In addition to the selection criteria indicated above, the selection of these nanomaterials was based on the fact that the addition of small amounts of 2D materials such as graphene or hexagonal boron nitride to base oils has shown significantly lower friction coefficients and wear rates than base oil, features that makes them attractive high-performance nanolubricants [90,94-99].

The h-BN NPs and GnP samples were provided by IoLiTec. GnP (lot NCP068011) have a claimed mole fraction purity equals to 0.95, a thickness between 11 and 15 nm, an average particle diameter of 15 μm and a bulk density of 2.25 g cm^{-3}. Their morphology was previously explored by Liñeira del Río et al. [98] and Guimarey et al. [155]. From these studies it can be concluded that GnP have a bended and wrinkled appearance. In addition, it was confirmed that the GnP of this lot have a carbon atomic composition of 95 %. Concerning h-BN NPs (lot MNC018001) have mole fraction purity of 0.99, average particle size of 70 nm, and bulk density of 2.29 g cm^{-3}, previous studies revealed a disc-like shaped morphology [90,103]. Regarding the iron oxide NPs, they were obtained by recycling the iron ions from the sludge of iron mine located in Bosnia and Herzegovina using the method of Stević et al. [4].

Table 2.1. Several properties of the lubricants used in this Doctoral Thesis

Base Oil	Supplier	Viscosity at 100°C, cSt	CAS Number
Polyalphaolefin, PAO32	REPSOL	31.5	533903-84-3
Polyalphaolefin, PAO32	Tehnosint	~32	533903-84-3
Polyalphaolefin, PAO10	Tehnosint	~10	856661-25-1

Table 2.2. Several properties of the nanoadditives used in this Doctoral Thesis

Nanomaterial	Supplier	CAS Number	Purity	Average Size (nm)
Graphene nanoplatelets, GnP	Iolitec	1034343-98-0	0.95	11-15[a]
Hexagonal boron nitride nanoparticles, h-BN	Iolitec	10043-11-5	0.995	70
Iron Oxide NPs	synthesized	1309-37-1	n.a.	5-30

[a]Referred to thickness
n.a: not available

Table 2.3. Several properties of the ionic liquids used in this Doctoral Thesis

Ionic Liquid	Supplier	CAS Number	Purity[a]	Chemical Structure
Trihexyltetradecylphosphonium bis(2-ethylhexyl)phosphate (IL1) **$[P_{6,6,6,14}][DEHP]$**	Iolitec	1092655-30-5	>0.98	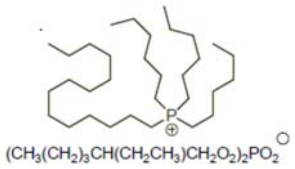
Tributylethylphosphonium diethylphosphate (IL2) **$[P_{2,4,4,4}][DEP]$**	Iolitec	20445-94-7	>0.95	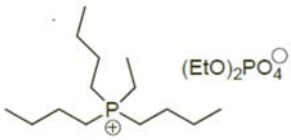
Trihexyltetradecylphosphonium bis(2,4,4-trimethylpentyl)phosphinate (IL3) **$[P_{6,6,6,14}][(iC8)_2PO_2]$**	Iolitec	465527-58-6	>0.90	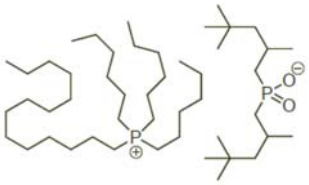

[a]Given by the supplier

In this Doctoral Thesis, three phosphonium ionic liquids (ILs) were also used as additives for the PAO32 sample supplied by Repsol. The ILs selected were trihexyltetradecylphosphonium bis(2-ethylhexyl) phosphate (IL1), tributylethylphosphonium diethylphosphate (IL2) and trihexyltetradecylphosphonium bis(2,4,4-trimethylpentyl)phosphinate (IL3). These ILs were selected since phosphonium based ILs are known as excellent lubricant additives due to their appropriate properties such as great oil miscibility and their both antiwear and anticorrosion properties, playing their organic phosphorus a fundamental role in tribo-chemistry [22,138,140,143,156-159].

2.2 CHARACTERIZATION TECHNIQUES

Fourier-transform infrared spectroscopy (FTIR), scanning electron microscopy (SEM) and Raman spectroscopy techniques, were used to characterize the base oils, additives, lubricants or tribological pairs as well as analyzing the surface of the discs and the pins used in this Doctoral Thesis. The analyses were carried out in collaboration with the Network of Infrastructures to Support Research and Technological Development (RIAIDT) of the University of Santiago de Compostela. In addition, a high-resolution transmission electronic

microscope (HRTEM) and an X-ray diffractometer (XRD) from Shinshu University were used to characterize the iron oxide NPs.

2.2.1 Fourier-transform infrared spectroscopy

This non-destructive analytical characterization technique, based on the interaction of infrared radiation with a sample, allows to identify chemical bonds of compounds. The positions of the peaks give information on the structure of the molecules in the sample and the peak intensity is function of the bond concentrations in the sample. Infrared spectra are unique, rich in information as well as being fast and easy to obtain [160]. This technique was used to analyze the chemical structures of PAO32 supplied by Repsol and the three phosphonium ILs selected. The nanomaterials, h-BN and GnP, were previously characterized by Liñeira del Río et al. [98,103] and Guimarey et al. [155]. In addition, FTIR spectra were carried out for the analysis of the mixtures (PAO32/ILs) and the nanodispersions containing h-BN NPs, comparing them with the spectrum corresponding to the pure base oil PAO32, aiming to detect any chemical bond formation in the mixtures and dispersions. This technique was also used to analyze the spectra of the ILs after the corrosion tests. An FTIR VARIAN 670-IR spectrometer (Fig. 2.2) assembled to 610 IR microscope mapping was used to obtain the spectra. For this task, the device was equipped with an Attenuated Total Reflection (ATR) accessory, ATR PIKE, which measures the absorbance spectrum of the sample.

Fig. 2.2. FTIR VARIAN 670-IR Fourier transform infrared spectrometer (RIAIDT of the University of Santiago de Compostela)

2.2.2 Scanning electron microscopy

Scanning electron microscopy (SEM) images were obtained by means of a scanning electron microscope Zeiss FESEM Ultra Plus (Fig. 2.3. a) operating in high vacuum mode. The sample under study is placed on a support plate (Fig. 2.3. b). The device has an acceleration voltage range between 0.02 and 30 kV and resolutions: 1.0 nm/15 kV, 1.7 nm/1 kV and 4.0 nm/0.1 kV. This technique was used to obtain high resolution images of the wear scar generated on the surface of the pins and discs after the tribological tests, to characterize the surface wear type, evaluate the morphological changes and identify the type of wear produced.

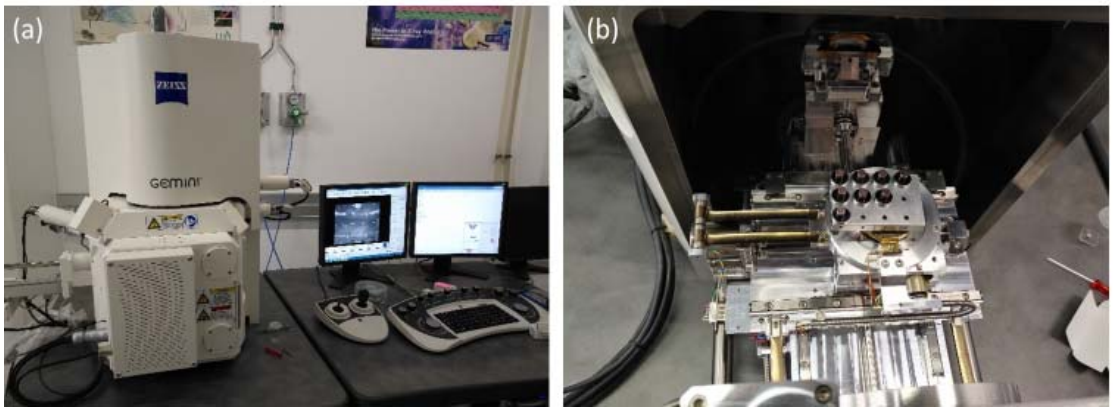

Fig. 2.3. (a) Zeiss FESEM Ultra Plus Scanning Electron Microscope device and (b) samples support including several discs for analysis (RIAIDT of the USC)

2.2.3 Raman spectroscopy

The device used to carry out Raman analysis is a confocal Renishaw Raman spectrometer Invia Reflex (Fig. 2.4. a), equipped with an argon ion laser operating at 514 nm. In addition, it is also equipped with a confocal LEICA DM microscope, an XYZ motorized platform for Raman mapping and a variable spot laser from 1 to 300 μm depending on the objective and the wavelength used. Raman spectroscopy of the GnP and h-BN NPs were previously reported [103,155], whereas this technique was used to obtain the Raman spectra of PAO32 and of the three ILs. Furthermore, to get details on the tribofilm compositions within the wear scar generated during the tribological tests, a WITec alpha300R+ confocal Raman microscope (Fig. 2.4. b) that can operate at different wavelengths: 488, 532 and 785 nm, was used. This device allows to generate a 3D image of the worn scar surface providing chemical and 3D optical information. In the present Doctoral Thesis, Raman spectra and elemental mapping of the worn surfaces lubricated with several designed lubricants were recorded at a wavelength of 532 nm.

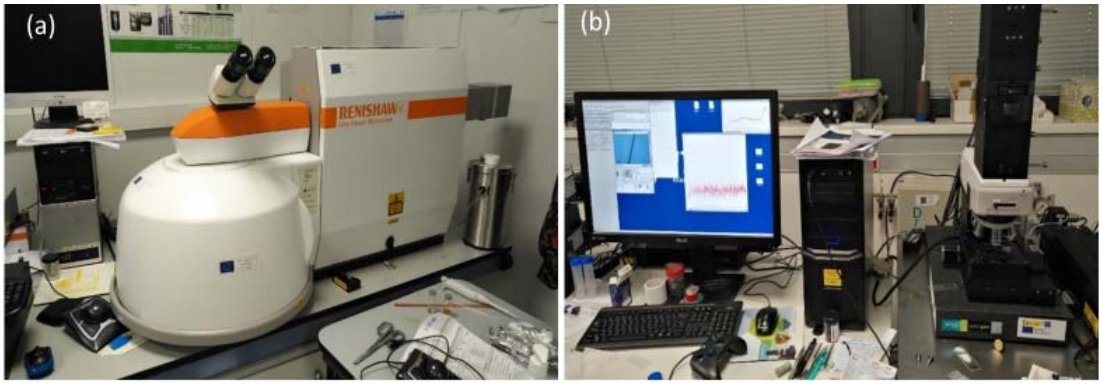

Fig. 2.4. (a) "InVia Reflex" Renishaw confocal Raman spectroscope and (b) WITec alpha300R+ confocal Raman microscope. (RIAIDT of the USC)

2.2.4 High-resolution transmission electron microscopy and X-ray diffractometer

Morphology and size of the iron oxide NPs were carried out with high-resolution transmission electron microscopy (HRTEM) (Fig. 2.5). Images were acquired using a JEOL JEM-2010 apparatus operated at 200 kV. This characterization was performed at the Division of Chemistry and Materials, Faculty of Textile Science and Technology, Shinshu University, (Japan) with the support of Prof. Yoshiyuki Hattori.

Fig. 2.5. JEOL JEM-2010 High-resolution transmission electron microscope

In addition, the composition of the iron oxide NPs was qualitatively determined by an Ultima IV Rigaku X-ray diffractometer (XRD) (Fig. 2.6), with a source Cu-Kα, λ = 1.5418 Å, also from Shinshu University.

Fig. 2.6. Ultima IV Rigaku X-ray diffractometer (XRD)

2.3 PREPARATION OF THE NANOLUBRICANTS

The preparation of homogenized and stable nanolubricants is an essential part to be considered since the instability of nanolubricants limits their use in industrial applications. The stability of the nanoadditives in the base oil is reduced due to their agglomeration that occurs due to van der Waals forces [161]. Two main techniques are used to prepare nanolubricants: the one-step method and the two-step method. The first one consists of the simultaneous production and dispersion of the particles in the fluid to minimize agglomeration of the nanoparticles. Its most important drawback is that residual reagents can remain in the nanolubricant due to failed reactions or stabilization. These residues could adversely affect the tribological functions and chemical stability of the different components of the nanolubricant. The two-step method is the most economically affordable for designing nanolubricants, with the two steps being: 1) NPs are obtained by chemical or physical methods as dry powders; 2) their dispersion in the base fluid using physical methods as high-sharp mixing, ultrasonic agitation, high-pressure

homogenization, intense magnetic force agitation, and/or ball milling dispersion, or chemical methods: electrostatic, steric and electrosteric methods [162,163].

The two-step method [164] was used to prepare the nanolubricants formed by PAO32 and PAO10 and the nanoadditives (GnPs, and h-BN or iron oxide). Moreover, the nanodispersions including ionic liquid (PAO32/NPs/ILs) were made following the method proposed by Sanes et al. [27]. In both cases, the mass concentrations of the nanoadditives and of the base oil were determined using a high precision polyrange microbalance Sartorius MC 210P (Fig. 2.7. a) with an uncertainty in the mass range of the measurements of this work of 0.00001 g. The procedure [26,27] followed to prepare these hybrid nanolubricants consists of: first, the appropriate amount of ionic liquid was drawn by a suction micropipette (mass to volume equivalent was calculated) (Fig. 2.7. b) and then it is mixed with the appropriate amount of nanomaterials (weighted by the microbalance Sartorius MC 210P), and finally, manually crushed by the pestle in continuous movement in an agate mortar (Fig. 2.7. c) for 10 minutes. The amount of base oil necessary to obtain a certain composition is then added to the mixture obtaining the required nanodispersion. For homogenization, the nanodispersion is sonicated uninterruptedly for 4 hours in a Fisherbrand TM 11203 ultrasonic bath, at a frequency of 37 kHz being 180 W the effective power (Fig. 2.7. d). During the sonication of the nanodispersions, their temperature can increase. In our case, the duration of the sonication was 4 hours, which may increase the temperature of the bath water and the samples up to 353.15 K. To keep the samples at room temperature, cold water is added, and hot water is extracted from the bath manually every 30 minutes until the end of the process. The same procedure [164] was also used to homogenize the nanodispersions based on the combination PAO32/iron oxide NPs or PAO10/iron oxide NPs. In this case, a Kern ABJ 220-4NM the analytical balance was used to measure the weight of the base oils and the NPs. This balance has a readability of 0.1 mg (Fig. 2.8. a). After preparation, the samples were sonicated in an ultrasonic bath UW 32 (Fig. 2.8. b) that operates at 38 kHz, for 4 hours continuously where the temperature of the bath was controlled with the same procedure above indicated.

Fig. 2.7. (a) High precision Sartorius MC 210P Microbalance, (b) micropipette, (c) 80 mm agate mortar with pestle and (d) Fisherbrand ultrasonic bath FB11203

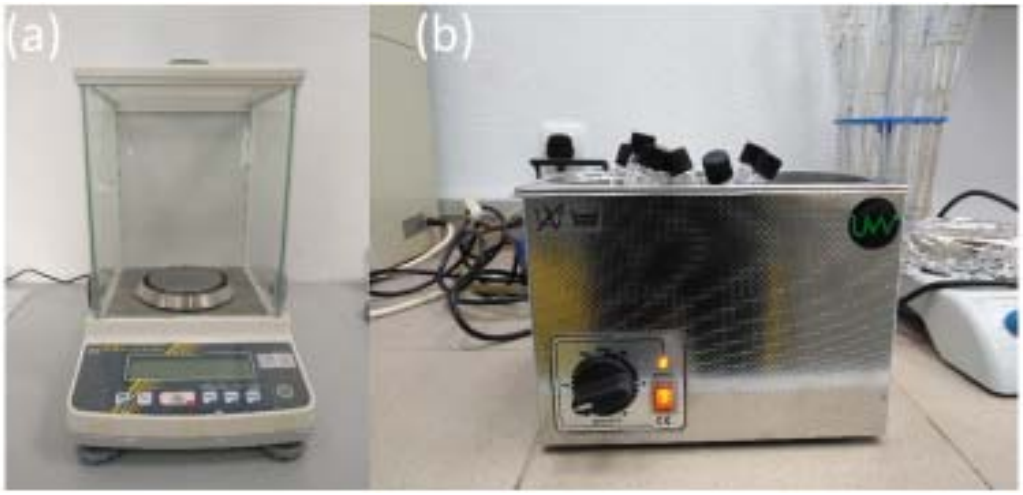

Fig. 2.8. (a) Analytical balance Kern ABJ 220-4NM, and (b) Ultrawave Ultrasonic Bath UW 32

2.4 STABILITY OF THE NANOLUBRICANTS

For industrial applications, the nanolubricant stability against sedimentation is a key factor. Therefore, obtaining stable suspensions of nanoadditives in base oils is essential. If the dispersion is homogeneous and stable, its ability to be used as an advanced lubricant attains better chance. From this point of view, one of the objectives of nanolubricant researches is to extend their stability time [18,123,165].

Several factors could influence the stability of nanolubricants, including the methods of preparing them, the structural properties (type, size, shape) of the nanoadditives as well as their thermophysical properties (density and viscosity) and the chemical structure of the oil. For spherical nanoparticles, Stokes law [123,166] relates the sedimentation speed, v, of the NPs that precipitate in the base fluid through their radius, r, and density, ρ_{NP}, and the density, ρ, and the dynamic viscosity, η, of the base oil, respectively.

$$\boldsymbol{v} = \frac{\mathbf{2}\boldsymbol{g}\boldsymbol{r}^{\mathbf{2}}(\boldsymbol{\rho}_{\boldsymbol{NP}}-\boldsymbol{\rho})}{\mathbf{9}\eta} \qquad (2.1)$$

Therefore, the larger the size of the nanoparticle and/or the greater the difference in the densities of the nanoadditives and the base oil, the faster the sedimentation. Several ways to improve the stability of the nanolubricant are considered useful. The use of surfactants is one of the simplest ways, but it must be taken into account that this technique can impact the lubricant characteristics by changing its properties, such as the viscosity, and therefore its antifriction and antiwear capabilities [162]. Another way is to chemically modify the surface of the nanoadditives (coating), this method is aided by means of modifying agents [167]. In this work, no surfactants or nanoparticle coatings were used as methods to improve the stability of the nanolubricant. Instead, in the preparation of several hybrid nanolubricants of PAO32 base oil, phosphonium based ILs were used. In fact, the addition of these ILs was carried out with a double purpose: on the one hand, to improve the stability of the nanolubricant since phosphonium based ILs have a good reputation as dispersants for the stabilization of nanoadditives [22,70] and dissolve in non-polar oils such as PAOs [24], and on the other hand, to improve the tribological behavior of the base oil.

Different ways to evaluate the stability time of the nanolubricants have been published in the literature [123]. Most of them are not applicable to dark-colored or highly viscous nanolubricants, as is the case here. In this Doctoral Thesis the simplest, cheapest, and most

common method was used, although it is time-consuming: the visual observation of the sedimentation, which consists of taking photographs of the nanodispersions periodically. In our case, the samples were photographed every day until initial, partial, or total sedimentation was detected at the bottom of the containers. The setup used for the visual control of several PAO dispersions with hybrid additives (ILs+nanoadditive), and the dispersions with double hybrid additives (ILs+nanoadditive1+nanoadditive2) is shown in Fig. 2.9 for some mixtures of ILs this setup was also used.

The stability of the PAO32/iron oxide NPs or PAO10/ iron oxide NPs nanodispersions was analyzed with two methods: the first one was also the visual observation by taking photos of the samples and the second through the UV spectra of the dispersions using a Perkin Elmer lambda 25 UV/VIS spectrometer (Fig. 2.10). The wavelength range of this device is 190-1100 nm and the fixed bandwidth was 1 nm. The wavelength used to measure the stability of the nanodispersions was 622 nm, being the nearest to the observed orange color of the samples.

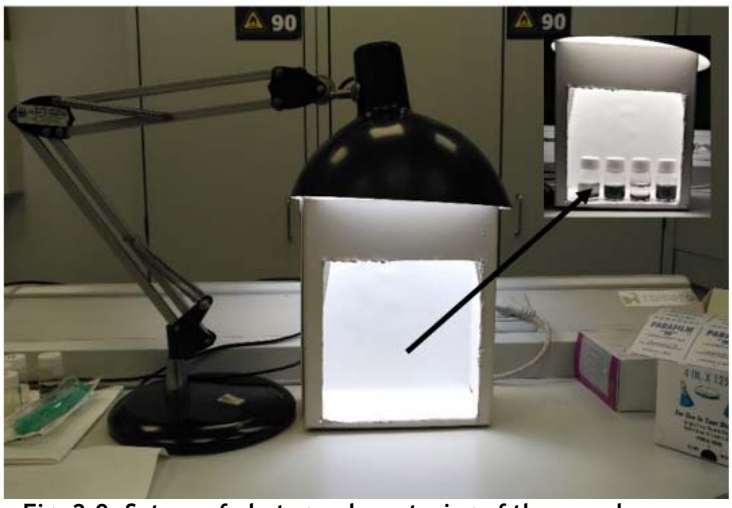

Fig. 2.9. Set-up of photograph capturing of the samples

Fig. 2.10. Perkin Elmer lambda 25 UV/VIS spectrometer

2.5 THERMOPHYSICAL CHARACTERIZATION

This section describes the apparatus used to characterize, at atmospheric pressure, the thermophysical properties of the base oils and the designed nanolubricants. Density, dynamic viscosity, and viscosity index were the measured thermophysical properties. This apparatus is a Stabinger SVM 3000 viscometer from Anton Paar (Fig. 2.11. a), that can operate in the

temperature range (233.15-378.15) K, in the density range (0.65-3) g/cm^3 and in the viscosity range (0.2-20000) mm^2/s, at atmospheric pressure. In this device two separate cells are assembled to measure viscosities and densities. The viscosity cell is a rotational Couette viscometer with a cylindrical geometry (Fig. 2.11. b), with a rapid rotating outer tube and an inner measuring bob which rotates slower [168]. The density cell is an oscillating glass U-tube. Both cells are filled in the same step and density and viscosity measurements are carried out simultaneously. The viscometer has a thermostat with Peltier cascade elements, which controls the cell temperature. A Pt100 probe is used to measure the temperature with an expanded uncertainty (k = 2) of 0.02 K in the range (288.15-378.15) K and of 0.05 K outside the indicated range. The expanded uncertainty for the density measurements is 0.0005 g·cm^{-3}, and the relative expanded dynamic viscosity uncertainty is 1 %.

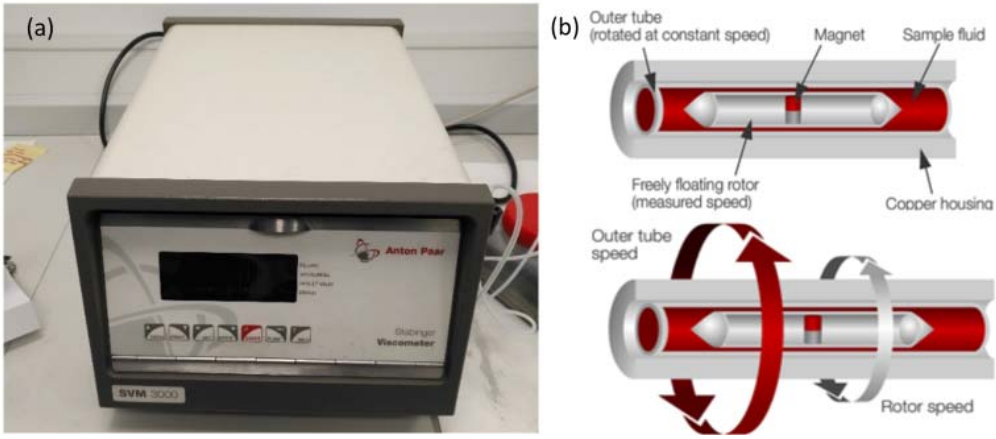

Fig. 2.11. (a) Anton Paar Stabinger SVM3000 visco-densimeter, (b) Operation diagram of the measuring system of the device

2.5 mL of each sample is needed to perform the measurements that were carried out automatically in temperature-ramp-scan mode from 278.15 K to 373.15 K with a step of 5 K, at atmospheric pressure. After measurements, both cells are immediately rinsed first with hexane and second with acetone and then dried by air. This cleaning is done several times until the density value of air reaches its standard value. In addition, the viscosity index (VI) is measured according to ASTM D2270 and ISO 2909 standards. VI is a dimensionless number that indicates the variation of viscosity with temperature, the higher the viscosity index, the lower the temperature dependence of viscosity. Its knowledge is necessary to characterize the lubricants, as there are often temperature changes during machinery operation and optimal lubrication should be ensured.

2.6 TRIBOLOGICAL CHARACTERIZATION

The tribological characterization in terms of friction coefficients and geometric characteristics of wear scar was carried out using base oils and most of the designed lubricants. The results were compared with each other in order to analyze the capacity of the nanoadditives as potential antifriction and antiwear improvers. Steel specimens were used as testers. This section presents a description of the different techniques used for this study. After comparison, the most efficient nanolubricants were selected as possible lubricants for industrial usage. As aforementioned, two tribological devices, a CSM Standard Tribometer and an Anton Paar MCR302 rheometer coupled to a T-PTD200 tribology cell, were used in this Doctoral Thesis.

2.6.1 CSM Standard Tribometer

Among other configurations, the CSM Standard tribometer (CSM Instruments: Peseux, Switzerland currently Anton Paar), can operate in ball-on-plate configuration with reciprocating motion or in rotational ball-on-disc configuration, the latter (Fig. 2.12) being the one used in this Doctoral Thesis to determine the antifriction capacity of the nanolubricants . In this configuration, a 6 mm diameter ball, made of AISI 52100 steel and with a roughness, Ra, of 0.05 μm and a 58–66 Rockwell "C" Scale hardness, runs against a 10 mm diameter disc also made of AISI 52100 steel, being the surface finish (Ra) 0.02 μm and the hardness 190–210 HV30. Initially and before mounting the specimens, they are cleaned and dried with hexane and hot air, respectively. A lubricant sample (3 drops, equivalent to 0.15 mL) is placed on the surface of the disc to cover the contact area during the ball trajectory. The ball is fixed on the arm that also supports the load chosen to perform the test. The base where the disc is attached is mounted on the rotating actuator. The ball is displaced from the center of the disc, generating during the test a circular groove of radius a (in our case a is 3 mm) at the surface of the disc. The ball is mounted on a rigid lever, which acts as a frictionless force transducer. As the disc rotates, the resulting friction forces between the disc and the ball are measured using a linear variable differential transformer (LVDT sensor) through the very small deflections produced in the lever. The coefficient of friction is determined from the tangential force, which is measured by the LVDT sensor, that provides accurate measurements of the tangential force and therefore friction coefficients.

All tests were performed under the following conditions: a normal load of 20 N corresponding to a maximum contact pressure of 1.79 GPa, trajectory radius of 3 mm, a speed of 0.10 $m \cdot s^{-1}$, sliding distance of 340 m and ambient temperature (~294 K). During each test, the software continuously records the tangential force measurements and translates them into the friction coefficient. All the tests were performed three times under the same conditions. The coefficient of friction is given as the mean value of the average friction coefficients along the sliding distance of the three tests and its corresponding standard deviation is also provided. Once the test is finished, the specimens are disassembled and cleaned again with hexane and hot air, being ready for other analysis.

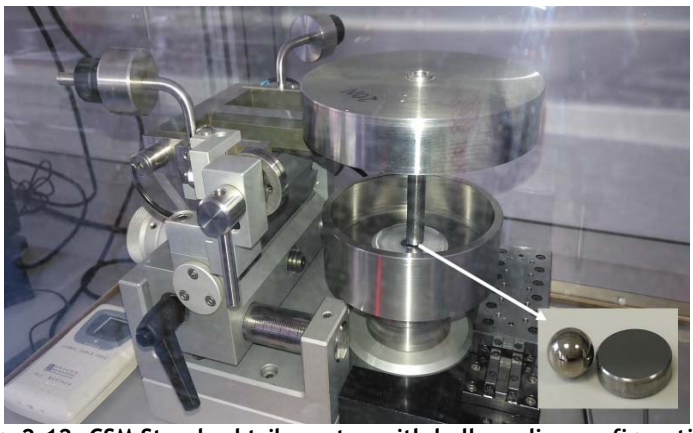

Fig. 2.12. CSM Standard tribometer with ball-on-disc configuration

2.6.2 Anton Paar T-PTD200 tribological cell

A tribology cell (Tribo-cell T-PTD200) mounted on an Anton Paar MCR302 rheometer was also used to measure the antifriction capacity of the nanolubricants (Fig. 2.13 a). This device is equipped with a Peltier hood H-PTD 200, which allows to control the temperature in the range (233.15 K-573.15 K). The measurements were performed in a ball on-three-pins

configuration. A 12.7 mm diameter ball of AISI 52100 chrome steel is fixed to the main axial shaft of the rheometer. This axial shaft, where the ball is mounted, is vertically fixed to a rotary motor. This rotary motor is driven by means of pressurized air nozzles, which in fact drives the shaft in a circular motion generating a rotational movement. Since the ball is mounted to the shaft, the rotational force is transferred to the ball similarly. The ball touches the three pins that the sample holder carries at three points of contact, one contact for each pin. The rotating shaft carrying the ball is vertically aligned with the sample holder that carries the pins that are tilted 45º angle as shown in Fig. 2.13. b. In addition, the pins are also made of AISI 52100 steel, and have a diameter and height equal to 6 mm, leading to a steel to steel contact pair.

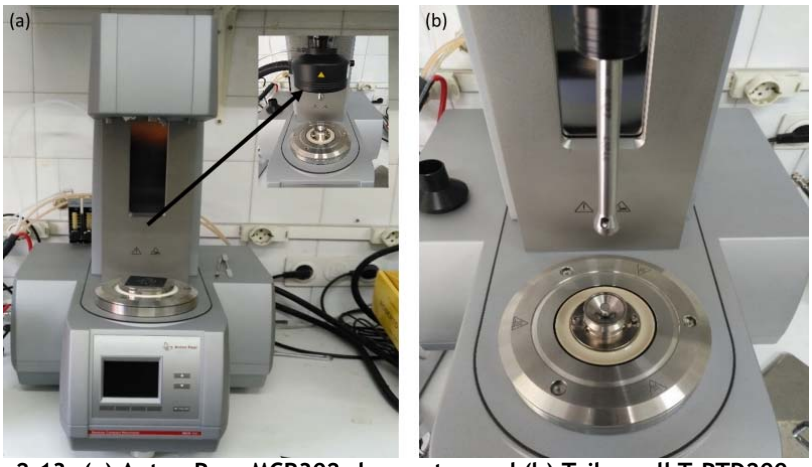

Fig. 2.13. (a) Anton Paar MCR302 rheometer and (b) Tribo-cell T-PTD200

This axial force, F, is transferred into three normal forces, F_N, perpendicular to the transversal surface of the pins at the contact points, because the ball presses the three pins (Fig. 2.14). The tangential force is determined from the torque needed to keep the sliding speed [169,170]. Flexibility is required in the pins so that the same normal force acts uniformly on the three contact points. The rheometer moves vertically down and then up the rotating ball to distribute the forces equally in three friction contacts. From Fig. 2.14, the relationship between the normal force F_N and the axial force F produced by the rheometer can be obtained:

$$F_N = \frac{F}{3\times\cos\alpha} \qquad (2.2)$$

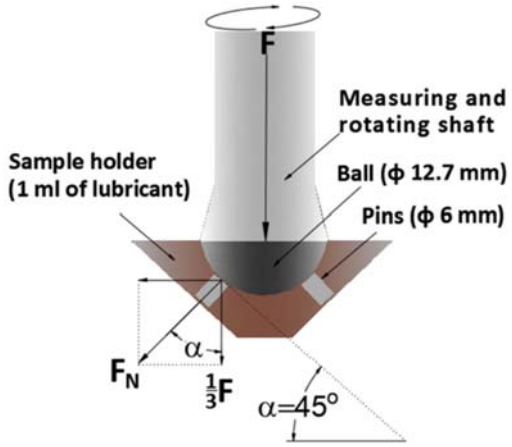

Fig. 2.14. 2D drawing of the tribometer test setup

During the test, the rotational movement of the main shaft produces a sliding speed of the ball with respect to the surfaces of the pins at the contact points, which can be constant or vary from 0 to 1.4 m/s. Automatic calibration of the system is made one time from the start to turnoff of the device, so continuous experiments can be carried out within this period with no need to recalibrate the device when initiating another different measuring test. Zero gap is automatically performed by the device when starting a test, ensuring that the ball touches the surface of the three pins with zero contact force. More details are given in the literature [79]. This step must be done before adding oil inside the sample holder. The last step before running the experiment is to fill the sample holder, where the pins are placed, with lubricant until these pins are completely submerged (~1.3 mL). The experiments were carried out under an axial force, F, of 42.43 N, which results in normal force F_N equal to 21.21 N, at an angular speed of rotation of 213 rpm (linear speed of the contact points of the ball 0.1 m s^{-1}), the sliding distance of the contact points of the ball was set at 340 m and the chosen temperatures were 298.15 K or 353.15 K. During the test, the friction coefficient is recorded as a function of time or of the sliding distance. The mean friction coefficient during the 340 m for each test is determined. Three repetitions were carried out for each condition/lubricant. The average coefficient of friction is calculated from the mean value of each of the three tests. Finally, the pins and the ball are disassembled and cleaned with hexane and hot air to analyze the wear.

2.6.3 3D Optical Profiler Sensofar S Neox

A 3D Sensofar S Neox optical profiler (Fig. 2.15.) was used to measure the parameters of the wear track generated on the discs or the pins due to the tribological test. For both specimens, the cross-section area, the maximum wear depth and the average roughness value (Ra) at the worn surface were measured. The wear scar of the pins has a form like a paraboloid, for which the volume and the diameter of the wear circumference at the surface of the pin is also measured. The wear scar in the disks has the shape of the volume generated by a parabolic surface perpendicular to the surface of the disk rotating about its axis. At the surface of the disk, the wear scar has the shape of a ring, whose width is also measured.

The profiler can operate in three different modes: confocal, interferometry and focus variation mode, and has three optical lenses, 10x, 20x and 50x. Moreover, the device has four LED sources (red, green, blue, and white) inside its optical core to optimize the lateral resolution (shorter wavelengths) or greater optical coherence (longer wavelengths). Furthermore, the red, green, and blue LEDs are pulsed to obtain true-color images and high-quality information in real time. In addition, the apparatus attains vertical and lateral resolutions up to 0.01 nm and 0.1 μm, respectively. During measurements, a 3D image is generated and transferred to SensoMap software, which allows a fast and precise analysis of the surface topology. In this Doctoral Thesis, the measurements were carried out in confocal mode with a 10x lens to analyze the wear scars produced from the tribological tests. In addition, roughness measurements were made for 6 discs in which one of the three selected ILs had been deposited for corrosion detection. The profiler in the confocal mode used for both types of measurements has a vertical resolution of 25 nm and a maximum slope of 14^0. The roughness value is determined according to the ISO4287 standard, applying a Gaussian filter with a wavelength cut-off of 0.08 mm.

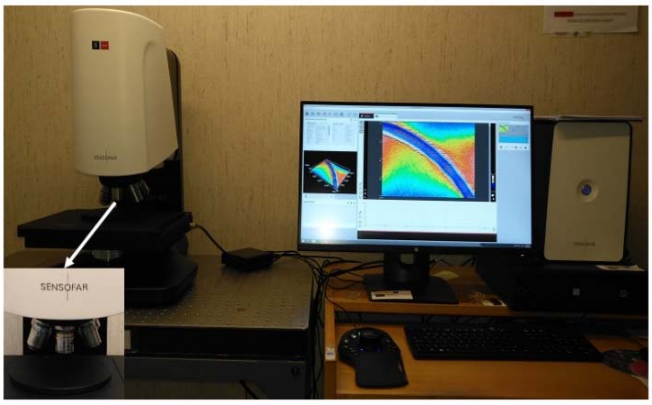

Fig. 2.15. 3D Optical Profiler Sensofar S Neox

2.7 CORROSION ANALYSIS

Apart from the use of ILs as enhancers of the stability of nanolubricants and as antifriction and antiwear additives, ILs can act as surface protectors against corrosion mainly for the lubrication of steel, especially phosphate-based ionic liquids, due to the formation of protective phosphate films. However, these ILs can be corrosive [133,171,172]. For this reason, simple corrosion tests were carried out for the three phosphonium ILs chosen in this Doctoral Thesis. Thus, each IL was evaluated separately to see the possible corrosion produced on the surfaces of the AISI 52100 steel discs. For this purpose, 0.15 mL of each ionic liquid (IL1, IL2, or IL3) were deposited on the surface of three smooth AISI 52100 steel discs (190–210 HV30 hardness). Two replicates were prepared with each IL forming two sets of samples. All the used discs were placed inside a Petri dish with lid to keep them in undisturbed conditions. One set was kept for 35 days at room conditions, whereas the other set was kept at 373.15 K (within 0.3 K) in a temperature chamber for 24 hours (Fig. 2.16.). After 35 days the Ra values of the surface of the discs were measured and compared to the Ra value of an unused disc. In addition, the ILs on the surfaces of the discs were collected and analyzed by infrared spectroscopy.

Fig. 2.16. Temperature chamber and pictures of three samples placed in Petri dishes

3 RESULTS

The publications derived from the work developed in the framework of this Doctoral Thesis are summarized in this chapter. Thus, three articles published in two reputed international scientific journals are included, as well as two contributions to scientific conferences. In addition, unpublished results obtained during a research stay at the University of Banja Luka (Bosnia and Herzegovina) are also reported.

3.1 PUBLISHED ARTICLES IN SCIENTIFIC JOURNALS AND COMMUNICATIONS TO CONFERENCES

A1: *Synergistic effects of hexagonal boron nitride nanoparticles and phosphonium ionic liquids as hybrid lubricant additives*

Khodor I. Nasser[a], José M. Liñeira del Río[a], Enriqueta R. López[a], Josefa Fernández[a]
[a]Laboratory of Thermophysical Properties, Nafomat Group, Department of Applied Physics, Faculty of Physics, University of Santiago de Compostela, 15782 Santiago de Compostela, Spain

Journal of Molecular Liquids 301, 113343, 2020
https://doi.org/10.1016/j.molliq.2020.113343
Editorial: ELSEVIER SCIENCE BV
ISSN: 0167-7322
2020 JCR: Physics, Atomic, Molecular & Chemical, 4/37, Q1 (Impact factor 6.165)

CRediT authorship contribution statement: Khodor I. Nasser: Validation, Formal analysis, Writing – original draft, Visualization. José M. Liñeira del Río: Formal analysis, Writing - review & editing. Enriqueta R. López: Methodology, Formal analysis, Writing - review & editing. Josefa Fernández: Conceptualization, Writing - review & editing, Supervision, Funding acquisition.

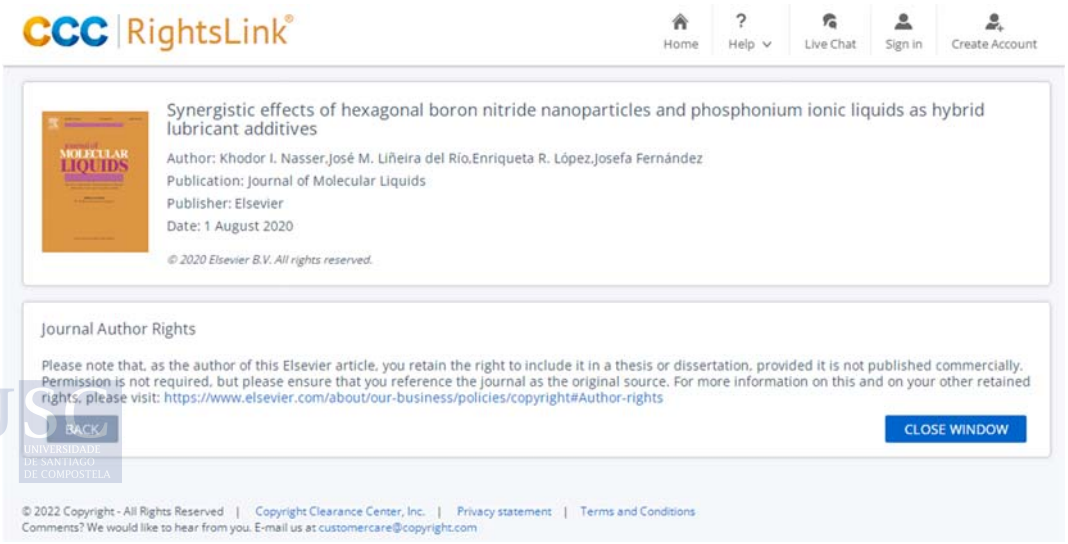

A2: *Hybrid combinations of graphene nanoplatelets and phosphonium ionic liquids as lubricant additives for a polyalphaolefin*

Khodor I. Nasser[a], José M. Liñeira del Río[a], Enriqueta R. López[a], Josefa Fernández[a]
[a]Laboratory of Thermophysical and Tribological Properties, Nafomat Group, Department of Applied Physics, Faculty of Physics, University of Santiago de Compostela, 15782 Santiago de Compostela, Spain

Journal of Molecular Liquids 325, 116266, 2021 (open access)
https://doi.org/10.1016/j.molliq.2021.116266
Editorial: ELSEVIER SCIENCE BV
ISSN: 0167-7322
2020 JCR: Physics, Atomic, Molecular & Chemical, 4/37, Q1 (Impact factor 6.165)

CRediT authorship contribution statement: Khodor I. Nasser: Validation, Formal analysis, Writing – original draft, Visualization. José M. Liñeira del Río: Formal analysis, Writing-review & editing. Enriqueta R. López: Methodology, Formal analysis, Writing - review & editing. Josefa Fernández: Conceptualization, Writing - review & editing, Supervision, Project administration.

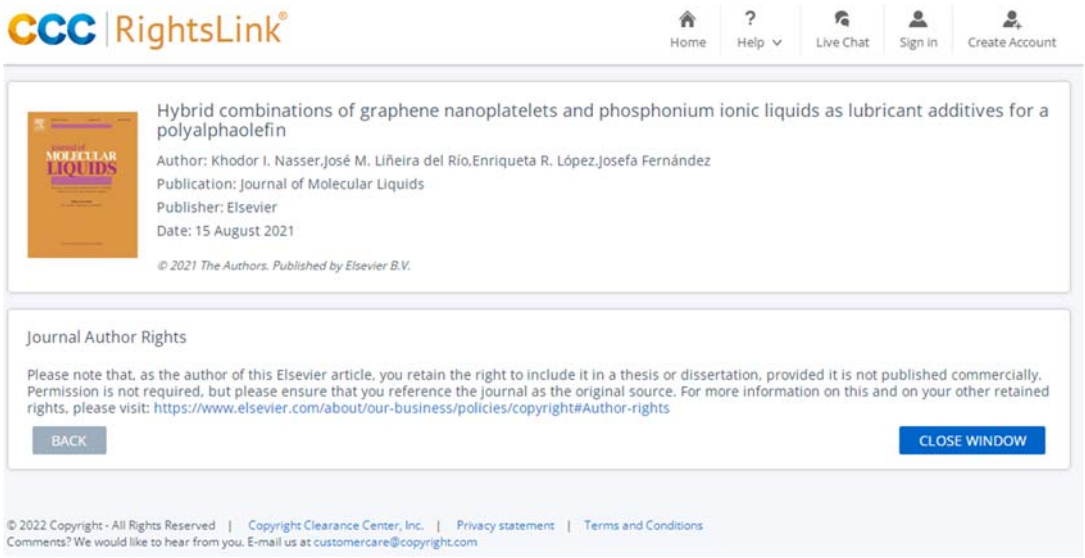

A3: *Double hybrid lubricant additives consisting of a phosphonium ionic liquid and graphene nanoplatelets/hexagonal boron nitride nanoparticles*

Khodor I. Nasser[a], José M. Liñeira del Río[a], Fátima Mariño[a], Enriqueta R. López[a], Josefa Fernández[a]
[a]Laboratorio de Propiedades Termofísicas y Tribológicas, Grupo Nafomat, Departamento de Física Aplicada, Facultad de Física, Universidade de Santiago de Compostela, 15782 Santiago de Compostela, Spain

Tribology International 163, 107189, 2021 (open access)
https://doi.org/10.1016/j.triboint.2021
ELSEVIER SCIENCE BV
ISSN: 0301-679X
2020 JCR: Engineering, Mechanical, 17/133, Q1 (Impact factor 4.872)

CRediT authorship contribution statement: Khodor Nasser: Validation, Formal analysis, Writing – original draft, Visualization. José M. Liñeira del Río: Formal analysis, Writing–review & editing. Fátima Mariño: Formal analysis, Writing – review & editing. Enriqueta R.

López: Methodology, Formal analysis, Supervision, Writing – review & editing. Josefa Fernández: Conceptualization, Writing – review & editing, Supervision, Project administration

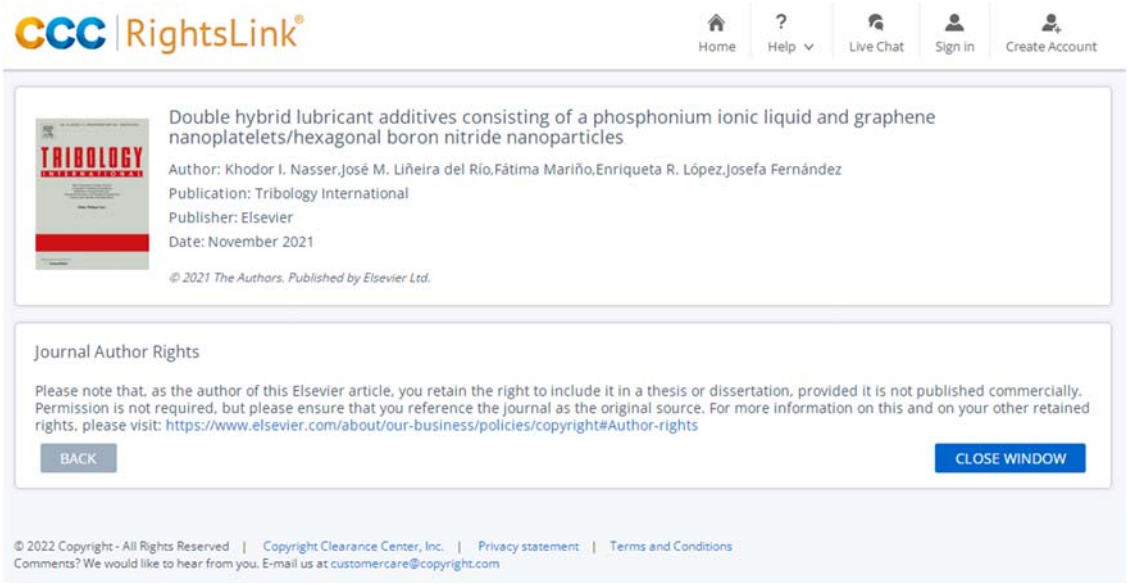

C1: Khodor I. Nasser, Fátima Mariño, Enriqueta R. López, Josefa Fernández
Synergistic Effects of Nanoparticles and Ionic Liquids as Hybrid Lubricant Additives in Energy System Applications
Conference: V Encontro da Mocidade Investigadora
Editorial of the abstract book: Universidade de Santiago de Compostela. Servizo de Publicacións e Intercambio Científico
ISBN: 978-84-17595-28-9
Year: 2019
https://dx.doi.org/10.15304/9788417595289
The purpose of this series of conferences is favoring the dynamics of collaboration, debate and diffusion of the knowledge generated among PhD students, presenting the main topics of each field of research.

C2: Khodor I. Nasser, José M. Liñeira del Río, Fátima Mariño, Enriqueta R. López, Josefa Fernández
Synergistic effects of nanoparticles and ionic liquids as hybrid lubricant additives for energy system applications
Organizer: Universitat Rovira i Virgili
Seminar: 10th International Seminar on Thermodynamic Engineering of Fluids (ISTEF), Tarragona (Spain)
ISBN: 978-84-09-32895-6
Year: 2021
These academic-scientific conferences are organized annually within the framework of the interuniversity doctoral program in Thermodynamic Fluid Engineering. Senior researchers present research lines and Ph.D. students the progress in their theses. It also involves invited researchers from outside the program.

3.2 SYNERGISTIC EFFECTS OF HEXAGONAL BORON NITRIDE NANOPARTICLES AND PHOSPHONIUM IONIC LIQUIDS AS HYBRID LUBRICANT ADDITIVES

This work reported the study of synergistic effects due to the combination of hexagonal boron nitride nanoparticles (h-BN) and three different phosphonium ionic liquids (ILs), trihexyltetradecylphosphonium bis(2-ethylhexyl)phosphate (IL1), tributylethylphosphonium diethylphosphate (IL2) and trihexyltetradecylphosphonium bis(2,4,4-trimethylpentyl)phosphinate (IL3) as hybrid additives of the base oil PAO32. FTIR and Raman spectra for PAO32, IL1, IL2 and IL3 were conducted. In addition, corrosion tests for the three ILs were carried out on the surface of smooth steel discs. Corrosion was detected with the presence of IL2 but not with IL1 nor with IL3. Moreover, seven lubricants were designed with 0.1 wt% of h-BN and/or 1 wt% of IL, namely the nanolubricants PAO32/h-BN, the hybrid nanolubricants PAO32/h-BN/ILX and the mixtures PAO32/ILX (X=1, 2 or 3). PAO32/h-BN nanolubricant was prepared with the two-step method whereas for the three hybrid nanolubricants the method proposed by Sanes et al. [27] was used. PAO32 and ILs were characterized by Raman and FTIR. The temporal stability of the four nanodispersions against sedimentation and of the three PAO32/ILX mixtures against separation was evaluated through visual observation by taking periodic photographs. The nanodispersions PAO32/h-BN/IL1 and PAO32/h-BN/IL3 were stable at least after 240 days since preparation whereas the mixtures did not present immiscibility signs two years after their preparation. The thermophysical properties (density and viscosity) at atmospheric pressure from 278.15 K to 373.15 K were analyzed for the prepared lubricants and for the base oil. In general, the density and viscosity increase, in comparison to PAO32, due the addition of h-BN, ILs, or h-BN/ILs. The relative increments in viscosity and in density owing to h-BN nanoparticles and/or ILs are lower than 7 % and 0.3 %, respectively. The tribological behavior of the mixtures, nanolubricants and the base oil was analyzed. The tests were carried out on an MCR 302 rheometer from Anton Paar equipped with a Peltier heated tribology cell T-PTD200 operating in the ball-on-three pins configuration. All the specimens are made of steel. The conditions of the setup during the tribological tests were: 213 rpm rotational speed, 42.43 N axial load (F) distributed equally at the surfaces of the three pins, two temperatures (298.15 K and 353.15 K) and for a duration of 3400 seconds. The friction coefficients obtained using the nanodispersions and the mixtures were compared with that obtained using the base oil. The best antifriction performance was exhibited by the nanolubricant PAO32/h-BN/IL2 at both temperatures, being 17 % and 28 % for 298.15 K and 353.15 K, respectively. A 3D optical profilometer Sensofar S neox was used to measure the produced wear scar in the pins. Three geometrical parameters (wear scar diameter (WSD), cross section area and maximum depth) were evaluated, being clearly identified at 353.15 K, and unmeasurable at 298.15 K. The WSD is reduced in comparison to that obtained with PAO32. The best antiwear reducer was the nanolubricant PAO32/h-BN/IL1 which minimized the WSD to 65 %, the worn volume reduced by 99 % and the depth by 92 %. In addition, the measured roughness values (Ra) at the worn surface of the pins shows synergistic effects between each IL and h-BN NPs by smoothing the surface. Ra reductions reached up to 60 % for IL2/h-BN additive in comparison to Ra values measured for PAO32. The hybrid additives noticeably improved the tribological performance of the lubricants with single additives, showing positive synergies. In addition, the Raman spectroscopy results of the worn surface of the pins illustrated protective IL and h-BN tribofilms. Finally, PAO32/IL1/h-BN was considered the nanolubricant that displays the best combined properties.

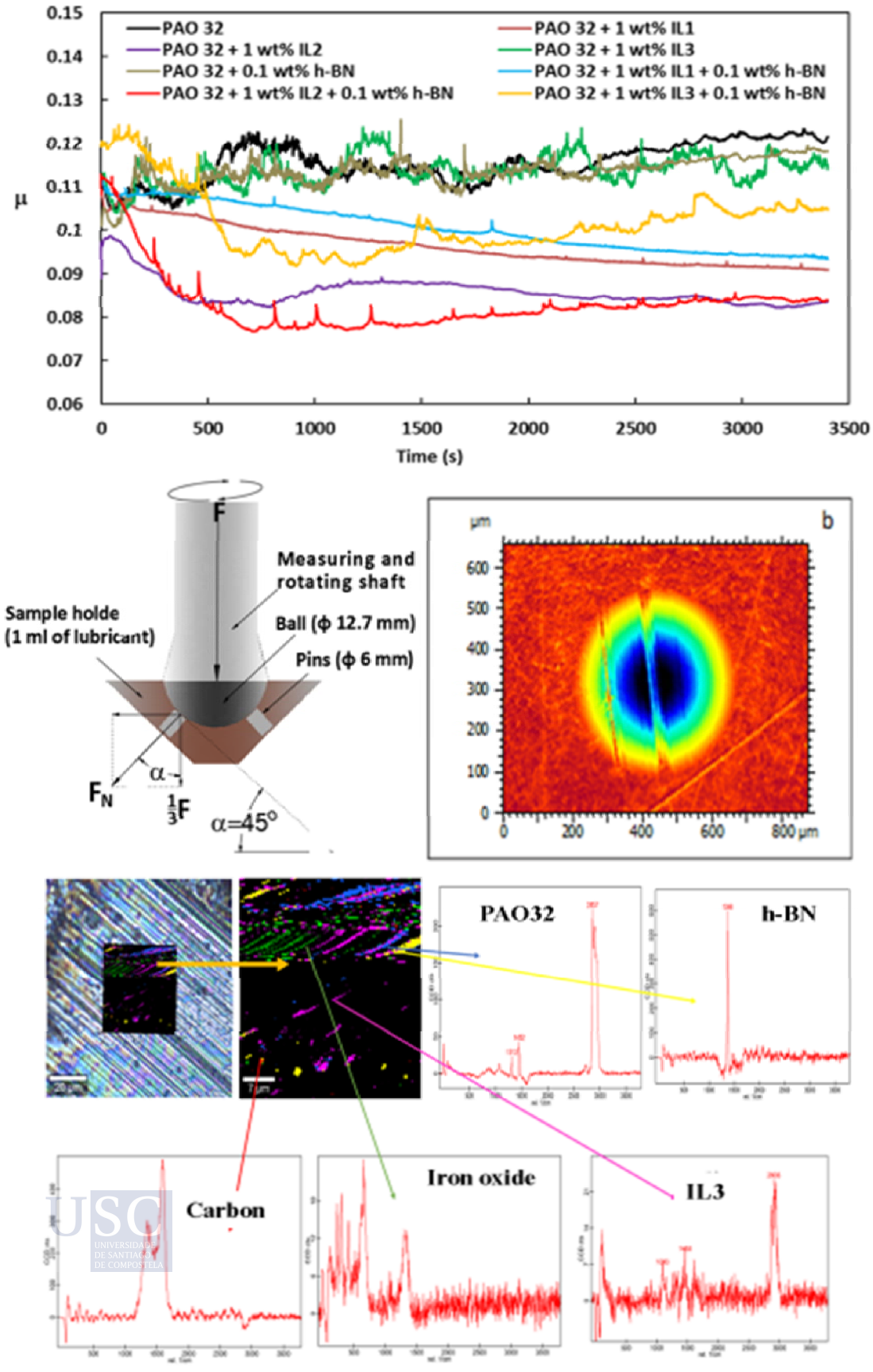

Fig. 3.1. Graphical abstract for article A1

3.3 HYBRID COMBINATIONS OF GRAPHENE NANOPLATELETS AND PHOSPHONIUM IONIC LIQUIDS AS LUBRICANT ADDITIVES FOR A POLYALPHAOLEFIN

This article presents the thermophysical and tribological properties of new developed nanolubricants based on the combination of graphene nanoplatelets (GnP) and the three phosphonium ILs used in the previous article. For this aim, eleven lubricants (three IL mixtures and eight nanodispersions) with different mass concentrations and combinations of GnP (0.05 wt% or 0.1 wt%), ILs or GnP/IL were formulated. To prepare the two single nanolubricants the two-step method was used whereas the method proposed by Sanes et al. [27] was used for the six hybrid nanolubricants. In order to know the effect of the GnP loading on the thermophysical and tribological properties, nanodispersions with 0.05 wt% and 0.1 wt% mass concentration of GnP were prepared with or without 1 wt% of IL. As in the previous article, the stability of the eight nanodispersions against sedimentation was evaluated. The nanodispersions PAO32/GnP, PAO32/GnP/ILX (X=1 or 3) for 0.05 wt% and 0.1 wt% of GnP showed no signs of sedimentation for at least 240 days after preparation. Thermophysical properties 0.1 MPa were evaluated for the eight nanodispersions with an SVM 3000 rotational Stabinger viscometer. The average density increases of the nanolubricants compared to PAO32 and due the addition of GnP and GnP/ILs ranged from 0.05 to 0.24 %. As regards to viscosity the average increments ranged from 2.2 % to 6.6 %. VI changes from -1.7 % to 0.53 %. Tribological performance of the nanolubricants in terms of friction coefficients were characterized with a CSM standard tribometer using ball-on-disc configuration applying 20 N normal load for 3400 seconds at room temperature and distance of 340 m in the relative motion of the ball against the rotating disc. The measured friction coefficient values for all the prepared nanolubricants and mixtures with ILs are lower than that corresponding to PAO32, being the nanolubricant PAO32/IL2/0.05 GnP the best anti frictional reducer by 24 %. The wear at the discs was measured in terms of the maximum wear scar width (WSW), transversal area and maximum depth of the worn scars using the 3D profiles. For all the designed lubricants, the wear scars were lower than those obtained with PAO32. The best antiwear behavior was achieved by the nanolubricant PAO32/IL2/0.05 GnP, which reduced the WSW by 13 %, the transversal area 23 % and the maximum depth 27 %, in comparison with the PAO32 base oil. From the profile measurements it was concluded that smoother contact surfaces were obtained with all mixtures and nanolubricants than with PAO32. With PAO32/IL2/0.05 GnP nanolubricant, the smoothest worn disc surfaces were obtained. Interestingly, the single dispersion with 0.05 wt% GnP is more effective (lower friction coefficient, transversal area, WSW and maximum depth) than that with 0.1 wt% GnP. Similar trends were found when comparing hybrid nanodispersions with 0.05 wt% GnP and 0.1 wt% GnP. SEM images of the worn scars show that the surfaces are smooth with neither marks of abrasion nor plowing, which agrees with the 3D profiles. In addition, small signs of plastic deformation were observed. Considering several behaviors, such stability worsening, higher viscosity rises, and corrosion production of IL2 made the selection of PAO32/IL2/0.05 GnP unfavorable. On the other hand, 0.05 wt% GnP with 1 wt% of any of the other ILs (IL1 or IL3) containing the cation $[P_{6,6,6,14}]^+$ lead to the best combined capabilities for the hybrid lubricants. Raman confocal microscopy was used to characterize the composition of the worn scar surface. Boundary tribofilms containing PAO32, ILs, carbon and iron oxides were found. These tribofilms act as excellent stress reducer leading to smoother wear tracks and avoiding partially the contact of the rubbing surfaces. Thus, when the load is applied, GnP acts as an efficient stress releaser and slides smoothly due to fragile interlayer bonds [173]. In addition, the protective tribofilms are formed because of the reaction of phosphonium ILs with the contact surface. As conclusion PAO32/IL1/0.05 GnP and PAO32/IL3/0.05 GnP are proposed as potential nanolubricants of PAO32.

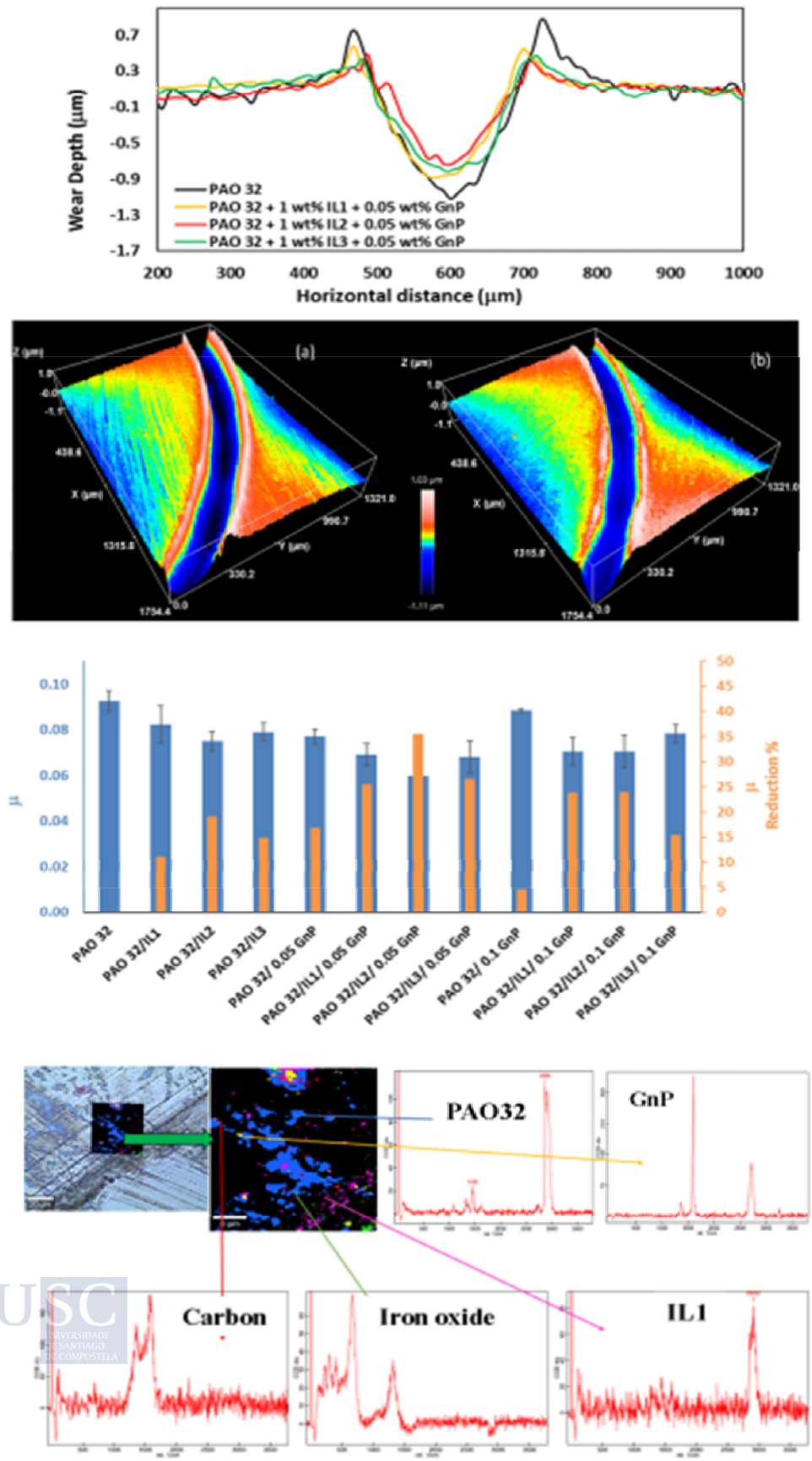

Fig. 3.2. Graphical abstract for article A2

3.4 DOUBLE HYBRID LUBRICANT ADDITIVES CONSISTING OF A PHOSPHONIUM IONIC LIQUID AND GRAPHENE NANOPLATELETS/HEXAGONAL BORON NITRIDE NANOPARTICLES

This article focuses on hybrid (IL/NP) and double hybrid (IL/NP1/NP2) combinations of the ILs and nanomaterials (h-BN and GnP) already used in previous articles A1 and A2 as additives for PAO32. The synergies found among ILs and these NPs on the tribological properties and on the stability led us to look for other ones in IL/NP1/NP2 combinations. Initially and for the purpose of selecting the optimum mass concentration of h-BN and GnP nanomaterials for PAO32, six nanodispersions were prepared based on the combination PAO/a wt% h-BN and PAO/b wt% GnP with a and b being 0.025, 0.05 or 0.1 wt%. Antifriction performance of these nanolubricants was measured with a CSM standard tribometer with ball-on-disc configuration. The test conditions were 20 N normal load, 3400 s duration, 340 m linear distance and room temperature. The obtained values of the coefficients of friction were compared to that obtained with PAO32. Results showed that 0.05 wt% GnP and 0.1 wt% h-BN additions led to best friction reductions among others. Based on these concentrations, a hybrid nanodispersion, PAO/0.05 wt% GnP/0.1 wt% h-BN and three double hybrid nanodispersions, PAO/ILX/0.05 wt% GnP/0.1 wt% h-BN were prepared following the same methods used in A1 and A2. For these nanolubricants, tribological performance, thermophysical properties (density, viscosity and viscosity index) and stability against time were characterized. The stability against sedimentation was analyzed through visual observation taking photographs to track the partial or full sedimentation. The hybrid nanodispersions PAO/IL1/GnP/h-BN and PAO/IL3/GnP/h-BN remained stable at least for 150 days whereas the other two PAO/IL2/GnP/h-BN and PAO/GnP/h-BN showed partial stability at 60 days from the first day of preparation. Thermophysical properties (density and viscosity) at atmospheric pressure from 278.15 K to 373.15 K were evaluated by SVM 3000 rotational Stabinger viscometer for the four prepared nanolubricants. The addition of additives (GnP/h-BN or ILX/GnP/h-BN) led to density increases respect to PAO32 from 0.21 % to 0.46 %, whereas the viscosity increments reached 8.9 %. The nanolubricant PAO/GnP/h-BN shown even better friction performance than PAO/GnP and PAO/h-BN nanolubricants showing the synergy of the hybrid combination of these nanoadditives. Moreover, maximum friction reduction of 40 % was obtained with the double hybrid nanodispersion PAO/IL3/GnP/h-BN. A 3D optical profilometer was used to measure several geometrical parameters of the wear scar at the discs. The double hybrid nanodispersions reduced the maximum wear scar width (WSW) in a range from 5 % to 11 %, the transversal area from 9 % to 18 % and the maximum depth from 13 % to 16 % being the best antiwear performance achieved by PAO/IL2/GnP/h-BN and PAO/IL1/GnP/h-BN. In addition, the roughness values (Ra), measured with 0.08 mm Gaussian filter long wavelength cut-off, and the Raman surface analysis assured the importance of the synergistic effects due to hybrid additives combination. Specifically, Ra of 0.071 μm, 0.058 μm and 0.062 μm were obtained with GnP/h-BN/IL1, GnP/h-BN/IL2 and GnP/h-BN/IL3, respectively, whereas the Ra value obtained when using the neat PAO was 0.151 μm. Hence there are an important improvement in the worn surface roughness when PAO/ILX/GnP/h-BN (X = 1, 2 or 3) is used as lubricant. Nevertheless, it must be indicated that no more anti-wear enhancements were found when h-BN is added to PAO/ILX/GnP nanodispersions. Raman, SEM and roughness analysis revealed that the mechanisms were tribofilm formation and repair effect on worn surfaces due to ILs/NPs combination as well as positive synergies among both nanoadditives and ILs. the layered structure of GnPs provides low shear strength between layers, preventing wear at the contact surfaces and their planar shape avoids that GnPs incise and deform the asperities of the contact surfaces.

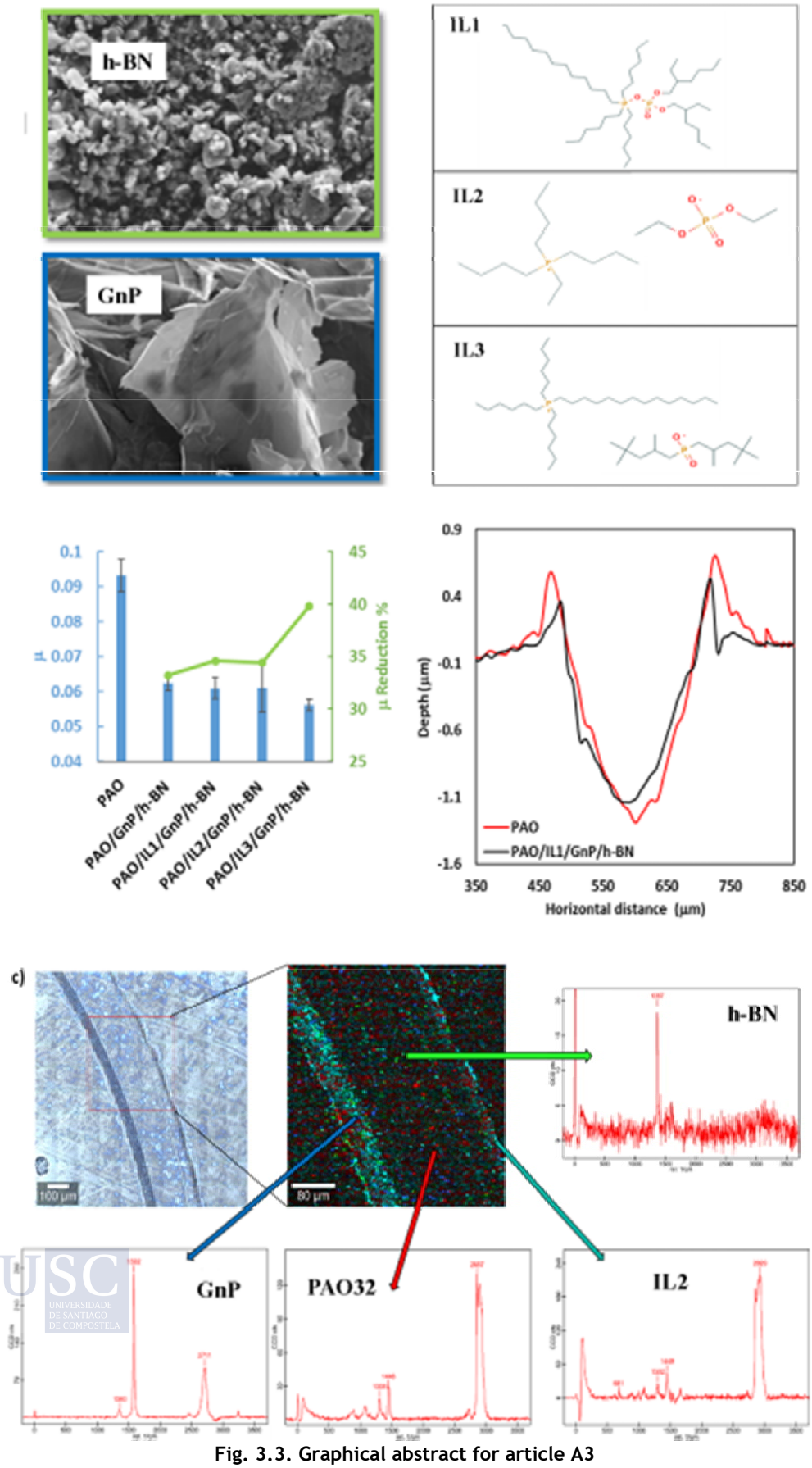

Fig. 3.3. Graphical abstract for article A3

3.5 NANODISPERSIONS OF IRON OXIDE NANOPARTICLES IN POLYALPHAOLEFIN OILS

3.5.1 Introduction

This study presents the synthesis of nanoparticles of iron oxide from waste sludge (tailings) which is always accumulated in iron mining areas. This was the main objective of the project entitled "Nanochemistry Solutions in Technical Lubricants Additive Improvements" (LubriCAD), which aims to use these NPs as lubricant additives [122]. The project focuses on the stability of the proposed nanodispersions. The sludge was collected at the Omarska mine located in Bosnia and Herzegovina which produces iron ore and mainly supplies ArcelorMittal's European subsidiaries [174]. The large amounts of iron normally accumulated at the bottom of artificial lakes can be used in different ways. In the case of LubriCAD, it is proposed to use them in the synthesis of iron oxide nanoparticles for their potential use as additives for lubricants. The synthesis of iron oxide NPs begins with the digestion of the sludge by acids and finishes with the crushing of the nanomaterials (Fig. 3.4.).

The aim of this study is not only to synthesize and use these nanomaterials in lubricants, but also to clean and recycle areas of nature negatively affected by accumulation of mining tailings. Thus, the extraction of iron ores from the sludge of mining deposits leads to better protection of the environment [5]. The synthetized iron oxide NPs were used as antifriction additives of two polyalphaolefin base oils: PAO32 and PAO10. The three mass concentrations of iron oxide NPs were: 0.1, 0.25 or 0.5 wt%. Stability of the six designed nanolubricants was evaluated by means of a Perkin Elmer lambda 25 UV/VIS spectrometer and through visual observation by taking periodic photographs of the nanodispersions.

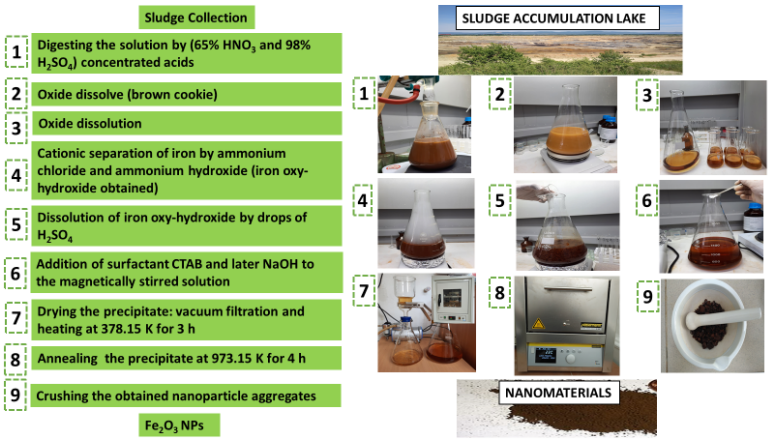

Fig. 3.4. Flow diagram of the followed procedure from the waste sludge collection to the iron oxide synthesis

3.5.2 Process of synthesis of iron oxide nanoparticles

Iron oxide nanoparticles were synthetized using a procedure similar to that of Stević et al. [4]. The process starts by collecting an adequate amount of sludge (around 2 kg of dense mud) from waste mine deposits (lakes). In a given sample of sludge, it is very possible that the iron ore is mixed with some other metals, as well as a significant amount of organic matter, clay, sand, etc. Following on, a digestion process of the collected sludge was used to remove the organic matter from the sample and convert metals that are in the form of compounds into free metals. For this purpose, 500 mL sample of sludge were taken and stored in a 2000 mL Erlenmeyer flask with 100 mL of distilled water. Afterwards, 5 mL of a solution of 65 % nitric acid (HNO_3) and 5 mL of 98 % sulfuric acid (H_2SO_4) were added to the flask, which was placed on top of a magnetic stirrer hot plate. Then, the obtained sample was gradually heated and

manually stirred. 5 mL of the concentrated HNO_3 were added twice, the first after 1 hour and the second after another hour. During this time, the sludge solidified and oxidized, giving rise to a solid brownish dough. The flask was removed from the hot plate and 100 mL of distilled water was added and then left overnight to prolong the acidic extraction of metal ions. The flask was removed from the hot plate and 100 mL of distilled water were added and then left overnight in order to complete the transformation from Fe^{2+} to Fe^{3+}. The next day the sample was filtered first using filter papers only and then by vacuum filtration through double filter paper (Fig. 3.5. a) to remove insoluble materials (such as sand).

After this procedure the separation of iron ions was done by adding ammonium chloride and ammonium hydroxide as a classical cationic separation procedure. A light brown iron oxy-hydroxide floating mass was obtained and again separated from the remaining colorless solution (in which other metal ions had remained).

Iron oxyhydroxide was dissolved by 500 mL of distilled water and 2 mL of concentrated H_2SO_4 resulting in turbid brownish liquid suspension. The flask was placed on the magnetic hot plate for continuous stirring set at 250 rpm and 443.15 K. During gradual heating, concentrated H_2SO_4 was again added drop-by-drop until the solution became transparent, which indicated that the iron ions are completely dissociated. Subsequently, 20 mL of concentrated H_2SO_4 were added until the solution turned from a brownish to dark brownish color to convert all iron ions to the Fe^{3+} form. During this last process 5 g of surfactant cetrimonium bromide (hexadecyltrimethylammonium bromide), CTAB 99 % (hereinafter CTAB) was added to the solution. A 2.5 M sodium hydroxide (NaOH) solution was gradually added to the iron ion solution, until after about 400 mL of 2.5 M NaOH was consumed, and the pH confirmed at constant 14. Some particles were observed first and then in significant quantities showing that the iron oxy-hydroxide nanoparticles were now formed within the surfactant micelles. Later, the solution flask was removed out of the mixer and 5 mL of hexane were added and left for cooling overnight and to let the micelles reorganize themselves. Filtration was performed, sample dried at 378.15 K for 3 hours (Fig. 3.5. b), and then kept at 973.15 K for 4 hours in a muffle furnace (Fig. 3.5. c). Obtained nanoparticles are collected and kept overnight for cooling inside the desiccator. The final product was crushed manually using an agate mortar for 15 minutes in a continuous motion (Fig. 3.5. d) to get the final powder of iron oxide NPs. Two modifications were performed respect the original synthesis procedure [4]. The first change was that a higher amount of CTAB was used and the second one was that the samples were not taken out of the oven immediately after the heat treatment but after two hours relaxation time. Samples were analyzed by means of HRTEM and XRD to confirm the structure and to know the size and the nature of the obtained nanomaterial.

Fig. 3.5. (a) Vacuum pump with sample, (b) Sterilizer SSW100, (c) Muffle Furnace Nabertherm L15/14, and (d) Agate mortar with pestle

Fig. 3.5. shows the vacuum pump used to filter the digested sample (a), the sterilizer SSW100 used to dry the sample after filtration kept at 373.15 K (b), the muffle furnace Nabertherm L15/14 used to heat the sample of the iron oxide NPs at 973.15 K for 4 hours continuously (c) and finally the agate mortar used to crush the sample leading to get the final brown colored fine powder of the iron oxide NPs (d).

3.5.3 Characterization of iron oxides nanoparticles

The morphology and the composition iron oxide NPs in powder form were analyzed using a high-resolution transmission electron microscope (HRTEM, JEOL JEM-2010, Japan), at 200 kV acceleration voltage and an X-ray diffractometer (XRD, Rigaku Ultima IV, Japan) in the 2θ range 0°-90° with Cu-Kα radiation (λ = 1.5418 Å), respectively [4]. Fig. 3.6. (a-d) illustrates HRTEM images of the iron oxide NPs at 5, 10, 20 and 50 nm magnifications, where the structural shape of the NPs is shown. The particles strongly vary in the shapes and morphologies. Most of the NPs have a rounded and laminated structure with sharp edges (Fig. 3.6. a) ranging between 5 and 30 nm in size, but also elongated cylindrical NPs are observed. More detailed images (1-3) at 20, 10 and 5 nm are extracted from Fig. 3.6. a. Thus, it can be said that for sure the micelle shape of the surfactant used in synthesis was playing the role. Namely, due to the increased concentration of CTAB surfactant, first spherical micelles are formed followed by the elongated cylindrical micelles which are defining the shape of several of the NPs obtained in this case. As regards to the second change the two hour relaxation time could have caused also elongation and interaction between the particles when comparing to the samples which are made by sudden annealing as in the previous work of the collaborating laboratory which was used as the reference [175]. In image (3) of Fig. 3.6, with 5 nm scale, laminated striped layers are shown inside a red square, which are considered essential to form reactions on the contact surfaces composed of iron oxides to accelerate the adsorption film and to provide higher wear resistance. This structural shape is an important factor of iron oxide NPs to smoothly interact with the surface to provide better tribological behavior [176,177]. In the previous publication by the collaborative laboratory at University of Banja Luka, more promising results were obtained [175].

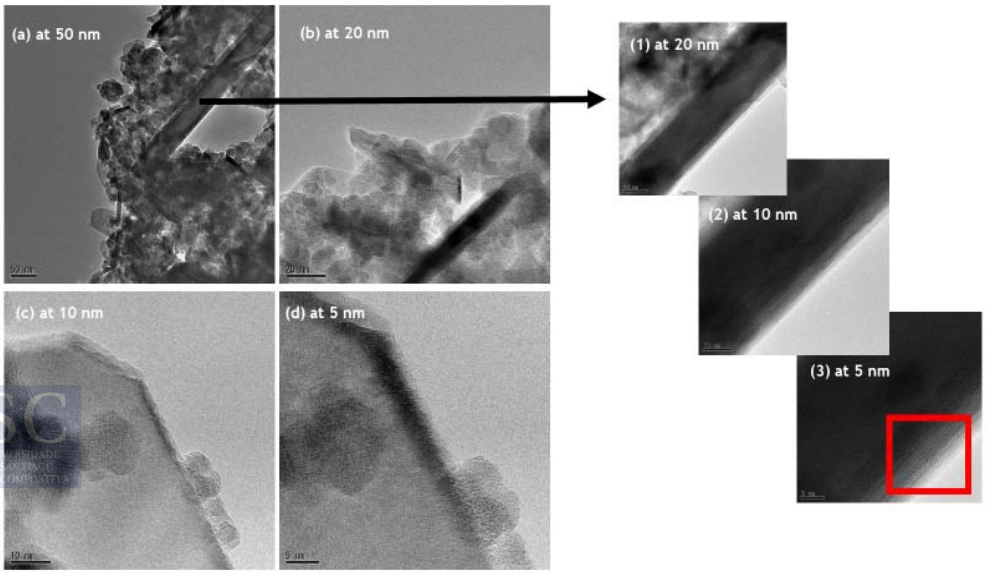

Fig. 3.6. High-resolution transmission electron microscope (HRTEM) images of the iron oxide NPs: (a) at 50 nm, (b) at 20 nm, (c) at 10 nm and (d) at 5 nm

Fig. 3.7 shows HRTEM of both the newly synthesized iron oxide NPs (NIO-A) in this study and the previously synthesized (NIO-C) by Stević, et al. [4]. The NIO-C particles were of pronounced crystallinity and more regular rectangular shape, whereas NIO-A shows more dominant amorphous phase than the crystalline one as can be seen from this figure. This was also confirmed by comparison of the XRD data presented here and the one from the literature.

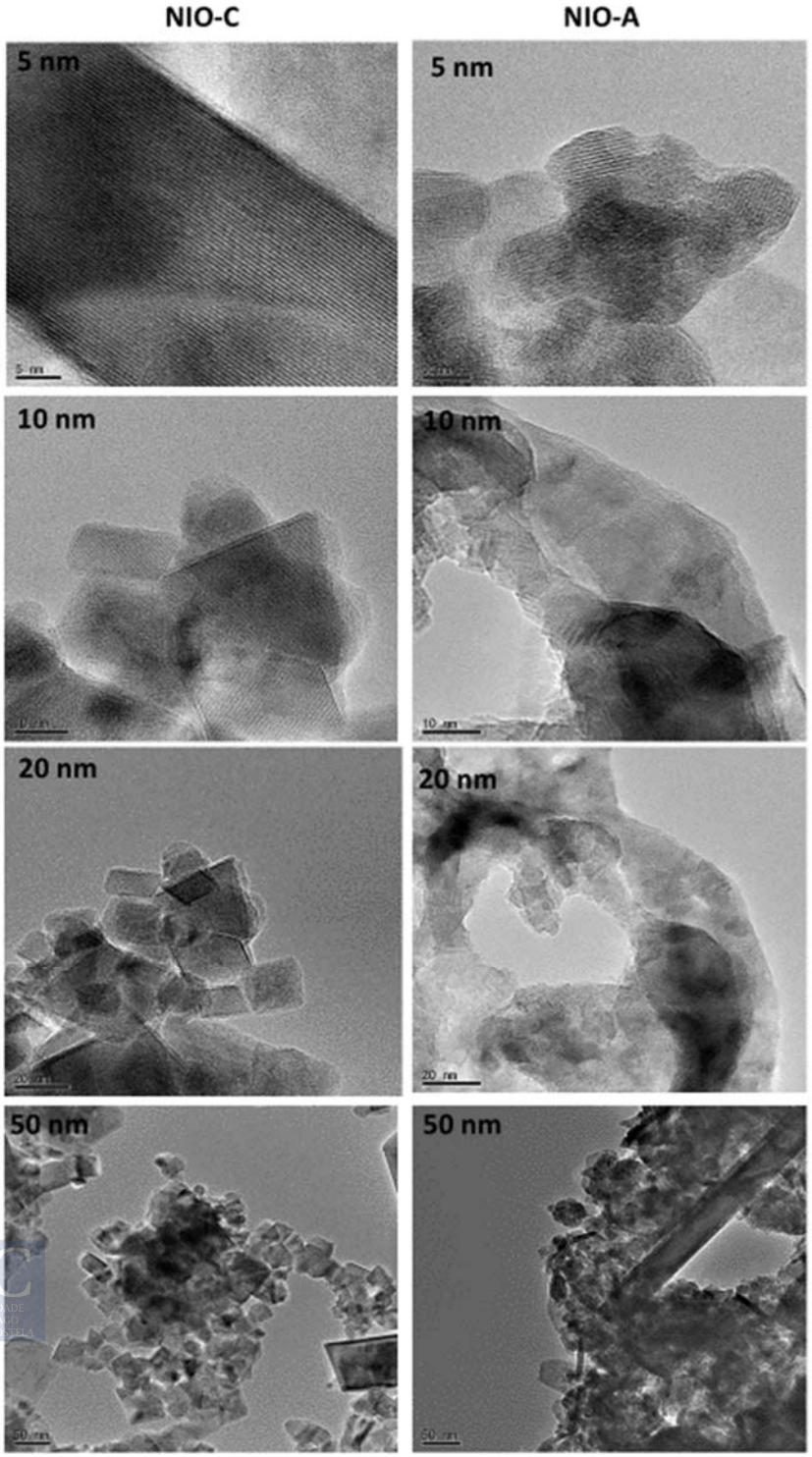

Fig. 3.7. Comparison of HRTEM images for the NIO-A and NIO-C [4] samples at different magnifications

Fig. 3.8 shows the X-ray powder diffractogram (XRD) for the synthesized iron oxide NPs. The results show the appearance of both hematite (Fe_2O_3) and magnetite (Fe_3O_4) [178,179] in the synthesized NPs structure. Dashed lines and circles show the coincidence of the iron oxide NPs peaks with the peaks of both oxides and Na_2SO_4. It seems that Fe_2O_3 iron oxide forms are predominant. In this sense, the NPs tend to be predominantly amorphous Fe_2O_3, so these nanomaterials tend to be immiscible in liquids and, consequently, are not able to promote the formation of crystalline phase [180], to penetrate the contact surface to improve the tribological properties and function as both antifriction and antiwear minimizers [181]. This result shows the importance of the morphology of iron oxide particles for their tribological application.

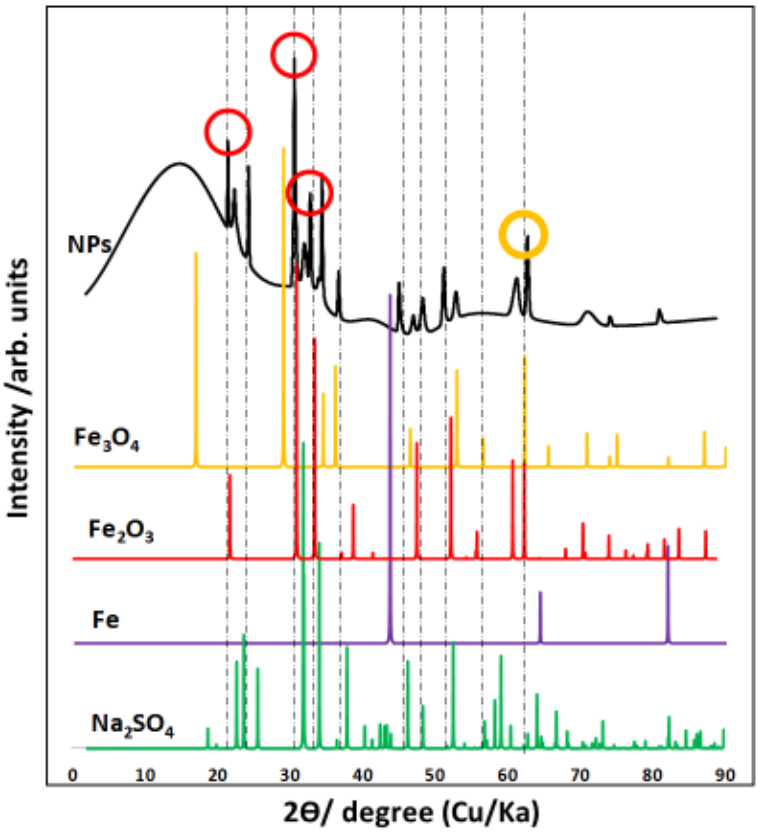

Fig. 3.8. X-ray powder diffractogram (XRD) for the iron oxide NPs with their corresponding peaks in comparison with Fe, Fe_2O_3, Fe_3O_4 and Na_2SO_4 structures

3.5.4 Samples preparation and stability behavior

Once obtained the iron oxide NPs, six nanodispersions were prepared: PAO32/aNPs and PAO10/aNPs being a 0.1, 0.25 or 0.5 wt%. All the dispersions were prepared using the two-step method. A Kern ABJ 220-4NM analytical balance was used to weight the base oils and the NPs. The nanodispersions were sonicated by an ultrasonic bath UW 32 at 38 kHz for 4 hours. The stability of the nanodispersions was detected by two ways: visual observation by taking photographs, and absorbance measurements using a Perkin Elmer lambda 25 UV/VIS spectrometer. All dispersions were tracked for 15 days. Fig. 3.9 and 3.10 show the photographs of the nanodispersions from the day of preparation to 15 days later of both PAO32/aNPs and PAO10/aNPs. The results showed that all the nanodispersions showed sedimentation in the first week of preparation.

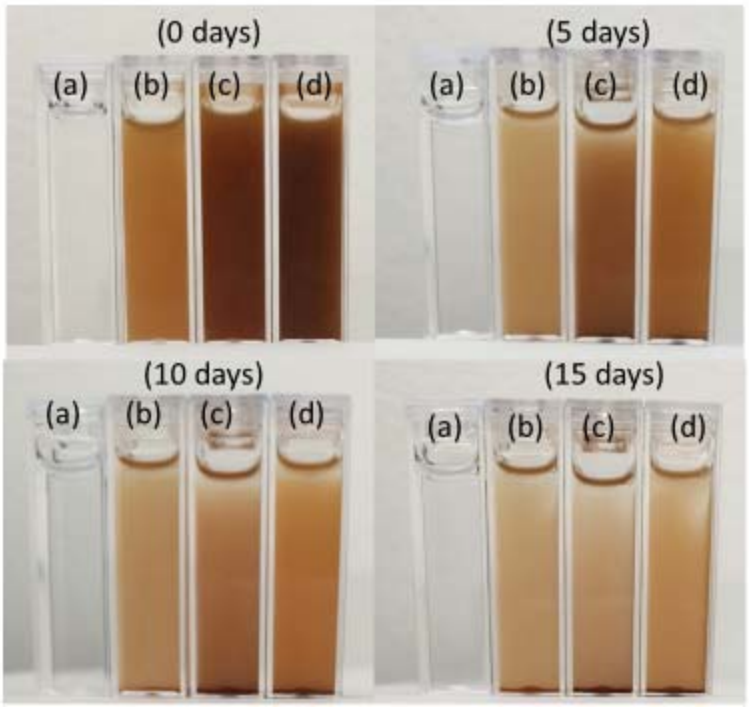

Fig. 3.9. Photographs of the PAO32 nanodispersions during two weeks of tracking: (a) Neat PAO32, (b) PAO32 + 0.1 wt% iron oxide NPs, (c) PAO32 + 0.25 wt% iron oxide NPs and (d) PAO32 + 0.5 wt% iron oxide NPs

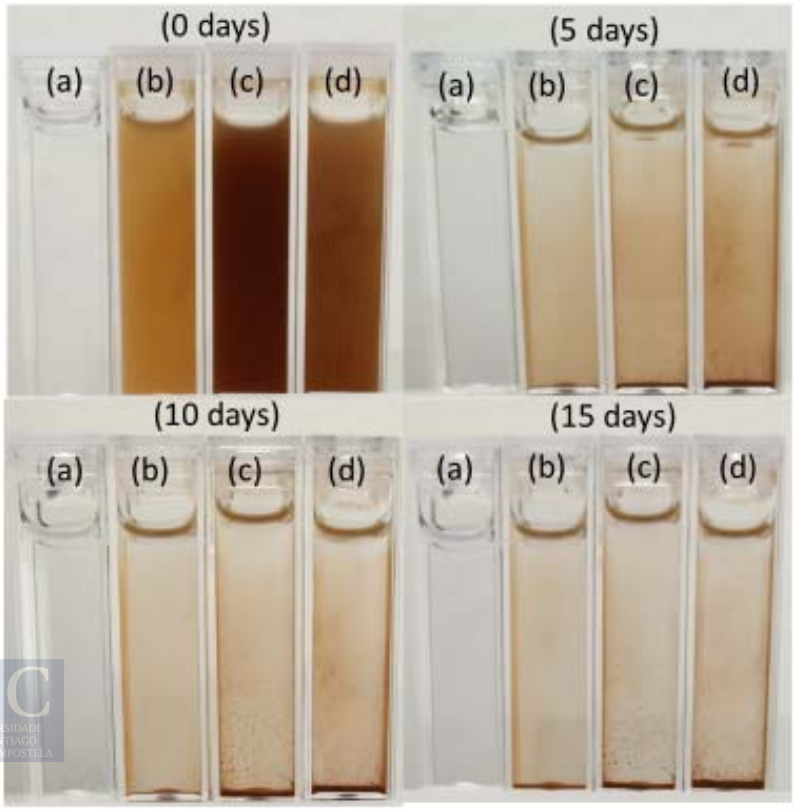

Fig. 3.10. Photographs of the PAO 10 nanodispersions during two weeks of tracking: (a) Neat PAO10, (b) PAO10 + 0.1 wt% iron oxide NPs, (c) PAO10 + 0.25 wt% iron oxide NPs and (d) PAO10 + 0.5 wt% iron oxide NPs

Fig. 3.11 shows the data collected by a Perkin Elmer lambda 25 UV/VIS spectrometer during the tracking stage of the nanodispersions at a wavelength of 622 nm. The UV/VIS measurements showed that all the samples tend to precipitate from the first day of preparation, being partial sedimentation in the first week and full sedimentation after two weeks.

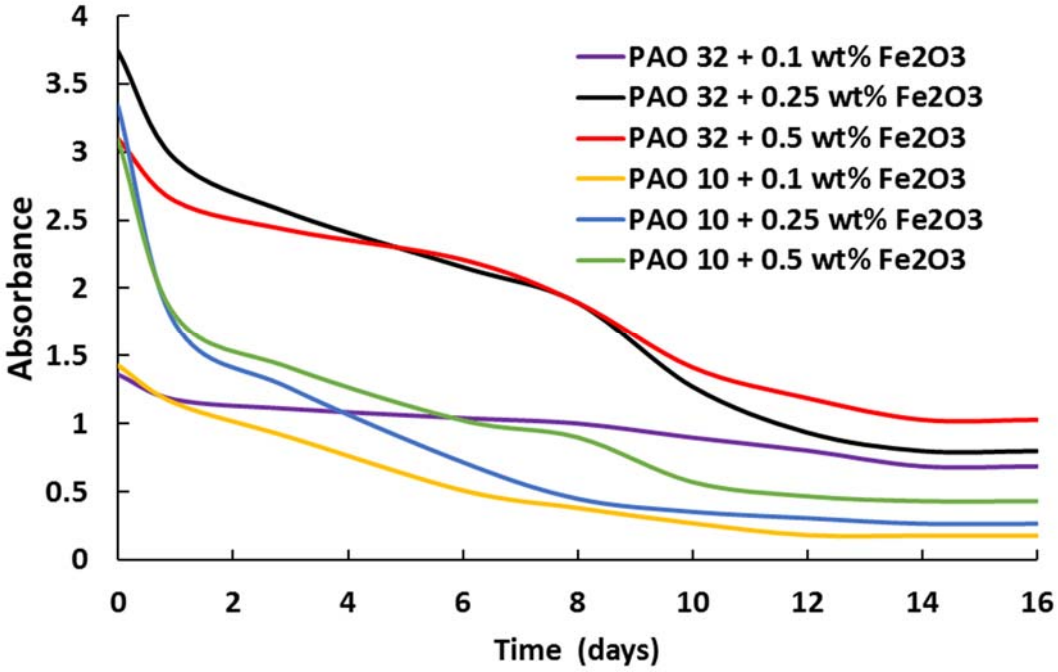

Fig. 3.11. Temporal evolution of the absorbance of the samples at 622 nm wavelength

3.5.5 Conclusions

Iron oxide NPs were synthesized from the sludge collected in the waste lake of Omarska mine located in Bosnia and Herzegovina, that produces iron ore to supply ArcelorMittal's European subsidiaries. The synthesized NPs were used as nanoadditives for two polyalphaolefin oils, PAO32 and PAO10, supplied by Tehnosint. This fundamental study aims to show the suspension ability of these synthesized iron oxide NPs in PAO32 and PAO10. The results showed that the addition of such NPs revealed poor stability in both polyalphaolefin base oils. For instance, and by visual observation, clear sedimentation of iron oxide NPs in PAO32 and PAO10 was observed after 5 days of preparation. More detailed results were illustrated by UV/VIS absorbance measurements along time being the sedimentation detected from the first day of preparation. According to the preliminary results, the synthesized iron oxide NPs are not considered very attractive to be used as additives to PAO32 and PAO10, but further trials may be suggested such as mass concentration selection, or addition of ionic liquids.

4 GENERAL DISCUSSION

The main goal of this Doctoral Thesis is to study the tribological performance of potential lubricants with nanoadditives aimed for application in renewable energy technologies, such as in wind turbine gearboxes. The use of nanoadditives in lubricants implies a challenge that must be considered in order to achieve homogeneous dispersions of nanoadditives in the base oil and to guarantee their temporary stability. Thus, small quantities of ionic liquids have also been incorporated into the dispersions with the intention of minimizing the level of aggregation of nanoadditives and improving the nanodispersion stability along time. The selection of the materials used in this study was introduced in Chapter 2, section 2.1. Briefly, polyalphaolefin 32 (PAO32, the most widely used PAO in wind turbine gearboxes systems) was selected as the main base oil, whereas hexagonal boron nitride (h-BN) nanoparticles (NPs) and/or graphene nanoplatelets (GnPs) were used as nanomaterials. These two 2D nanomaterials are promising as antifriction and antiwear additives. Finally, trihexyltetradecylphosphonium bis(2-ethylhexyl)phosphate (IL1), tributylethylphosphonium diethylphosphate (IL2) and trihexyltetradecylphosphonium bis(2,4,4-trimethylpentyl)phosphinate (IL3) were the phosphonium based ionic liquids used as dispersants because they show better miscibility and excellent tribological performance as additives of current lubricants than other ILs. In addition, PAO32 and PAO10, supplied by Tehnosint company from Bosnia and Herzegovina, were also used as base oils for a stability study with iron oxide NPs as additives. These iron oxide NPs were synthesized from the sludge of Omarska mine located in Bosnia and Herzegovina, as the primary raw material. In this chapter a general discussion of the results included in Chapter 3 is presented. This includes the characterization of the selected materials (ILs and PAO32), the corrosion tests performed with the three selected ILs, the synthesis and characterization of iron oxide NPs, the preparation of the mixtures and nanodispersions, the stability tracking of the prepared samples, the thermophysical properties measurements, and the tribological investigation conducted with the prepared samples.

4.1 MATERIALS AND CHARACTERIZATION

After selection of the materials, a detailed characterization for PAO32 and the ILs was done by FTIR and Raman. FTIR technique was previously described (Chapter 2, section 2.2.1) and the spectra are reported in publication A1 (Figures 1 and 2). PAO32 FTIR spectrum showed several bands and peaks, a band corresponding to C-H stretching vibrations of the aliphatic carbon chain of intense peaks at 2852 and 2920 cm^{-1}, other band of two peaks at 1377 and 1462 cm^{-1}, corresponding to C-H deformation of the aliphatic group $–CH_3$ [155,182] and a vibration peak at 721 cm^{-1} attributable to in-plane bending or rocking of the methylene groups ($–CH_2–$) [183,184]. Besides, and due to the presence of alkyl chains, FTIR bands of PAO32 also existed in the FTIR spectra of the three ILs. In addition, in the three ILs spectra a peak corresponding to the anion P=O bond stretch is presented between 1229 and 1249 cm^{-1}, and for IL3 an additional strong peak also characteristic of a P=O bond stretch is observed at 1170 cm^{-1} [172,185].

A confocal Raman microscope (Chapter 2, section 2.2.3) was used to generate the Raman spectra of PAO32, IL1, IL2 and IL3. Several bands were detected showing peaks attributable to: C-H stretching (at 857 and 2908, 2909 and 2930 cm^{-1}), $\delta(CH_2)$ (at 1310, 1314 and 1322

cm^{-1}) and δ(CH_3) vibrations (at 451, 1456 and 1457 cm^{-1}). Aliphatic chain vibrations ν(CC) were found at 894, 899, 1082, 1086, 1089 and 1094 cm^{-1} [186,187]. Results are presented in publication A1, Figures S1 and S2.

Two of the three nanomaterials used in this study (h-BN and GnP) were previously characterized by Liñeira del Río et al.[101] and Guimarey et al.[155] (Chapter 2, section 2.1). The characterization showed that GnPs have a bended and wrinkled appearance, being a multilayer GnPs type, whereas a disc-like shaped morphology was revealed for h-BN. In addition, iron oxide nanoparticles were synthetized from the sludge of a mine, being the procedure of this synthesis explained in chapter 3 section 3.5. Briefly, digestion, dissolving, filtration, drying, baking and crushing were the steps followed to obtain the iron oxide NPs. The HRTEM images of these NPs show that their size ranges between 5 and 30 nm, being most of the NPs rounded and with laminated structure whereas some of them are elongated and cylindrical. XRD revealed the majority presence of Fe_2O_3 in the sample as well as Fe_3O_4 to a lesser extent. From here on, the iron oxide NPs will be called as Fe_2O_3 (major component).

4.2 SELECTION AND PREPARATION OF THE NANOLUBRICANTS

The first step was to select the nanoadditive composition that optimizes the antifriction capability of the nanolubricants. For this task six nanodispersions (PAO32/NPs) were prepared using the two-step method and are presented in Table 4.1. In this table, the nanodispersions based on h-BN NPs or GnP for which the friction coefficient (COF) was minimal are marked in bold.

The reductions of the COFs of these nanodispersions in respect to the COF of neat PAO32 are presented in Fig. 4.1. As can be observed, the optimum concentration when h-BN was used as nanoadditive in PAO32 was 0.1 wt%, leading to a 26 % friction reduction, whereas the optimum composition was 0.05 wt% when using GnP being the reduction of COF 17 %. Thus, these compositions were selected to be added to the base oil to subsequently prepare the hybrid nanolubricants.

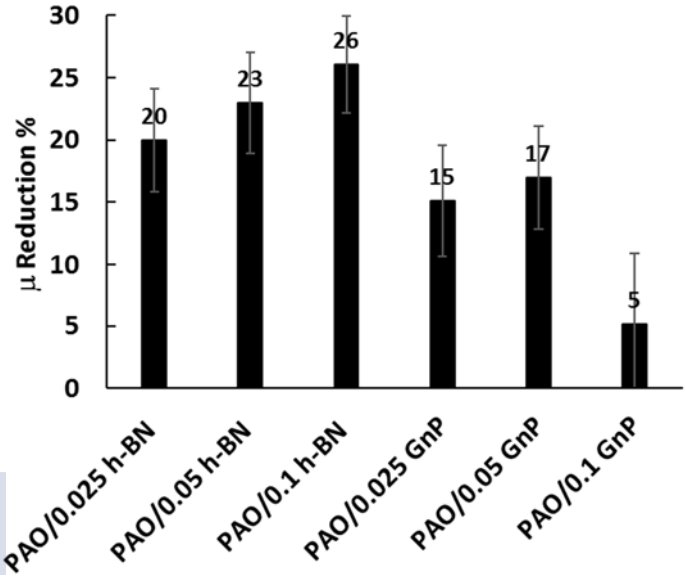

Fig. 4.1 Average friction coefficient (μ) reduction obtained with nanodispersions of different concentrations of h-BN or GnP compared to that obtained with PAO32 at room temperature

Table 4.1. Preliminary h-BN or GnP nanodispersions

Nanodispersions	*Publication*
PAO32/0.025 wt% h-BN	A3
PAO32/0.05 wt% h-BN	A3
PAO32/0.1 wt% h-BN	A1 and A3
PAO32/0.025 wt% GnP	A3
PAO32/0.05 wt% GnP	A2
PAO32/0.1 wt% GnP	A2

Table 4.2 The prepared mixtures and nanodispersions together with the articles in which results are reported

Lubricant	*Samples*	*Publication*
Mixtures	PAO32/1 wt% IL1	A1 and A2
	PAO32/1 wt% IL2	A1 and A2
	PAO32/1 wt% IL3	A1 and A2
Nanodispersions	PAO32/0.1 wt% h-BN	A1 and A3
	PAO32/0.05 wt% GnP	A2
	PAO32/0.1 wt% Fe_2O_3	Unpublished
	PAO32/0.25 wt% Fe_2O_3	Unpublished
	PAO32/0.5 wt% Fe_2O_3	Unpublished
	PAO10/0.1 wt% Fe_2O_3	Unpublished
	PAO10/0.25 wt% Fe_2O_3	Unpublished
	PAO10/0.5 wt% Fe_2O_3	Unpublished
Hybrid Nanodispersions	PAO32/0.1 wt% h-BN/0.05 wt% GnP	A3
	PAO32/0.1 wt% h-BN/1 wt% IL1	A1
	PAO32/0.1 wt% h-BN/1 wt% IL2	A1
	PAO32/0.1 wt% h-BN/1 wt% IL3	A1
	PAO32/0.05 wt% GnP/1 wt% IL1	A2
	PAO32/0.05 wt% GnP/1 wt% IL2	A2
	PAO32/0.05 wt% GnP/1 wt% IL3	A2
	PAO32/0.1 wt% GnP/1 wt% IL1	A2
	PAO32/0.1 wt% GnP/1 wt% IL2	A2
	PAO32/0.1 wt% GnP/1 wt% IL3	A2
Double Hybrid Nanodispersions	PAO32/0.1 wt% h-BN/0.05 wt% GnP/1 wt% IL1	A3
	PAO32/0.1 wt% h-BN/0.05 wt% GnP/1 wt% IL2	A3
	PAO32/0.1 wt% h-BN/0.05 wt% GnP/1 wt% IL3	A3

The following step was to evaluate the miscibility of the three ILs in PAO32. Based on previous results [21,22,138]. The mixture composition 1 wt% of IL in PAO32 was selected for the three mixtures. After that, hybrid nanodispersions PAO/NP1/NP2 and PAO/NPs/ILs and double hybrid nanodispersions PAO/NPs/NPs/ILs were prepared using different methods depending on the nature of the final nanolubricant. Detailed information on the preparation methods can be found in the publications A1-A3 and in Chapter 2, section 2.3. In all the cases, two sets of samples were prepared, one set was kept stationary at room temperature for visual stability analyses and image tracking, and the other one was used for thermophysical and tribological

studies. In case of nanodispersions that are based on Fe_2O_3 NPs, one set was prepared (PAO/NPs) and used for visual tracking and UV spectrum for stability analyses (Chapter 3, section 3.5). Table 4.2 shows all the prepared samples with their different concentrations and presentation in the related publications.

4.3 MISCIBILITY OF IL MIXTURES AND STABILITY OF NANOLUBRICANTS

As indicated for the GnP and h-BN nanodispersions, one of the sets of the prepared samples was kept undisturbed to analyze the temporal stability of these samples. This task was carried out through their visual observation and documented by taking pictures in defined time intervals. Photographs are valuable to show partial and/or complete sedimentation of nanolubricants or signs of immiscibility in case of the mixtures. It should be noted that the photos were stopped 240 days after samples preparation (or 150 days in the case of the double hybrid nanodispersions). That is why when it is indicated that the stability is 240 days (or 150 days), it should be clearly understood that it is greater than this period. Table 4.3 and Fig. 4.2 show all the samples and their corresponding stability time in days. In addition, it must be noted that no signs of immiscibility were observed for none of the three mixtures PAO/IL even two years after their preparation.

Table 4.3. Miscibility of the mixtures and time stability of the designed nanolubricants

Mixture	*Miscibility*
PAO32/1 wt% IL1	Miscible
PAO32/1 wt% IL2	Miscible
PAO32/1 wt% IL3	Miscible
Nanolubricant	*Stability Time (days)*
PAO32/0.1 wt% h-BN	30-60
PAO32/0.05 wt% GnP	> 240
PAO32/0.1 wt% GnP	> 240
PAO32/0.1 wt% Fe_2O_3	< 5
PAO32/0.25 wt% Fe_2O_3	< 5
PAO32/0.5 wt% Fe_2O_3	< 5
PAO10/0.1 wt% Fe_2O_3	< 5
PAO10/0.25 wt% Fe_2O_3	< 5
PAO10/0.5 wt% Fe_2O_3	< 5
PAO32/0.1 wt% h-BN/1 wt% IL1	Up to 150
PAO32/0.1 wt% h-BN/1 wt% IL2	Between 60 and 90
PAO32/0.1 wt% h-BN/1 wt% IL3	Up to 150
PAO32/0.05 wt% GnP/1 wt% IL1	> 240
PAO32/0.05 wt% GnP/1 wt% IL2	Up to 150
PAO32/0.05 wt% GnP/1 wt% IL3	> 240
PAO32/0.1 wt% GnP/1 wt% IL1	> 240
PAO32/0.1 wt% GnP/1 wt% IL2	Up to 60

PAO32/0.1 wt% GnP/1 wt% IL3	> 240
PAO32/0.1 wt% h-BN/0.05 wt% GnP	Up to 60
PAO32/0.1 wt% h-BN/0.05 wt% GnP/1 wt% IL1	> 150
PAO32/0.1 wt% h-BN/0.05 wt% GnP/1 wt% IL2	Up to 60
PAO32/0.1 wt% h-BN/0.05 wt% GnP/1 wt% IL3	> 150

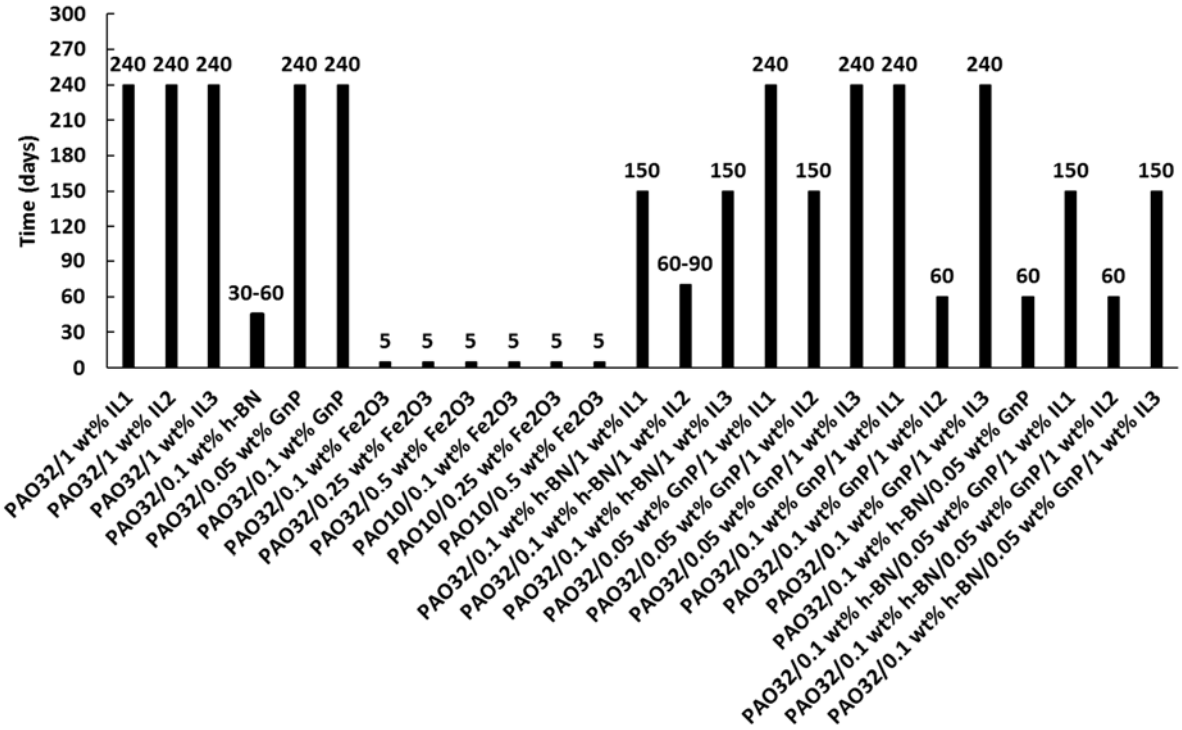

Fig. 4.2. Miscibility of the mixtures and stability of the PAO32 and PAO10 nanolubricants along time (days)

Regarding the h-BN or GnP nanolubricants, the addition of ILs to the samples elongated the stability time of the nanodispersions, in general. The photos showed that nanolubricants containing IL1 or IL3, both with the same cation $[P_{6,6,6,14}]^+$, showed longer time stabilities than those containing IL2. This fact could indicate a positive effect on the stability of ILs that contain cations with longer alkyl chains as IL1, $[P_{6,6,6,14}][DEHP]$, and IL3, $[P_{6,6,6,14}][(iC8)_2PO_2]$.

As regards to the nanodispersions based on PAO32 and PAO10 with iron oxide NPs as additives, photographs and UV spectra indicated partial sedimentation at the fifth day and total sedimentation in two weeks (chapter 3, section 3.5.3). So, no additional experimental studies were performed with these nanodispersions.

4.4 THERMOPHYSICAL PROPERTIES

As mentioned before, a second set of h-BN or GnP dispersions was prepared and used to evaluate the thermophysical properties of the nanolubricants as well as to characterize their tribological behavior. PAO32 and the IL mixtures were also thermophysically and tribologically characterized. Thermophysical properties (dynamic viscosity, density and viscosity index) were measured using an SVM 3000 rotational Stabinger viscometer from Anton Paar in the temperature range from 278.15 to 373.15 K with an interval 5 K as detailed in Chapter 2 section 2.5. In Fig. 4.3 the average relative density ($\Delta\rho/\rho$) change in the full

temperature range for each sample respect to density of PAO32 is shown. In general, as can be observed, the addition of additives to the base oil, either ILs, nanoadditives or both, increases both thermophysical properties, corresponding the highest increments to those containing double hybrid additives. In particular, the highest change in $\Delta\rho/\rho$ was obtained with the double hybrid combination PAO32/0.1 wt% h-BN/0.05 wt% GnP/1 wt% IL2, being 0.460 %, and the lowest one was achieved for the nanodispersion PAO32/0.05 wt% GnP, being 0.053 %.

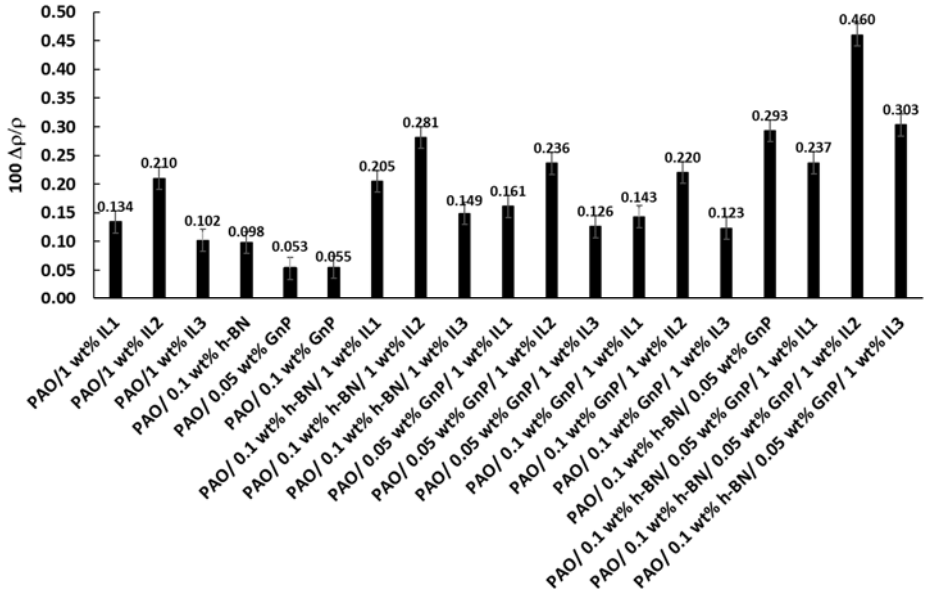

Fig. 4.3. Average relative density change, 100 $\Delta\rho/\rho$, of the PAO32 samples respect to density of PAO32 in the temperature range from 278.15 K to 373.15 K

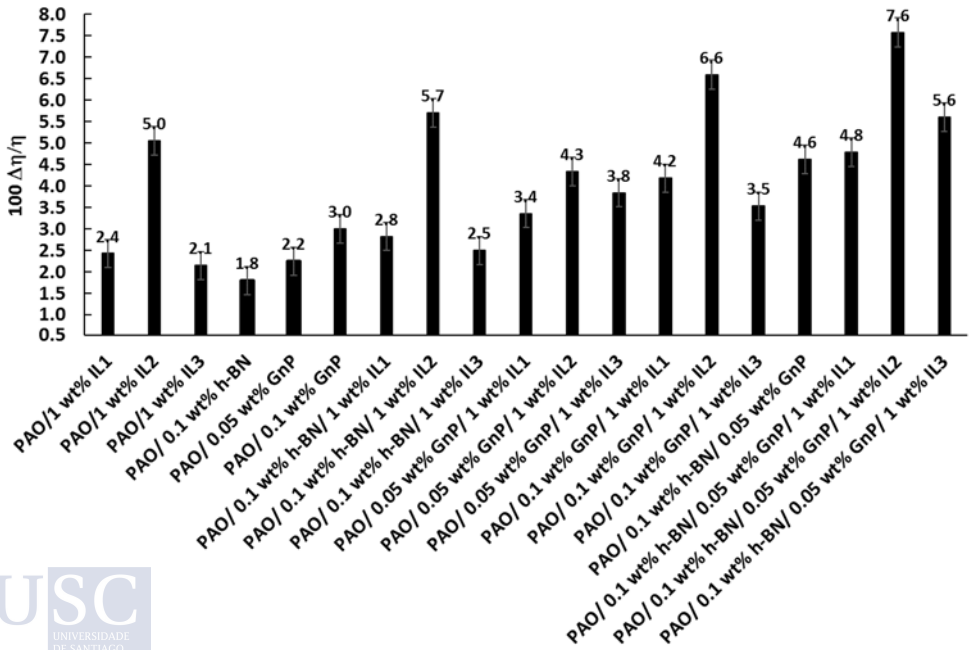

Fig. 4.4. Average relative viscosity change, 100 $\Delta\eta/\eta$, of the samples respect to viscosity of PAO32 in the temperature range from 278.15 K to 373.15 K

The average relative increase in viscosity ($\Delta\eta/\eta$) over the whole temperature range is shown in Fig. 4.4. As can be observed, the highest increase corresponds to the double hybrid

combination PAO/h-BN/GnP/IL2 (7.579 %) and the lowest change to the nanodispersion PAO/0.1 wt% h-BN, being 1.795 %. In addition, the viscosity index (VI) of several nanolubricants was measured using the same device and according to ASTM D227. The VI of the samples shows small variations, ranging from -1.7 % to 0.53 %. This lubricant parameter is very important, because it quantifies the viscosity changes due to temperature variation. The higher the VI value, the lower the viscosity temperature dependence.

4.5 IONIC LIQUIDS: CORROSION TESTS

As it was indicated in Chapter 2, section 2.1, the two tribological pairs (ball-on-disc and ball-on-pins) used to perform the tribological tests were steel/steel. Specifically, the four different specimens (the two balls, the pin and the disc) were made of AISI 52100 steel.

Previously to the lubricant tribological characterization, and due to the nature of the ILs, corrosion tests on unused discs were carried out with the three ILs. The procedure was explained in Chapter 2, section 2.7. Thus, two types of tests were conducted, one at room temperature and a second one at high temperature (373.15 K). The first type of test consisted of depositing three drops of the corresponding IL on a mirror-polished disc (Ra=0.0076 μm), placing the discs inside covered Petri dishes for 35 days under room conditions. During this time, the appearance of the plates was visually observed daily. Although no corrosion signs were detected when applying IL1 or IL3 (as shown in publication A1, section 3.3), a rapid corrosion on the surface of the steel disc was noticed with IL2 24 hours after its deposition on the surface of the disc.

After these 35 days, the ILs were collected to be analyzed, and the discs were cleaned to assess their roughness. From these last tests it was concluded that the roughness of the discs tested with IL1 and IL3 hardly changes after the test with respect to the roughness of an unused disc, whereas the roughness of the disc tested with IL2 increases strongly as shown in Fig. 4.5. With the collected IL samples, FTIR analyses were carried out, which indicate the presence of water, especially in the case of IL2.

Afterwards, a second type of tests was designed to evaluate if humidity could influence the appearance of corrosion. This new set of tests are very similar to the first type, but in this case the Petri dishes were located inside a chamber at 373.15 K for 24 hours. After this time, the appearance of the discs did not change, but the FTIR spectra showed the presence of peaks corresponding to water, which indicates that in contact with air, the three ILs are quickly hydrated. Finally, it was noticed that IL2 could be an enhancer of corrosion which is an unfavorable property. Added to the fact that the nanolubricants containing IL2 have shown the lowest stability time, its usage as friction and wear enhancer is less attractive than IL1 or IL3.

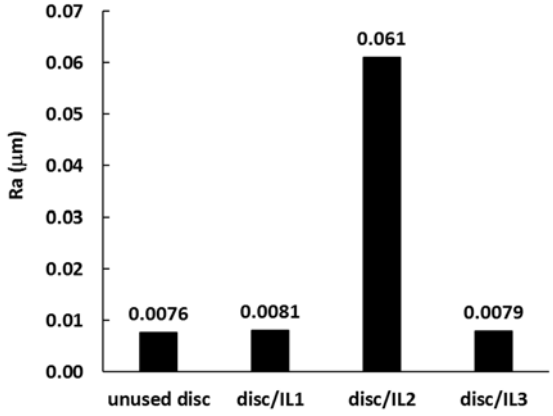

Fig. 4.5. Roughness values (Ra) of the surfaces for unused disc and discs wet with different ILs obtained with a Gaussian filter of 0.08 mm

4.6 TRIBOLOGICAL STUDIES

Finally, tribological analyses were carried out with the nanolubricants to investigate their behavior in terms of antifriction and antiwear capabilities in comparison to the neat oil PAO32. The measurements were carried out with a MCR 302 rheometer from Anton Paar provided with a tribology cell (Tribo-cell T-PTD200) (Chapter 2, section 2.6.2) at two different temperatures, 298.15 K and 353.15 K, and with a CSM standard tribometer (Chapter 2, section 2.6.1) only at ambient temperature. Basically, all the prepared samples improved the tribological behavior when compared to neat PAO32, especially those formed of hybrid additives combinations.

The antifriction capability of each lubricant was evaluated by measuring the average coefficient of friction (COF) between a steel to steel (AISI 52100/AISI 52100) contact pair. After each test, a wear track (also called as groove or wear scar) is formed on the disc. Thus, different wear parameters were evaluated from the topography of these tracks: the wear scar diameter (WSD), wear scar width (WSW), cross-section area (A), wear volume (V), maximum wear depth (D) and the surface roughness (Ra). All tribological measurements were performed three times (three replicates), and the different tribological parameters are reported as the mean value together with its standard deviation. Additionally, SEM images (Chapter 2, section 2.2.2) of the discs and pins surfaces were taken to evaluate the wear mechanisms. Finally, Raman analysis (Chapter 2, section 2.2.3) on the worn surfaces was done, aiming to reveal the mapping distribution of the materials sticking on the rubbed surfaces. The following sections describe three scenarios according with the different published articles (A1, A2 and A3). In the first one, (article A1), h-BN NPs were selected as nanoadditives and the three ILs as separate dispersants. An Anton Paar MCR 302 rheometer fitted with a T-PTD200 tribology cell operating with a ball on three pins configuration was used. The concentration of h-BN NPs in the PAO32 nanodispersions was selected based on results from the literature [109], in addition to our own results.

In this first scenario, two temperatures were selected for the measurements, 298.15 K and 353.15 K. In the second scenario, the nanoadditives selected were GnP at two different concentrations (0.05 wt% and 0.1 wt%), and the same ILs tested as dispersants, as in the previous scenario. Finally, in scenario three, the results of using both h-BN and GnP and the three ILs as hybrid additives was analyzed. In the second and third scenarios, measurements were carried out at room temperature with the aid of a CSM tribometer. After completing the tribological tests corresponding to scenario 1, the equipment broke down, delaying the repair process for a long time due to its high cost. That is why the tribometer used in scenarios two and three was not the same.

4.6.1 Scenario one:

In this scenario a case study using h-BN and the three ILs as additives into PAO32 was performed. The results of this study were reported in publication A1. Three PAO32/IL mixtures and four PAO32 nanodispersions (Table 4.2) were prepared to study the influence on the tribological behavior of h-BN and ILs separately or combined as additives to PAO32.

Tests were performed at two different temperature maintaining the other setup conditions the same (Chapter 2, section 2.6.2). The temperatures, 298.15 K and 353.15 K, were selected based on the real application where PAO32 is used as lubricant base oil: wind turbines gearboxes. Their operation temperatures do not usually exceed 353.15 K but peaks up to this temperature are reached. In addition, the minimum temperature of the oil required for starting up a wind turbine for normal operation must be higher than 300 K [188,189]. Table 4.4 and Fig. 4.6 show the reductions of the COFs obtained with the different mixtures and nanodispersions.

As it can be observed, the highest reductions at both temperatures correspond to the results obtained using as lubricant PAO32/1 wt% IL2/0.1 wt% h-BN, being 17 % at 298.15 K and 28 % at 353.15 K. The second nanolubricant with best antifriction improvements was PAO32/1 wt% IL1/0.1 wt% h-BN, which resulted in reductions of 10 % at 298.15 K and 13 % at 353.15 K. It must be noted that the COF at high temperature is strongly dependent on the nanolubricant (publication A1, Figure 8b) while at low temperature the fluctuations of COF are small (publication A1, Figure 8a).

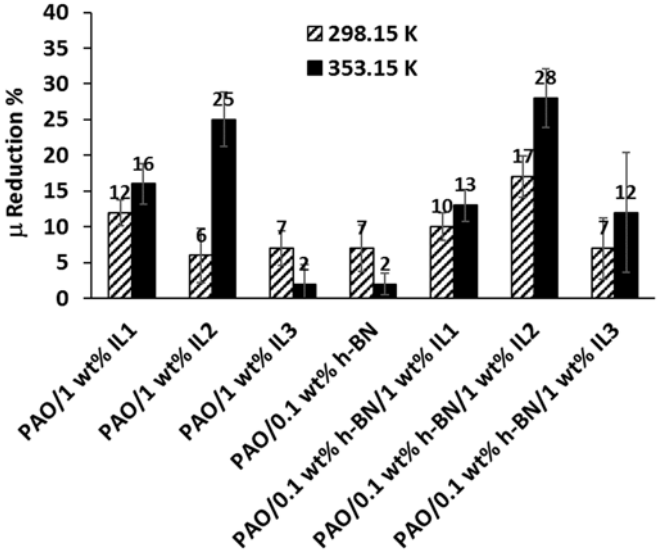

Fig. 4.6. Friction coefficient (μ) reduction for several lubricants compared with that obtained with PAO32 at T = 298.15 K (pattern fill) and at T = 353.15 K (solid fill)

Table 4.4. Tribological reduction results of the designed mixtures and PAO32 nanolubricants at 298.15 K and 353.15 K respect to those of PAO32

Mixture	*% Friction reduction at 298.15 K*	*% Friction reduction at 353.15 K*	*% Wear reduction (WSD) at 353.15 K*	*% Roughness reduction (Ra) at 353.15 K*
PAO/1 wt% IL1	12	16	50	0
PAO/1 wt% IL2	6	25	48	5
PAO/1 wt% IL3	7	2	22	13
Nanolubricant				
PAO/0.1 wt% h-BN	7	2	5	-25
PAO/0.1 wt% h-BN/1 wt% IL1	10	13	65	55
PAO/0.1 wt% h-BN/1 wt% IL2	17	28	35	75
PAO/0.1 wt% h-BN/1 wt% IL3	7	12	37	38

Next, the antiwear capacity of the designed lubricants was analyzed by using a 3D optical profiler Sensofar S neox (Chapter 2, section 2.6.3). For the discs tested at 298.15 K, the wear tracks were hardly noticeable. Therefore, the measurements of the different wear parameters would be affected by a very large uncertainty, so wear was not analyzed. The mean wear parameters extracted from the wear tracks obtained at 353.15 K, together with their corresponding uncertainties, as well as the average surface roughness values were reported in

publication A1. As can be observed in Fig. 4.7, the hybrid nanolubricant PAO32/1 wt% IL1/0.1 wt% h-BN showed the best antiwear behavior being the reduction 65 % whereas only 5 % was achieved with the nanodispersion PAO32/1 wt% h-BN. Average roughness values (Ra) reductions respect to the unused disc corresponding to the hybrid nanolubricants PAO32/1 wt% IL2/0.1 wt% h-BN and PAO32/1 wt% IL1/0.1 wt% h-BN were 75 % and 55 %, respectively.

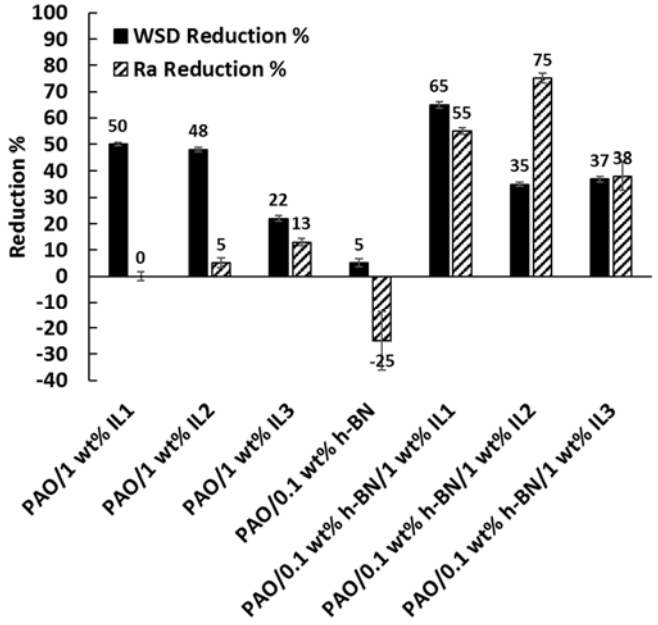

Fig. 4.7. Average wear scar diameter (WSD) reduction (Solid fill) and average roughness value (Ra) reduction (Pattern fill) at the contact surface of the steel pins of several lubricant respect to those obtained with PAO32 at 353.15 K

4.6.2 Scenario two

In this scenario a case study using GnP with two different concentrations and the three ILs as additives into PAO32 is carried out and reported in publication A2. The combinations shown in Table 4.5 were prepared to analyze the influence on the tribological behavior of GnP and ILs separately or combined added as additives to PAO32, at room temperature. The other experimental conditions are described in Chapter 2, section 2.6.1. The COFs were measured by means of a CSM standard tribometer and using ball on disc configuration at room temperature (Chapter 2, section 2.6.1). In addition, the selection of 0.05 wt% and 0.1 wt% of GnP was proposed. This selection was based on the optimal concentrations of graphene derivatives in oils obtained by other authors [98,184,190-192]. As in the previous study, the IL concentration was 1 wt%.

The COFs obtained using each one of the designed mixtures or nanodispersions as lubricants were, in all the cases, lower than that using bare PAO32 as lubricant. The COF reductions respect to that obtained with neat PAO32 are reported in Table 4.5 and shown in Fig. 4.8. As previously shown, it was concluded that the use of PAO32 with 0.05 wt% concentration of GnP is more efficient in reducing friction than that with 0.1 wt% or with 0.025 wt% (Fig. 4.1). Thus, an optimal concentration of 0.05 wt% was achieved. Optimal concentrations were also found for other nanolubricants [79,98,103,190,192,193]. At lower concentrations, the base oil governs the behavior because the quantity of nanoparticles is not enough to decrease strongly the friction, whereas when the concentration is too high, the agglomeration allows the creation of new asperities and prevents particles from entering the contact area of working surfaces, which lead to an increase of friction [194]. Moreover, the greatest reduction corresponded to

the friction results obtained using as lubricant PAO32/1 wt% IL2/0.05 wt% GnP, being 36 %. However, the latter nanolubricant was not globally considered the best, as the IL2 content limits its capabilities as nanolubricant. This is because IL2 promotes corrosion, led to the poorest time stabilities among the different nanolubricants tested, and produced the biggest change of thermophysical properties of the base oil. In contrast, the hybrid lubricants corresponding to PAO32/1 wt% IL1/0.05 wt% GnP and PAO32/1 wt% IL3/0.05 wt% GnP do not present these last disadvantages and led to 25 and 27 % of friction reductions, respectively.

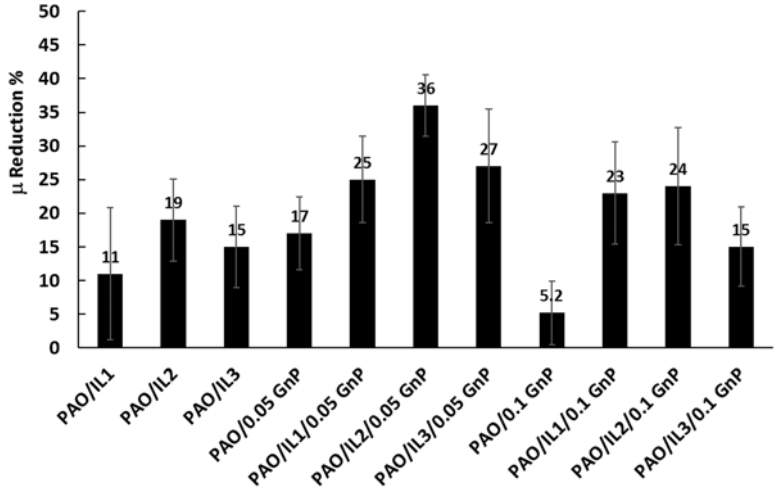

Fig. 4.8. Friction coefficients (μ) reduction for several lubricants respect to that obtained with PAO32 at room temperature

Table 4.5. Tribological results of the designed mixtures and nanolubricants based on PAO32 at room temperature

Mixture	*% Friction reduction*	*% Wear reduction (WSW)*	*% Roughness reduction (Ra)*
PAO/1 wt% IL1	11	4.2	19
PAO/1 wt% IL2	19	4.6	21
PAO/1 wt% IL3	15	3.8	16
Nanolubricant			
PAO32/0.05 wt% GnP	17	6.5	32
PAO32/1 wt% IL1/0.05 wt% GnP	25	12	36
PAO32/1 wt% IL2/0.05 wt% GnP	36	13	37
PAO32/1 wt% IL3/0.05 wt% GnP	27	12	34
PAO32/0.1 wt% GnP	5.2	5.8	31
PAO32/1 wt% IL1/0.1 wt% GnP	23	7.7	32
PAO32/1 wt% IL2/0.1 wt% GnP	24	9.6	33
PAO32/1 wt% IL3/0.1 wt% GnP	15	7.3	30

The 3D Optical Profiler Sensofar S neox presented in Chapter 2, section 2.6.3, was then used to measure the antiwear capacity of the designed lubricants. The mean wear parameters generated from the wear tracks obtained at room temperature, their corresponding uncertainties,

and the average surface roughness values were reported in publication A2. Additionally, Table 4.5 and Fig. 4.9 show the mean WSW and the average surface roughness (Ra) reductions, referred to those corresponding to the wear track obtained by the neat lubricant PAO32. Compared with PAO32, the hybrid nanolubricants with 0.05 wt% of GnP and each one of the three ILs resulted in the best antiwear reductions. PAO32/1 wt% IL2/0.05 wt% GnP showed the best antiwear reduction being 13 % followed by 12 % corresponding to both hybrid nanodispersions PAO32/1 wt% IL1/0.05 wt% GnP and PAO32/1 wt% IL3/0.05 wt% GnP. As regards Ra, reductions corresponding to the hybrid nanolubricants PAO32/1 wt% IL1/0.05 wt% GnP, PAO32/1 wt% IL2/0.05 wt% GnP and PAO32/1 wt% IL3/0.05 wt% GnP were 36, 37, and 34 %, respectively. Finally, the obtained results also showed that 0.05 wt% of GnP as antiwear additive to PAO32 is more efficient than 0.1 wt%. Hence, 1 wt% of any of IL1 or IL3, both containing the cation $[P_{6,6,6,14}]^+$, combined with 0.05 wt% GnP as hybrid additives for PAO32 produced synergistic effects. Therefore, IL1/0.05 wt% GnP and IL3/0.05 wt% GnP as hybrid additives can be considered as great improvers of the tribological behavior of PAO32 and may be suitable as potential additives of PAO32. The tribological, thermophysical and stability results obtained with IL1 and IL3 are very similar because of both ILs have the same cation $[P_{6,6,6,14}]^+$, whereas both anion and cation of IL2 have the shortest alkyl chains. These structural differences can also explain the greater affinity of IL2 with water and hence its corrosiveness.

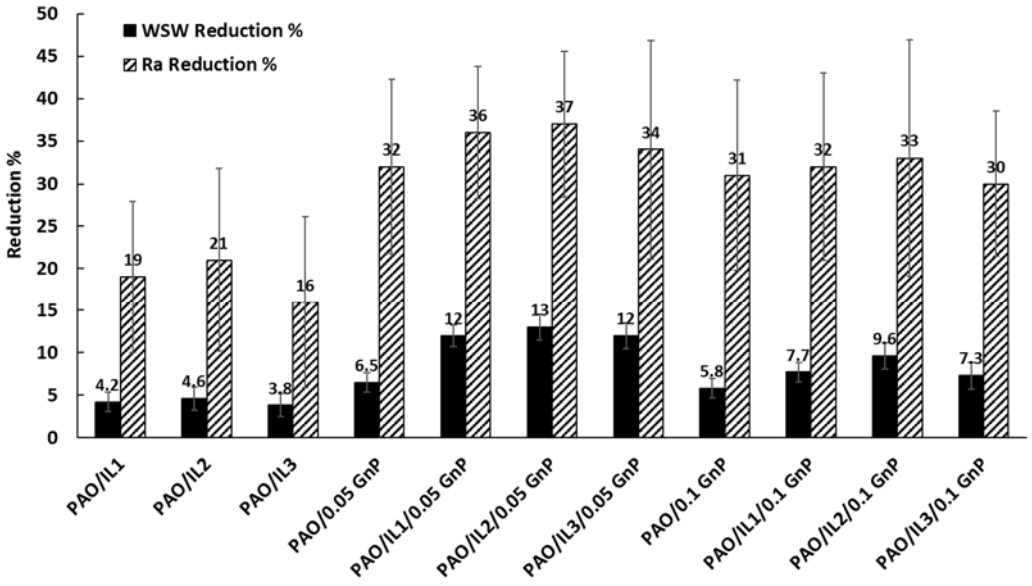

Fig. 4.9 . Average wear scar width (WSW) reduction (solid fill) and average roughness value (Ra) reduction (pattern fill) at the contact surface of the steel discs of several samples respect to those obtained with PAO32 at room temperature

4.6.3 Scenario three

Encouraged by the good results obtained in the first two scenarios, it was decided to analyze whether there were also synergies between both nanoadditives as well as among both nanoadditives and each IL. Then, in this third scenario a case study using h-BN and GnP and the three ILs as additives in PAO32 was performed (publication A3). In addition, four single nanodispersions, indicated in Table 4.2, were also studied. The COF values were determined by means of a standard CSM tribometer operating in the ball-on-disc configuration at room temperature (Chapter 2, section 2.6.1). The values of the parameters corresponding to the wear

profile were obtained by the 3D Optical Profiler Sensofar S neox (Chapter 2, section 2.6.3) extracting profiles from the grooves generated in the steel discs lubricated with the prepared nanolubricants.

Initially, the single nanodispersions listed in Table 4.1 were tested as lubricants for a steel to steel contact pair to select the best concentrations of both h-BN and GnP nanomaterials which can lead to better reductions in friction and consequently helps in minimizing the wear generated at the surface of the discs. In the case of h-BN NPs the best concentration was 0.1 wt%. For GnPs it was found that the 0.025 wt% did not perform better than 0.05 wt%. Hence, the optimal concentrations selected for the hybrid and the double hybrid nanodispersions were 0.1 wt% for h-BN NPs and 0.05 wt% for GnPs. Subsequently, PAO/0.05 wt% GnP/0.1 wt% h-BN nanolubricant was tested, which reduced the friction coefficient more than the individual addition of either 0.1 wt% h-BN or 0.05 wt% GnP separately as additives to PAO32 as can be seen in Fig. 4.10. Thus, the performance of PAO/GnP/h-BN led to COF reductions of 33 %, outperforming the friction reduction of 0.1 wt% h-BN and 0.05 wt% GnP nanodispersions, which resulted in COF reductions of 26 %, and 17 %, respectively. These results show the relevance of the hybrid combinations that drive the presence of the synergetic effects between both nanomaterials.

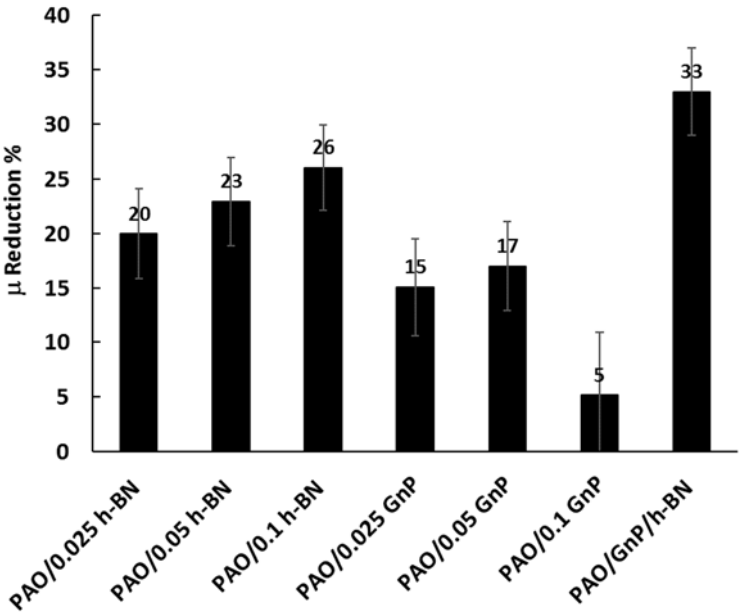

Fig. 4.10. Average reduction of the friction coefficient (μ) obtained using as lubricant nanodispersions with different nanoadditive concentration compared with that obtained with PAO32 at room temperature

For the three nanodispersions (PAO/IL/GnP/h-BN), GnP and h-BN nanoadditives were added to each IL in an agate mortar and crushed using the pestle for 10 min, obtaining three blends: IL1/GnP/h-BN, IL2/GnP/h-BN and IL3/GnP/h-BN. Each one of these blends is then added to a measured amount of PAO32 base to obtain three double hybrid nanodispersions PAO/ILX/GnP/h-BN (X=1, 2 or 3). The new friction tests yielded better achievements showing that the combinations including an IL are even more efficient than PAO/GnP/h-BN nanodispersion, due to a double hybrid synergy between the two nanomaterials and the IL.

Fig. 4.11 shows the friction reductions with respect to PAO32 obtained with PAO/ILX/GnP/h-BN nanodispersions together with those corresponding to PAO/h-BN/GnP. 33 % reduction was obtained with PAO/GnP/h-BN nanolubricant and those obtained with the three mixtures PAO/ILX were exceed with the double hybrid nanolubricants tested. Therefore,

the existence of synergistic effects between the combination of both nanomaterials and each one of the ILs were found, leading to a further reduction in friction up to 40 % regarding the neat base oil, in the case of the double hybrid nanodispersion PAO/IL3/GnP/h-BN.

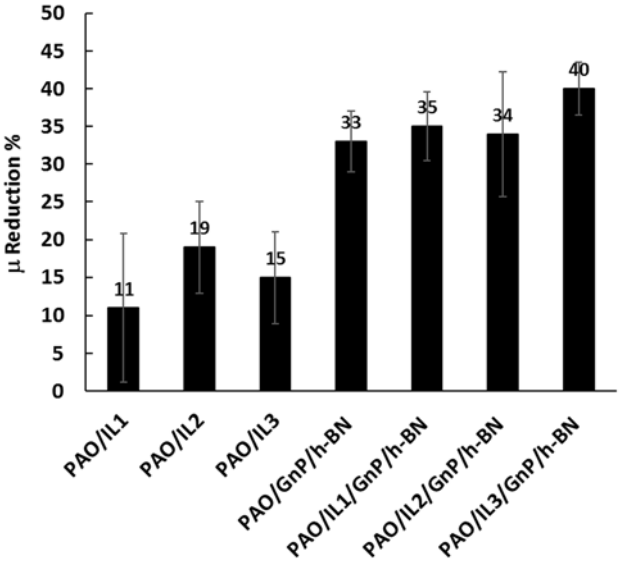

Fig. 4.11. Average friction coefficient (μ) reduction obtained using as lubricant the double hybrid nanodispersions together with those obtained compared with PAO32 and PAO/IL at room temperature

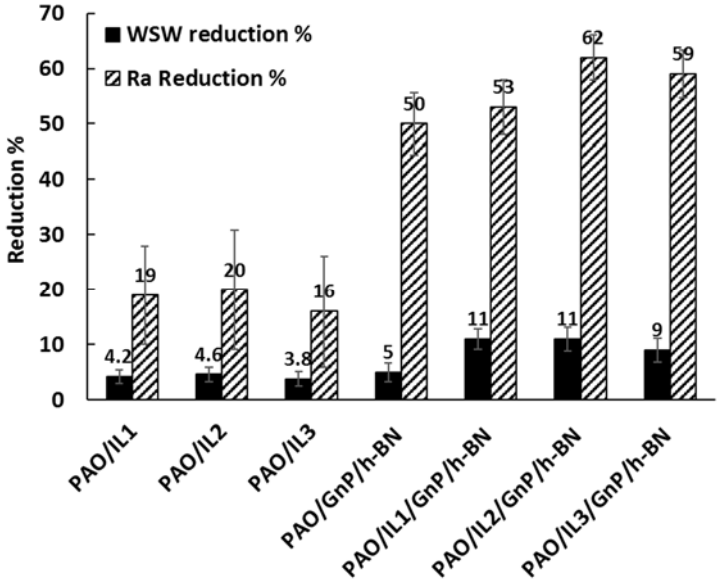

Fig. 4.12. Average wear scar width (WSW) reduction (solid fill) and average roughness value (Ra) reduction (pattern fill) at the contact surface of the steel discs of several samples using as lubricant the double hybrid nanodispersions together with those obtained compared with PAO32 and PAO/IL at room temperature

The double hybrid nanodispersions PAO/ILX/GnP/h-BN led also to more antiwear enhancements compared to the reduction achieved by PAO/GnP/h-BN and by PAO/ILX mixtures. For instance, and as shown in Fig. 4.12, the reductions in WSW were 11, 11, and 9 %, respect to WSW obtained with the base oil, when adding IL1, IL2 and IL3 to PAO/GnP/h-BN, respectively. The influence on the surface roughness was also noted. For example, the

combination PAO/IL2/GnP/h-BN reduced the average Ra value up to 62 %. In addition, the WSW and the Ra reductions corresponding to the scars of the discs lubricated with the mixtures and some of the nanolubricants are shown in Fig. 4.13. For most of the samples the WSW and Ra reductions showed similar trends, namely when WSW reduction increases, the corresponding Ra reduction also rises. Nevertheless, for the nanodispersions containing both GnP and h-BN, the Ra reductions are higher than expected. For all the samples included in Fig. 4.13, the wear scars show no signs of abrasion but of plastic flow (Figures S3 in A2 and A3), more evident in the case of the four nanolubricants containing both nanomaterials, increasing the contact area. Again, these results point up the importance of the combinations of ILs and nanomaterials to generate synergies. In addition to the mentioned before, Table 4.6 presents a summary of the tribological results and achievements. This table shows each nanolubricant with its corresponding reduction in friction, wear (in terms of WSW), and surface roughness. All these reductions are calculated with respect to the results obtained with tests of base oil PAO32.

Table 4.6. Tribological results of all the designed nanolubricants and IL mixtures at room temperature

Mixture	*% Friction reduction (μ)*	*% Wear reduction (WSW)*	*% Roughness reduction (Ra)*
PAO/1 wt% IL1	11	4.2	19
PAO/1 wt% IL2	19	4.6	21
PAO/1 wt% IL3	15	3.8	16
Nanolubricant			
PAO/0.025 wt% h-BN	20	-	-
PAO/0.05 wt% h-BN	23	-	-
PAO/0.1 wt% h-BN	26	-	-
PAO/0.025 wt% GnP	15	-	-
PAO/0.05 wt% GnP	17	6.5	32
PAO/0.1 wt% GnP	5.0	5.8	31
PAO/0.05 wt% GnP/IL1	25	12	36
PAO/0.05 wt% GnP/IL2	36	13	37
PAO/0.05 wt% GnP/IL3	27	12	34
PAO/0.1 wt% GnP/IL1	23	7.7	32
PAO/0.1 wt% GnP/IL2	24	9.6	33
PAO/0.1 wt% GnP/IL3	15	7.3	30
PAO/h-BN/GnP	33	5.0	50
PAO/h-BN/GnP/ IL1	35	11	53
PAO/h-BN/ GnP/IL2	34	11	62
PAO/h-BN/ GnP/IL3	40	9.0	59

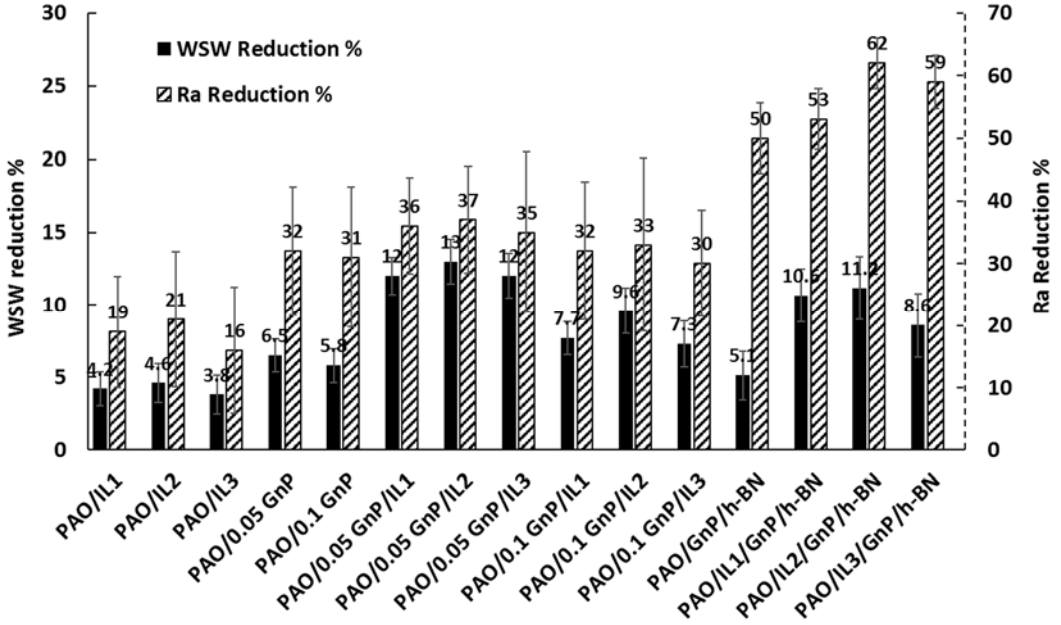

Fig. 4.13. Average wear scar width (WSW) reduction (sold fill) and average roughness value (Ra) reduction (pattern fill) at the contact surface of the steel discs of several samples respect to those obtained with PAO32 at room temperature

4.6.4 Nanolubricants and worn surfaces: FTIR, Raman and SEM

Mixtures and single nanolubricants based on h-BN NPs as additives and PAO32 as base oil were analyzed by FTIR spectroscopy (Chapter 2 section 2.2.1). Moreover, the pins and discs worn surfaces lubricated with PAO32, IL mixtures and nanolubricants were studied by confocal Raman microscopy (Chapter 2 section 2.2.3) and scanning electron microscopy (Chapter 2 section 2.2.2).

FTIR of nanolubricants: The FTIR spectra of some of the lubricants indicated in Table 4.2 are shown in publication A1, Figure S4. These spectra are compared to the spectrum of neat PAO32 (Figure 1, publication A1). It was clearly noted that there are no significant differences between the FTIR spectra of PAO32, PAO32/IL, PAO32/h-BN and PAO32/IL/h-BN. This fact shows the absence of the formation of new chemical bonds in the dispersions or in the mixtures.

Raman and SEM analysis of the worn surfaces: Raman spectra on the worn surfaces of the pins tested at 353.15 K, scenario one, were performed and illustrated in publication A1, Figures 15 and S8-S13. These spectra permit to identify the compounds present in the worn surface and their distribution. As regards to the IL mixtures, it was found that both IL1 and IL2 are present on the worn surface in larger portions than IL3. Linking this presence to tribological behavior, IL1 ($[P_{6,6,6,14}][DEHP]$) showed best antifriction behavior and antiwear capability at 298.15 K and 353.15 K, respectively.

Regarding PAO32/h-BN dispersion, weak presence of h-BN was detected on the surface, which could be related to the little antiwear enhancement obtained with this nanolubricant. The hybrid combination of IL/h-BN helped in protecting the steel surface, specially that containing IL1, whose tribofilms protect the steel surface more effectively (better antiwear capability despite the lower presence of both additives than in the other two hybrid combinations). In addition, SEM images were conducted for all the worn surfaces of the pins and shown in A1, Figure 12. These images illustrate some abrasive wear, barely perceptible in the case of lubricants containing IL1. In this regard, size and diameter of the wear scar shown in the SEM images agree with those of wear profiles (A1, Figure 13).

In relation to scenario two, Raman spectra on the disc worn surfaces lubricated with the nanodispersions and IL mixtures and their corresponding SEM images were reported in publication A2. Raman spectra, Figures 10 and S4-S13, confirm that the tribofilms formed by PAO32/GnP and PAO32/ILX/GnP nanolubricants containing 0.05 wt% GnP contain lower GnP areas on the contact surface than those containing 0.1 wt% GnP. Raman mappings corresponding to the hybrid nanolubricants (Figures 10 and S9-S13), present lower oxide area sizes than the other lubricants tested, especially those containing IL1 and IL2, as well as 0.05 wt% GnP. As regards to the area size of the IL tribofilm, there was no strong differences, being slightly higher for the hybrid nanolubricant containing IL2 and 0.05 wt% GnP. Regarding SEM images shown in A2, Figures S1-S3, it is evidenced that, for all the lubricants the worn surfaces are smooth, without signs of plowing or abrasion, which can be due to the fact that graphene derivatives prevent the formation of large abrasive particles. Mild abrasive wear was observed in the case of the surface lubricated with bare PAO32.

In scenario three, both Raman and SEM analyses were carried out on the worn surfaces lubricated with PAO/GnP/h-BN and PAO/ILX/GnP/h-BN (X=1,2 or 3) and shown in publication A3. Raman mapping of PAO/GnP/h-BN shows areas containing GnP and others with h-BN. Both components are also presented on the worn scars lubricated with each one of the three nanodispersions PAO/ILX/GnP/h-BN (A3, Figures 9-11) together with a significant tribofilm on the edges of the worn surface due to the corresponding IL. In the case of PAO/IL3/GnP/h-BN, the areas corresponding to h-BN are significantly larger than when the other two double hybrid nanolubricants are used. SEM images (A3, Figure S3) show plastic deformation in all cases as well as smoother surfaces for the scars corresponding to the nanolubricants than that to PAO32. WSW values obtained from SEM micrographs agree with those obtained with the 3D profilometer.

It is interesting to note that for all the mixtures and dispersions in the three scenarios iron oxides were found on the worn surfaces of the pins or discs, except for the nanolubricants PAO/ILX/GnP/h-BN. From Raman mappings, SEM images and roughness measurements, it can be concluded that the main tribological mechanisms occurring are IL tribofilm formation and mending/repairing effect due to GnP and h-BN nanoadditives, decreasing friction and wear modifying the surface roughness.

5 CONCLUSIONS AND FUTURE WORK

This Doctoral thesis was carried out to develop new oil lubricants. New advanced nanolubricants were prepared for reducing friction and minimize the wear in between contact surfaces. All the results achieved in this study are briefly presented as follows:

1 *Selection of nanoadditives to design new potential nanolubricants and synthesis and characterization of iron oxide NPs from mining sludge:* Hexagonal boron nitride NPs (h-BN) and graphene nanoplatelets (GnP) were selected due to their excellent properties as friction and wear reducers shown in previous literature and because their low cost and availability in addition to the h-BN ecofriendly nature. Iron oxide nanoparticles were selected to contribute to the development of a research line on iron oxide based lubricant additives obtained from the sludge of the iron mine to clean and recycle areas of nature negatively affected by accumulation of mining tailings. Fe_2O_3 NPs which are nontoxic and available were synthetized used a procedure developed in the chemistry department of the university of Banja Luka (Bosnia and Herzegovina). The size of the NPs determined by HRTEM is between 5 nm to 30 nm. The morphology of most of these NPs is round with laminated structure whereas some of them are elongated and cylindrical. XRD analysis shows the predominant presence of hematite (Fe_2O_3) NPs but also some magnetite (Fe_3O_4) NPs.

2 *Selection and characterization of ionic liquids (ILs) as lubricant additives of a polyalphaolefin, PAO32:* Three phosphonium ionic liquids, trihexyltetradecylphosphonium bis(2-ethylhexyl) phosphate (IL1), tributylethylphosphonium diethylphosphate (IL2) and trihexyltetradecylphosphonium bis(2,4,4-trimethylpentyl) phosphinate (IL3) were selected due to their better miscibility and performance as friction and wear reducers as compared with other ILs, whereas PAO32 was selected because it is used in the gearboxes of wind turbines. The three ILs and PAO32 were analyzed by Fourier transform infrared spectrometry (FTIR) and by confocal Raman spectrometry. In comparison to the Raman spectrum of PAO32, no significant changes were found. We are not aware of any previous Raman spectra of IL1 and IL2 reported in the literature.

3 *Evaluation of possible corrosion produced by selected ionic liquids on AISI 52100 steel*: At room temperature, only the disk tested with IL2 showed corrosion. For the test carried out at 373.15 K, no corrosion due to the ILs was detected. It was concluded that at room temperature the reason for the corrosion of the steel was the water content of IL2.

4 *Obtaining long-time stable dispersions of nanoadditives in lubricant base oils (PAO32 and PAO10):* The stability of 22 nanodispersions was checked. For the PAO32 dispersions the most stable are: PAO32/0.05 wt% GnP, PAO32/0.1 wt% GnP and eight PAO32 nanodispersions containing IL1 or IL3, which were stable for the overall analyzed time (150 or 240 days). Hence, IL1 and IL3 improved the stability of the h-BN nanodispersions. The nanodispersions based on PAO32 or PAO10 and iron oxide NPs with three different concentrations, 0.1,0.25 and 0.5 wt%, showed stability lower than five-days.

5 *Thermophysical characterization (density, viscosity and viscosity index) of PAO32, some of its mixtures with ILs, several of its dispersions with hybrid additives (ILs+nanoadditive), and with double hybrid additives (ILs+nanoadditive1+nanoadditive2):* Respect to the corresponding properties of PAO32, the average relative change in density ranged between 0.053 % and 0.44 %, the average relative change in viscosity ranged between

1.8 % and 7.6 % and the relative change in viscosity index ranged from -1.7 % to 0.53 %, being IL2 the additive which led to the highest variation of the thermophysical properties of PAO32.

6 *Evaluation of the tribological behavior of steel/steel contacts lubricated with PAO32, several of its mixtures with ILs, and of its nanolubricants with hybrid additives and lubricants with double hybrid additives.* The three PAO32/IL mixtures and 16 of the 22 designed nanolubricants tribologically tested improved the antifriction and antiwear capabilities of neat PAO32. Specifically, the best friction reduction (40 %) was achieved using as lubricant the double hybrid nanodispersion PAO32/IL3/GnP/h-BN at room temperature. The best wear reductions were obtained with PAO/IL1/h-BN at 353.15 K (99 % in terms of wear scar volume) and with PAO32/IL2/0.05 wt% GnP at room temperature (27 % in terms of maximum depth of the wear scar). Thus, several synergistic effects were presented between the two NPs with the ILs for IL/NP hybrid additives and for IL/NP1/NP2 as double hybrid additives to PAO32. From roughness measurements and confocal Raman microscopy it was concluded that the main tribological mechanisms are film formation due to ILs and surface repairing effect due to NPs.

7 From the overall tribological results, once that the additive IL2 was discarded due to its possible corrosive effect and the stability problems of its nanodispersions, it can be concluded that

a) the best antifriction additives are the double hybrid IL3/GnP/h-BN (40 %) and IL1/GnP/h-BN (35 %) as well as the hybrid GnP/h-BN (33 %);
b) for the additives analyzed at 353.15 K, the best antiwear behavior in terms of volume (99 %), maximum depth (92 %), transversal area (97 %) and diameter (65 %) of the scar is obtained with the hybrid IL1/h-BN additive;
c) for the additives analyzed at room temperature, the best antiwear behavior in terms of maximum depth (24 %, 23 %), transversal area (21 %, 20 %) and width (12 %, 12%) of the scar are obtained, respectively, with the hybrid IL1/GnP and IL3/GnP additives;

Based on the results of this doctoral thesis, some *recommendations and future work* can be proposed for the design of new advanced nanolubricants, which are briefly presented below:

1 For the nanodispersions which lead to the lowest friction and wear (conclusion 7), Stribeck curves, film thickness and friction torque measurements as well as other tests with tribometers whose characteristics (loads, configurations, speeds) are similar to those of the operational conditions of the gearboxes, can be carried out in future. Additional studies of the synergies of the NPs and the ILs with other additives needed for this kind of lubricants are also envisaged. Once, all these studies were finished, the formulated lubricants based on IL1, IL2, h-BN and/or GnP could be introduced in a gearbox of a wind turbine to analyze their performance.

2 As fundamental studies, several strategies come from the results obtained in this work as: a) Analyze the stability. Antifriction and antiwear synergies of IL1 and of IL3 with other NPs, quantum dots, WS_2 or MoS_2; b) To combine spherical carbon nanodots with GnP as additives to combine the rolling and the exfoliation mechanisms; c) mixing two ILs and one NPs being the combination, PAO/NPs/IL/IL instead of PAO/NPs/NPs/IL.

3 It was indicated that the synthesized Fe_2O_3 NPs from the sludge of an iron ore production mine showed weak stability in apolar lubricants (polyalphaolefins 10 and 32), so further work such as thermophysical and tribological researches were not carried out. However, the stability of the synthesized Fe_2O_3 NPs could be improved using ionic liquids, coating their surface or using polar base oils. Future work using these alternatives is envisaged.

6 REFERENCES

[1] K. Holmberg, P. Kivikytö Reponen, P. Härkisaari, K. Valtonen, A. Erdemir, Global energy consumption due to friction and wear in the mining industry, Tribology International 115 (2017) 116-139, https://doi.org/10.1016/j.triboint.2017.05.010.

[2] K. Holmberg, A. Erdemir, Influence of tribology on global energy consumption, costs and emissions, Friction 5 (2017) 263-284, https://doi.org/10.1007/s40544-017-0183-5.

[3] L.D. Danny Harvey, Iron and steel recycling: Review, conceptual model, irreducible mining requirements, and energy implications, Renewable and Sustainable Energy Reviews 138 (2021) 110-553, https://doi.org/10.1016/j.rser.2020.110553.

[4] D. Stević, D. Mihajlović, R. Kukobat, Y. Hattori, K. Sagisaka, K. Kaneko, S.G. Atlagić, Hematite Core Nanoparticles with Carbon Shell: Potential for Environmentally Friendly Production from Iron Mining Sludge, Journal of Materials Engineering and Performance 25 (2016) 3121-3127, https://doi.org/10.1007/s11665-016-1964-0.

[5] S.G. Atlagić, L. Tankosić, S. Prźulj, D. Mirošljević, Recent Patents in Reuse of Metal Mining Tailings and Emerging Potential in Nanotechnology Applications, Recent patents on nanotechnology 15 (2021) 256-269, https://doi.org/10.2174/1872210514666201224104555.

[6] S. Randalls, History of the 2°C climate target, Climate Change 1 (2010) 598-605, https://doi.org/10.1002/wcc.62.

[7] J. Rogelj, D. L. McCollum, A. Reisinger, M. Meinshausen, K. Riahi, Probabilistic cost estimates for climate change mitigation, Nature 493 (2013) 79-83, https://doi.org/10.1038/nature11787.

[8] J. Rogelj, M. Schaeffer, M. Meinshausen, R. Knutti, J. Alcamo, K. Riahi, W. Hare, Zero emission targets as long-term global goals for climate protection, Environmental Research Letters 10 (2015) 105-007, https://doi.org/10.1088/1748-9326/10/10/105007.

[9] N. Vincent Emodi, T. Chaiechi, ABM Rabiul Alam Beg, The impact of climate variability and change on the energy system: A systematic scoping review, Science of The Total Environment 676 (2019) 545-563, https://doi.org/10.1016/j.scitotenv.2019.04.294.

[10] D.E.H.J. Gernaat, H.S. de Boer, V. Daioglou, S.G. Yalew, C. Müller, D.P. van Vuuren, Climate change impacts on renewable energy supply, Nature Climate Change 11 (2021) 119-125, https://doi.org/10.1038/s41558-020-00949-9.

[11] S. W.D. Turner, M. Hejazi, S. H. Kim, L. Clarke, J. Edmonds, Climate impacts on hydropower and consequences for global electricity supply investment needs, Energy 141 (2017) 2081-2090, https://doi.org/10.1016/j.energy.2017.11.089.

[12] N.L. Panwar, S.C. Kaushik, S. Kothari, Role of renewable energy sources in environmental protection: A review, Renewable and Sustainable Energy Reviews 15 (2011) 1513-1524, https://doi.org/10.1016/j.rser.2010.11.037.

[13] E. Commission, https://ec.europa.eu/clima/eu-action/climate-strategies-targets/2030-climate-energy-framework_en, 2021.

[14] I. Tzanakis, M. Hadfield, B. Thomas, S.M. Noya, I. Henshaw, S. Austen, Future perspectives on sustainable tribology, Renewable and Sustainable Energy Reviews 16 (2012) 4126-4140, https://doi.org/10.1016/j.rser.2012.02.064.

[15] Y. Zhang, Boundary lubrication—An important lubrication in the following time, Journal of Molecular Liquids 128 (2006) 56-59, https://doi.org/10.1016/j.molliq.2005.12.002.

[16] B. J. Hamrock, S. R. Schmid, B. O. Jacobson, Fundamentals of Fluid Film Lubrication, 2nd Edition, CRC Press. (2004).https://doi.org/10.1201/9780203021187.
[17] L. Kong, J. Sun, Y. Bao, Preparation, characterization and tribological mechanism of nanofluids, RSC Advances 7 (2017) 12599-12609, http://dx.doi.org/10.1039/C6RA28243A.
[18] Y. Chen, P. Renner, H. Liang, Dispersion of nanoparticles in lubricating oil: A critical review, Lubricants 7 (2019) 7, https://doi.org/10.3390/lubricants7010007.
[19] I. Minami, Ionic Liquids in Tribology, Molecules 14 (2009) 2286-2305, https://doi.org/10.3390/molecules14062286.
[20] E.A. Somers, C.P. Howlett, R.D. MacFarlane, M. Forsyth, A Review of Ionic Liquid Lubricants, Lubricants 1 (2013) 3-21, https://doi.org/10.3390/lubricants1010003.
[21] M.D. Bermúdez, A.E. Jiménez, J. Sanes, F.J. Carrión, Ionic liquids as advanced lubricant fluids, Molecules 14 (2009) 2888-2908, https://doi.org/10.3390/molecules14082888.
[22] Y. Zhou, J. Qu, Ionic Liquids as Lubricant Additives: A Review, ACS Applied Materials & Interfaces 9 (2017) 3209-3222, https://doi.org/10.1021/acsami.6b12489.
[23] M.T. Donato, R. Colaço, L.C. Branco, B. Saramago, A Review on Alternative Lubricants: Ionic Liquids as Additives and Deep Eutectic Solvents, Journal of Molecular Liquids 333 (2021) 116-004, https://doi.org/10.1016/j.molliq.2021.116004.
[24] M. Cai, Q. Yu, W. Liu, F. Zhou, Ionic liquid lubricants: when chemistry meets tribology, Chemical Society Reviews (2020) 7481-7846, https://doi.org/10.1039/D0CS00126K.
[25] T. Naveed, R. Zahid, R.A. Mufti, M. Waqas, M.T. Hanif, A review on tribological performance of ionic liquids as additives to bio lubricants, Proceedings of the Institution of Mechanical Engineers, Part J: Journal of Engineering Tribology 235 (2021) 1782-1806, https://doi.org/10.1177/1350650120973805.
[26] J.M. Liñeira del Río, E.R. López, J. Fernández, Synergy between boron nitride or graphene nanoplatelets and tri(butyl)ethylphosphonium diethylphosphate ionic liquid as lubricant additives of triisotridecyltrimellitate oil, Journal of Molecular Liquids 301 (2020) 112442, https://doi.org/10.1016/j.molliq.2020.112442.
[27] J. Sanes, M.D. Avilés, N. Saurín, T. Espinosa, F.J. Carrión, M.D. Bermúdez, Synergy between graphene and ionic liquid lubricant additives, Tribology International 116 (2017) 371-382, https://doi.org/10.1016/j.triboint.2017.07.030.
[28] J.M. Liñeira del Río, E.R. López, D.E.P. Gonçalves, J.H.O. Seabra, J. Fernández, Tribological properties of hexagonal boron nitride nanoparticles or graphene nanoplatelets blended with an ionic liquid as additives of an ester base oil, Lubrication science 33 (2021) 269-278, https://doi.org/10.1002/ls.1543.
[29] T. Mang, W. Dresel, Lubricants and lubrication , second edition (2007).
[30] J. Zhao, Y. Huang, Y. He, Y. Shi, Nanolubricant additives: A review, Friction 9 (2020) 891-917, https://doi.org/10.1007/s40544-020-0450-8.
[31] J. Singh, D. Kumar, N. Tandon, Tribological and Vibration Studies on Newly Developed Nanocomposite Greases Under Boundary Lubrication Regime, Journal of Tribology 140 (2017) 032-001, https://doi.org/10.1115/1.4038100.
[32] J. A.Brandão, M. Meheux, F. Ville, J. H.O. Seabra, J. Castro, Comparative overview of five gear oils in mixed and boundary film lubrication, Tribology International 47 (2012) 50-61, https://doi.org/10.1016/j.triboint.2011.10.007.
[33] Y. Guo, P. Guo, L. Sun, X. Li, P. Ke, Q. Li, A. Wang, Tribological properties of Ti-doped diamond-like carbon coatings under dry friction and PAO oil lubrication, Surface and Interface Analysis 51 (2019) 361-370, https://doi.org/10.1002/sia.6588.

[34] M. J. Schertzer, P. Iglesias, Meta-Analysis Comparing Wettability Parameters and the Effect of Wettability on Friction Coefficient in Lubrication, Lubricants 6 (2018) 70, https://www.mdpi.com/2075-4442/6/3/70.
[35] Z. Xie, Z.-s. Rao, L. Liu, R. Chen, Theoretical and experimental research on the friction coefficient of water lubricated bearing with consideration of wall slip effects, Mechanics Industry 17 (2016) 13, https://doi.org/10.1051/meca/2015039.
[36] H.A. Spikes, Mixed lubrication — an overview, Lubrication science 9 (1997) 221-253, https://doi.org/10.1002/ls.3010090302.
[37] G. Guangteng, H.A. Spikes, An Experimental Study of Film Thickness in the Mixed Lubrication Regime, Tribology Series 32 (1997) 159-166, https://doi.org/10.1016/S0167-8922(08)70445-0.
[38] H.A. Spikes, A.V. Olver, Basics of mixed lubrication, Lubrication Science 16 (2003) 1-28, https://doi.org/10.1002/ls.3010160102.
[39] D. Zhu, Q.J. Wang, On the λ ratio range of mixed lubrication, Journal of Engineering Tribology 226 (2012) 1010-1022, https://doi.org/10.1177/1350650112461867.
[40] K.J. Sharif, H.P. Evans, R.W. Snidle, Modelling of elastohydrodynamic lubrication and fatigue of rough surfaces: The effect of lambda ratio, Journal of Engineering Tribology 226 (2012) 1039-1050, https://doi.org/10.1177/1350650112458220.
[41] J. W. Robinson, Y. Zhou, P. Bhattacharya, R. Erck, J. Qu, J.T. Bays, L. Cosimbescu, Probing the molecular design of hyper-branched aryl polyesters towards lubricant applications, Scientific Reports 6 (2016) 1-10, https://doi.org/10.1038/srep18624.
[42] M.M. Khonsari, E.R. Booser, Applied Tribology: Bearing Design and Lubrication, John Wiley & Sons, second edition. John Wiley & Sons. (2008).
[43] Y. Fu, A. W.Batchelor, N.K. Loh, K.W. Tan, Effect of lubrication by mineral and synthetic oils on the sliding wear of plasma nitrided AISI 410 stainless steel, Wear 219 (1998) 169-176, https://doi.org/10.1016/S0043-1648(98)00184-7.
[44] L. R. Rudnick, Synthetics, Mineral Oils, and Bio-Based Lubricants, Boca Raton: CRC Press. (2020).
[45] F.J. Owuna, M.U. Dabai, M.A. Sokoto, S.M. Dangoggo, B.U. Bagudo, U.A. Birnin-Yauri, L.G. Hassan, I. Sada, A.L. Abubakar, M.S. Jibrin, Chemical modification of vegetable oils for the production of biolubricants using trimethylolpropane: A review, Egyptian Journal of Petroleum 29 (2019) 75-82, https://doi.org/10.1016/j.ejpe.2019.11.004.
[46] T. Issariyakul, A. K. Dalai, Biodiesel from vegetable oils, Renewable and Sustainable Energy Reviews 31 (2014) 446-471, https://doi.org/10.1016/j.rser.2013.11.001.
[47] R. Benda, J. Bullen, A. Plomer, Synthetics basics: Polyalphaolefins — base fluids for high-performance lubricants, Journal of Synthetic Lubrication 13 (1996) 41-57, https://doi.org/10.1002/jsl.3000130105.
[48] T. Zolper, Z. Li, C. Chen, M. Jungk, T. Marks, Y.-W. Chung, Q. Wang, Lubrication Properties of Polyalphaolefin and Polysiloxane Lubricants: Molecular Structure–Tribology Relationships, Tribology Letters 48 (2012) 355-365, https://doi.org/10.1007/s11249-012-0030-9.
[49] J.F. Carpenter, Biodegradability and toxicity of polyalphaolefin base stocks, Journal of Synthetic Lubrication 12 (1995) 13-20, https://doi.org/10.1002/jsl.3000120103.
[50] S. Bair, P. Vergne, M. Querry, A unified shear-thinning treatment of both film thickness and traction in EHD, Tribology Letters 18 (2005) 145-152, https://doi.org/10.1007/s11249-004-1770-y.

[51] Y. Liu, Q.J. Wang, I. Krupka, M. Hartl, S. Bair, The Shear-Thinning Elastohydrodynamic Film Thickness of a Two-Component Mixture, Journal of Tribology 130 (2008) 021502, https://doi.org/10.1115/1.2842298.
[52] L. R. Rudnick, Lubricant Additives: Chemistry and Applications,3rd Edition, CRC Press Taylor and Francis Group. Boca Raton. (2017).https://doi.org/10.1201/9781420059656.
[53] H. Salah, M.R. Elkatory, M. Abdel Fattah, Novel zinc-polymer complex with antioxidant activity for industrial lubricating oil, Fuel 305 (2021) 121536, https://doi.org/10.1016/j.fuel.2021.121536.
[54] J.Q. Hu, J.J. Zhang, L. Guo, C.Q. Miao, S.Z. Yang, J. Ma, X. Xu, F. Xie, Synthesis of Styrenated Sulfur- and Phosphorus-Free Organic Titanate and Evaluation of Its Tribological and Antioxidant Properties as an Additive in Poly-α-olefin, Industrial & Engineering Chemistry Research 58 (2019) 1754-1759, https://doi.org/10.1021/acs.iecr.8b04652.
[55] Z. Yang, C. Sun, C. Zhang, S. Zhao, M. Cai, Z. Liu, Q. Yu, Amino acid ionic liquids as anticorrosive and lubricating additives for water and their environmental impact, Tribology International 153 (2021) 106663, https://doi.org/10.1016/j.triboint.2020.106663.
[56] D. Zheng, X. Wang, M. Zhang, Z. Liu, C. Ju, Anticorrosion and lubricating properties of a fully green lubricant, Tribology International 130 (2019) 324-333, https://doi.org/10.1016/j.triboint.2018.08.014.
[57] G. Tsagkaropoulou, C.P. Warrens, P.J. Camp, Interactions between Friction Modifiers and Dispersants in Lubricants: The Case of Glycerol Monooleate and Polyisobutylsuccinimide-Polyamine, ACS Applied Materials & Interfaces 11 (2019) 28359-28369, https://doi.org/10.1021/acsami.9b05718.
[58] M. J. Covitch, K. J.Trickett, How polymers behave as viscosity index improvers in lubricating oils, Advances in Chemical Engineering and Science 5 (2015) 134-151, http://dx.doi.org/10.4236/aces.2015.52015.
[59] A. Neville, A. Morina, T. Haque, M. Voong, Compatibility between tribological surfaces and lubricant additives—How friction and wear reduction can be controlled by surface/lube synergies, Tribology International 40 (2007) 1680-1695, https://doi.org/10.1016/j.triboint.2007.01.019.
[60] U. Abdulfatai, A. Uzairu, S. Uba, G.A. Shallangwa, Molecular modelling and design of lubricant additives and their molecular dynamic simulations studies of Diamond-Like-Carbon (DLC) and steel surface coating, Egyptian Journal of Petroleum 28 (2019) 111-115, https://doi.org/10.1016/j.ejpe.2018.12.004.
[61] U. Abdulfatai, A. Uzairu, G.A. Shallangwa, S. Uba, Computational modelling of some anti-friction lubricant additives, South African Journal of Chemical Engineering 32 (2020) 27-31, https://doi.org/10.1016/j.sajce.2020.01.003.
[62] F.P. Bowden, J.N. Gregory, D. Tabor, Lubrication of Metal Surfaces by Fatty Acids, Nature 156 (1945) 97-101, https://doi.org/10.1038/156097a0.
[63] X. Feng, H. Jianqiang, Z. Fazheng, J. Feng, Y. Junbing, Antiwear performance of organomolybdenum compounds as lubricant additives, Lubrication Science 19 (2007) 81-85, https://doi.org/10.1002/ls.31.
[64] Z. Tang, S. Li, A review of recent developments of friction modifiers for liquid lubricants (2007–present), Current Opinion in Solid State and Materials Science 18 (2014) 119-139, https://doi.org/10.1016/j.cossms.2014.02.002.
[65] H. Spikes, Friction Modifier Additives, Tribology Letters 60 (2015) 26, https://doi.org/10.1007/s11249-015-0589-z.

[66] B. Li, X. Wang, W. Liu, Q. Xue, Tribochemistry and antiwear mechanism of organic–inorganic nanoparticles as lubricant additives, Tribology Letters 22 (2006) 79-84, https://doi.org/10.1007/s11249-005-9002-7.
[67] S. Shahnazar, S. Bagheri, S.B. Abd Hamid, Enhancing lubricant properties by nanoparticle additives, International Journal of Hydrogen Energy 41 (2016) 3153-3170, https://doi.org/10.1016/j.ijhydene.2015.12.040.
[68] A. Singh, P. Chauhan, M. Gangadhar, A review on tribological performance of lubricants with nanoparticles additives, Materials Today: Proceedings 25 (2019) 586-591, https://doi.org/10.1016/j.matpr.2019.07.245.
[69] N. G. Demas, E. V. Timofeeva, J. L. Routbort, G. R. Fenske, Tribological Effects of BN and MoS2 Nanoparticles Added to Polyalphaolefin Oil in Piston Skirt/Cylinder Liner Tests, Tribology Letters 47 (2012) 91-102, https://doi.org/10.1007/s11249-012-9965-0.
[70] V. Khare, M.Q. Pham, N. Kumari, H.S. Yoon, C.S. Kim, J.I.L. Park, S.H. Ahn, Graphene–Ionic Liquid Based Hybrid Nanomaterials as Novel Lubricant for Low Friction and Wear, ACS Applied Materials & Interfaces 5 (2013) 4063-4075, https://doi.org/10.1021/am302761c.
[71] O. Konur, Nanotechnology Applications in Diesel Fuels and Related Research Fields: A Review of the Research. Biodiesel Fuels. (2021).
[72] J.E. Contreras, E.A. Rodriguez, J. Taha Tijerina, Nanotechnology applications for electrical transformers—A review, Electric Power Systems Research 143 (2017) 573-584, https://doi.org/10.1016/j.epsr.2016.10.058.
[73] European Commission, Commission recommendation on the definition of nanomateria, (2011), https://ec.europa.eu/environment/chemicals/nanotech/faq/definition_en.htm.
[74] M. F. Ashby, P. J. Ferreira, D. L. Schodek, Nanomaterials, nanotechnologies and design: an introduction for engineers and architects. Butterworth-Heinemann. (2009).https://doi.org/10.1016/B978-0-7506-8149-0.X0001-3.
[75] H. Xiao, S. Liu, 2D nanomaterials as lubricant additive: A review, Materials & Design 135 (2017) 319-332, https://doi.org/10.1016/j.matdes.2017.09.029.
[76] J.K. Patel, A. Patel, D. Bhatia, Introduction to Nanomaterials and Nanotechnology. Springer. (2021).https://doi.org/10.1007/978-3-030-50703-91.
[77] W. Dai, B. Kheireddin, H. Gao, H. Liang, Roles of nanoparticles in oil lubrication, Tribology International 102 (2016) 88-98, https://doi.org/10.1016/j.triboint.2016.05.020.
[78] P. Rabaso, F. Ville, F. Dassenoy, M. Diaby, P. Afanasiev, J. Cavoret, B. Vacher, T. Le Mogne, Boundary lubrication: Influence of the size and structure of inorganic fullerene-like MoS_2 nanoparticles on friction and wear reduction, Wear 320 (2014) 161-178, https://doi.org/10.1016/j.wear.2014.09.001.
[79] J.M. Liñeira del Río, E.R. López, M. González Gómez, S. Yáñez Vilar, Y. Piñeiro, J. Rivas, D.E.P. Gonçalves, J.H.O. Seabra, J. Fernández, Tribological Behavior of Nanolubricants Based on Coated Magnetic Nanoparticles and Trimethylolpropane Trioleate Base Oil, Nanomaterials 10 (2020) 683, https://doi.org/10.3390/nano10040683.
[80] M. Gulzar, H.H. Masjuki, M.A. Kalam, M. Varman, N.W.M. Zulkifli, R.A. Mufti, R. Zahid, Tribological performance of nanoparticles as lubricating oil additives, Journal of Nanoparticle Research 18 (2016) 18:223, https://doi.org/10.1007/s11051-016-3537-4.
[81] L. Rapoport, V. Leshchinsky, I. Lapsker, Y. Volovik, O. Nepomnyashchy, M. Lvovsky, R. Popovitz Biro, Y. Feldman, R. Tenne, Tribological properties of WS_2 nanoparticles under mixed lubrication, Wear 255 (2003) 785-793, https://doi.org/10.1016/S0043-1648(03)00044-9.

[82] Y.Y. Wua, W.C. Tsuia, T.C. Liub, Experimental analysis of tribological properties of lubricating oils with nanoparticle additives, Wear 262 (2007) 819-825, https://doi.org/10.1016/j.wear.2006.08.021.
[83] Z. Xiaodong, F. Xun, S. Huaqiang, H. Zhengshui, Lubricating properties of Cyanex 302-modified MoS_2 microspheres in base oil 500SN, lubrication science 19 (2007) 71-79, https://doi.org/10.1002/ls.32.
[84] G. Liu, X. Li, B. Qin, D. Xing, Y. Guo, R. Fan, Investigation of the mending effect and mechanism of copper nano-particles on a tribologically stressed surface, Tribology Letters 17 (2004) 961-966, https://doi.org/10.1007/s11249-004-8109-6.
[85] T. Sui, B. Song, F. Zhang, Q. Yang, Effect of particle size and ligand on the tribological properties of amino functionalized hairy silica nanoparticles as an additive to polyalphaolefin, Journal of Nanomaterials 2015 (2015) 9, https://doi.org/10.1155/2015/492401.
[86] V. Cortes, J. A. Ortega, Evaluating the Rheological and Tribological Behaviors of Coconut Oil Modified with Nanoparticles as Lubricant Additives, Lubricants 7 (2019) 76, https://www.mdpi.com/2075-4442/7/9/76.
[87] I. Minami, Molecular Science of Lubricant Additives, Applied Sciences 7 (2017) 445, https://doi.org/10.3390/app7050445.
[88] T. Rimza, S. Singh, P. Kumar, Chapter 19 - Two-dimensional nanomaterials for cancer application.(R. Khan, A. Parihar, S.K. Sanghi Eds.): Academic Press. (2022).https://doi.org/10.1016/B978-0-12-823424-2.00025-9.
[89] L. Liu, M. Zhou, L. Jin, L. Li, Y. Mo, G. Su, X. Li, H. Zhu, Y. Tian, Recent advances in friction and lubrication of graphene and other 2D materials: Mechanisms and applications, Friction 7 (2019) 199-216, https://doi.org/10.1007/s40544-019-0268-4.
[90] P.C. Uzoma, H. Hu, M. Khadem, O.V. Penkov, Tribology of 2D Nanomaterials: A Review, Coatings 10 (2020) 897, https://www.mdpi.com/2079-6412/10/9/897.
[91] W. Zhai, N. Srikanth, L.B. Kong, K. Zhou, Carbon nanomaterials in tribology, Carbon 119 (2017) 150-171, https://doi.org/10.1016/j.carbon.2017.04.027.
[92] D. Berman, A. Erdemir, A. V. Sumant, Graphene: a new emerging lubricant, Materials Today 17 (2014) 31-42, https://doi.org/10.1016/j.mattod.2013.12.003.
[93] G. De Bellis, A. Tamburrano, A. Dinescu, M. Laura Santarelli, M. Sabrina Sarto, Electromagnetic properties of composites containing graphite nanoplatelets at radio frequency, Carbon 49 (2011) 4291-4300, https://doi.org/10.1016/j.carbon.2011.06.008.
[94] S.S. Kiong Kiu, S. Yusup, C. Vui Soon, T. Arpin, S. Samion, R.N. Mohamad Kamil, Tribological investigation of graphene as lubricant additive in vegetable oil, Journal of Physical Science 28 (2017) 257-267, http://dx.doi.org/10.21315/jps2017.28.s1.17.
[95] V. Eswaraiah, V. Sankaranarayana, S. Ramaprabhu, Graphene-based engine oil nanofluids for tribological applications, ACS Applied Materials & Interfaces 3 (2011) 4221-4227, https://doi.org/10.1021/am200851z.
[96] D. Zheng, Z. Cai, M. Shen, Z. Li, M. Zhu, Investigation of the tribology behaviour of the graphene nanosheets as oil additives on textured alloy cast iron surface, Applied Surface Science 387 (2016) 66-75, https://doi.org/10.1016/j.apsusc.2016.06.080.
[97] P. Radhika, C.B. Sobhan, S. Chakravorti, Improved tribological behavior of lubricating oil dispersed with hybrid nanoparticles of functionalized carbon spheres and graphene nano platelets, Applied Surface Science 540 (2021) 148402, https://doi.org/10.1016/j.apsusc.2020.148402.
[98] J. M. Liñeira del Río, M. J. G. Guimarey, M. J. P. Comuñas, E. R. López, A. Amigo, J. Fernández, Thermophysical and tribological properties of dispersions based on graphene and a

trimethylolpropane trioleate oil, Journal of Molecular Liquids 268 (2018) 854-866, https://doi.org/10.1016/j.molliq.2018.07.107.
[99] J.M. Liñeira del Río, E.R. López, J. Fernández, Tribological properties of graphene nanoplatelets or boron nitride nanoparticles as additives of a polyalphaolefin base oil, Journal of Molecular Liquids 333 (2021) 115911, https://doi.org/10.1016/j.molliq.2021.115911.
[100] M.J.G. Guimarey, J.L. Viesca, A.M. Abdelkader, B. Thomas, A. Hernández Battez, M. Hadfield, Electrochemically exfoliated graphene and molybdenum disulfide nanoplatelets as lubricant additives, Journal of Molecular Liquids 342 (2021) 116959, https://doi.org/10.1016/j.molliq.2021.116959.
[101] J.M. Liñeira del Río, M.J.G. Guimarey, J.I. Prado, L. Lugo, E.R. López, M.J.P. Comuñas, Improving the tribological performance of a biodegradable lubricant adding graphene nanoplatelets as additives, Journal of Molecular Liquids 345 (2022) 117-797, https://doi.org/10.1016/j.molliq.2021.117797.
[102] T. Mosuang, J. Lowther, Relative stability of cubic and different hexagonal forms of boron nitride, Journal of Physics and Chemistry of Solid 63 (2002) 363-368, https://doi.org/10.1016/S0022-3697(00)00254-7.
[103] J.M. Liñeira del Río, M.J.G. Guimarey, M.J.P. Comuñas, E.R. López, J.I. Prado, L. Lugo, J. Fernández, Tribological and Thermophysical Properties of Environmentally-Friendly Lubricants Based on Trimethylolpropane Trioleate with Hexagonal Boron Nitride Nanoparticles as an Additive, Coatings 9 (2019) 509, https://doi.org/10.3390/coatings9080509.
[104] T.Q.P. Vuong, S. Liu, A. Van der Lee, R. Cuscó, L. Artús, T. Michel, P. Valvin, J. H.Edgar, G. Cassabois, B. Gil, Isotope engineering of van der Waals interactions in hexagonal boron nitride, Nature materials 17 (2018) 152-158, https://doi.org/10.1038/nmat5048.
[105] N. Ay, G.M. Ay, Y. Göncü, Environmentally friendly material: Hexagonal boron nitride, Journal of Boron 1 (2016) 66-73,
[106] F.U. Shah, S. Glavatskih, O.N. Antzutkin, Boron in Tribology: From Borates to Ionic Liquids, Tribology Letters 51 (2013) 281-301, https://doi.org/10.1007/s11249-013-0181-3.
[107] D. V. Shtansky, K. L. Firestein, D. V. Golberg, Fabrication and application of BN nanoparticles, nanosheets and their nanohybrids, Nanoscale 10 (2018) 17477-17493, http://doi.org/10.1039/C8NR05027A.
[108] P.D. Srivyas, M.S. Charoo, Nano lubrication behaviour of Graphite, h-BN and Graphene Nano Platelets for reducing friction and wear, Materials Today: Proceedings 44 (2020) 7-11, https://doi.org/10.1016/j.matpr.2020.04.785.
[109] Q. Wan, Y. Jin, P. Sun, Y. Ding, Tribological Behaviour of a Lubricant Oil Containing Boron Nitride Nanoparticles, Procedia Engineering 102 (2015) 1038-1045, https://doi.org/10.1016/j.proeng.2015.01.226.
[110] O.N. Çelik, N. Ay, Y. Göncü, Effect of Nano Hexagonal Boron Nitride Lubricant Additives on the Friction and Wear Properties of AISI 4140 Steel, Particulate Science and Technology 31 (2013) 501-506, https://doi.org/10.1080/02726351.2013.779336.
[111] S. Ramteke, H. Chelladurai, Examining the role of hexagonal boron nitride nanoparticles as an additive in the lubricating oil and studying its application, Proceedings of the Institution of Mechanical Engineers, Part N: Journal of Nanomaterials, Nanoengineering and Nanosystems 234 (2020) 19-36, https://doi.org/10.1177/2397791420911811.
[112] Y. Wang, Z. Wan, L. Lu, Z. Zhang, Y. Tang, Friction and wear mechanisms of castor oil with addition of hexagonal boron nitride nanoparticles, Tribology International 124 (2018) 10-22, https://doi.org/10.1016/j.triboint.2018.03.035.

[113] I.E. Uflyand, V.A. Zhinzhilo, V.E. Burlakova, Metal-containing nanomaterials as lubricant additives: State-of-the-art and future development, Friction 7 (2019) 93-116, http://10.1007/s40544-019-0261-y.
[114] M. Chirita, I. Grozescu, L. Taubert, H. Radulescu, E. Princz, Fe_2O_3–nanoparticles, physical properties and their photochemical and photoelectrochemical applications, Chem. Bull 54 (2009) 1-8,
[115] M. S. Chavali, M. P. Nikolova, Metal oxide nanoparticles and their applications in nanotechnology, SN Applied Sciences 1 (2019) 607, https://doi.org/10.1007/s42452-019-0592-3.
[116] M. Tahmasebi Sulgani, A. Karimipour, Improve the thermal conductivity of 10w40-engine oil at various temperature by addition of Al_2O_3/Fe_2O_3 nanoparticles, Journal of Molecular Liquids 283 (2019) 660-666, https://doi.org/10.1016/j.molliq.2019.03.140.
[117] A. Majeed Faraj Saeid, N. Bin Mohd Yusof, M. Azlan Suhaimi, N. Mejid Elsiti, S. Norbiha bt A. Aziz, Effect of paraffin oil with XGnP and Fe_2O_3 nanoparticles on tribological properties, Materials Today: Proceedings 27 (2020) 1685-1688, https://doi.org/10.1016/j.matpr.2020.03.576.
[118] S. B, P. Tamilarasu, P. Amutha, S. N, Triboengineered Industrial Lubricant Using Perlite Loaded Fe_2O_3 Nano-Additives: A Greener Approach, (2021),
[119] M. Parashar, V.K. Shukla, R. Singh, Metal oxides nanoparticles via sol–gel method: a review on synthesis, characterization and applications, Journal of Materials Science: Materials in Electronics 31 (2020) 3729-3749, https://doi.org/10.1007/s10854-020-02994-8.
[120] S. Akin, S. Sonmezoglu, Metal oxide nanoparticles as electron transport layer for highly efficient dye-sensitized solar cells, Emerging materials for energy conversion and storage (2018) 39-79, https://doi.org/10.1016/B978-0-12-813794-9.00002-8.
[121] V.S. Mello, M.F. Trajano, A.E.D.S. Guedes, S.M. Alves, Comparison Between the Action of Nano-Oxides and Conventional EP Additives in Boundary Lubrication, Lubricants 8 (2020) 54, https://www.mdpi.com/2075-4442/8/5/54.
[122] LubriCAD-national project, nanochemistry solutions in technical lubricants additive improvements, https://pmf.unibl.org/lubricad/, 2021.
[123] N.F. Azman, S. Samion, Dispersion Stability and Lubrication Mechanism of Nanolubricants: A Review, International Journal of Precision Engineering and Manufacturing-Green Technology 6 (2019) 393-414, https://doi.org/10.1007/s40684-019-00080-x.
[124] R.D. Rogers, K.R. Seddon, Ionic Liquids--Solvents of the Future?, Science 302 (2003) 792-793, https://doi.org/10.1126/science.1090313.
[125] D. R. MacFarlane, M. Kar, J. M. Pringle, Fundamentals of ionic liquids: from chemistry to applications. John Wiley & Sons. (2017).http://dx.doi.org/10.1002/9783527340033.
[126] S.K. Singh, A.W. Savoy, Ionic liquids synthesis and applications: An overview, Journal of Molecular Liquids 297 (2020) 112038, https://doi.org/10.1016/j.molliq.2019.112038.
[127] J.D. Holbrey, K.R. Seddon, Ionic Liquids, Clean Products and Processes 1 (1999) 223-236, https://doi.org/10.1007/s100980050036.
[128] G. Tiago, J. Restolho, A. Forte, R. Colaço, L. Branco, B. Saramago, Novel ionic liquids for interfacial and tribological applications, Colloids Surfaces A: Physicochemical Engineering Aspects 472 (2015) 1-8, https://doi.org/10.1016/j.colsurfa.2015.02.030.
[129] C. Ye, W. Liu, Y. Chen, L. Yu, Room-temperature ionic liquids: a novel versatile lubricant, Chemical Communications (2001) 2244-2245, https://doi.org/10.1039/B106935G.
[130] A.J. Greer, J. Jacquemin, C. Hardacre, Industrial Applications of Ionic Liquids, Molecules 25 (2020) 5207, https://www.mdpi.com/1420-3049/25/21/5207.

[131] A. E. Somers, R. E. Yunis, M. B. Armand, J. M. Pringle, D. R. MacFarlane, M. Forsyth, Towards phosphorus free ionic liquid anti-wear lubricant additives, Lubricants 4 (2016) 22, https://doi.org/10.3390/lubricants4020022.
[132] H. Xiao, Ionic Liquid Lubricants: Basics and Applications, Tribology Transactions 60 (2017) 20-30, https://doi.org/10.1080/10402004.2016.1142629.
[133] M. Uerdingen, C. Treber, M. Balser, G. Schmitt, C. Werner, Corrosion behaviour of ionic liquids, Green Chemistry 7 (2005) 321-325, https://doi.org/10.1039/B419320M.
[134] L. Pisarova, C. Gabler, N. Dörr, E. Pittenauer, G. Allmaier, Thermo-oxidative stability and corrosion properties of ammonium based ionic liquids, Tribology International 46 (2012) 73-83, https://doi.org/10.1016/j.triboint.2011.03.014.
[135] C.M.C.G. Fernandes, A. Hernandez Battez, R. González, R. Monge, J. Viesca, A. García, R. C. Martins, J.H.O. Seabra, Torque loss and wear of FZG gears lubricated with wind turbine gear oils using an ionic liquid as additive, Tribology International 90 (2015) 306-314, https://doi.org/10.1016/j.triboint.2015.04.037.
[136] M. Cai, Y. Liang, M. Yao, Y. Xia, F. Zhou, W. Liu, Imidazolium ionic liquids as antiwear and antioxidant additive in poly (ethylene glycol) for steel/steel contacts, ACS Applied Materials & Interfaces 2 (2010) 870-876, https://doi.org/10.1021/am900847j.
[137] E. Cigno, C. Magagnoli, M. S. Pierce, P. Iglesias, Lubricating ability of two phosphonium-based ionic liquids as additives of a bio-oil for use in wind turbines gearboxes, Wear 376-377 (2017) 756-765, https://doi.org/10.1016/j.wear.2017.01.010.
[138] I. Otero, E. R. López, M. Reichelt, M. Villanueva, J. Salgado, J. Fernández, Ionic Liquids Based on Phosphonium Cations As Neat Lubricants or Lubricant Additives for a Steel/Steel Contact, ACS Applied Materials & Interfaces 6 (2014) 13115-13128, https://doi.org/10.1021/am502980m.
[139] R. González, M. Bartolomé, D. Blanco, J.L. Viesca, A. Fernández González, A. Hernández Battez, Effectiveness of phosphonium cation-based ionic liquids as lubricant additive, Tribology International 98 (2016) 82-93, https://doi.org/10.1016/j.triboint.2016.02.016.
[140] P. Oulego, D. Blanco, D. Ramos, J.L. Viesca, M. Díaz, A. Hernández Battez, Environmental properties of phosphonium, imidazolium and ammonium cation-based ionic liquids as potential lubricant additives, Journal of Molecular Liquids 272 (2018) 937-947, https://doi.org/10.1016/j.molliq.2018.10.106.
[141] J. Qu, H. Luo, M. Chi, C. Ma, P. J. Blau, S. Dai, M. B. Viola, Comparison of an oil-miscible ionic liquid and ZDDP as a lubricant anti-wear additive, Tribology International 71 (2014) 88-97, https://doi.org/10.1016/j.triboint.2013.11.010.
[142] N. Murthy, A.K. Rai, S. Berkebile, Improved Loss-of-Lubrication Performance with Lubricants Containing Nano-Graphene Platelets and Ionic Liquids, Journal of Applied Sciences 10 (2020) 7958, https://doi.org/10.3390/app10227958.
[143] M. A. Gutierrez, M. Haselkorn, P. Iglesias, The Lubrication Ability of Ionic Liquids as Additives for Wind Turbine Gearboxes Oils, Lubricants 4 (2016) 14, https://www.mdpi.com/2075-4442/4/2/14.
[144] K.J. Fraser, D.R. MacFarlane, Phosphonium-based ionic liquids: an overview, Australian journal of chemistry 62 (2009) 309-321, https://doi.org/10.1071/CH08558.
[145] S. Khazalpour, M. Yarie, E. Kianpour, A. Amani, S. Asadabadi, J.Y. Seyf, M. Rezaeivala, S. Azizian, M.A. Zolfigol, Applications of phosphonium-based ionic liquids in chemical processes, Journal of the Iranian Chemical Society 17 (2020) 1775-1917, https://doi.org/10.1007/s13738-020-01901-6.

[146] J. Yu, R.T. Wheelhouse, M.A. Honey, N. Karodia, Synthesis and characterisation of novel nopyl-derived phosphonium ionic liquids, Journal of Molecular Liquids 316 (2020) 113857, https://doi.org/10.1016/j.molliq.2020.113857.
[147] Z. He , P. Alexandridis, Ionic liquid and nanoparticle hybrid systems: Emerging applications, Advances in Colloid Interface Science 244 (2017) 54-70, https://doi.org/10.1016/j.cis.2016.08.004.
[148] A. Sani, A. Sahab, A.R. Erween, T. Norfazillah, K. Kamaruddin, R. Mohammad Zulafif, Performance Evaluation of Palm-Olein TMP Ester Containing Hexagonal Boron Nitride and an Oil Miscible Ionic Liquid as Bio-Based Metalworking Fluids, Journal of Mechanical Engineering (2017) 223-234, https://ir.uitm.edu.my/id/eprint/39264.
[149] M. Upendra, V. Vasu, Synergistic Effect Between Phosphonium-Based Ionic Liquid and Three Oxide Nanoparticles as Hybrid Lubricant Additives, Journal of Tribology 142 (2020) 052101, https://doi.org/10.1115/1.4045769.
[150] A.V. Bondarev, A. Fraile, T. Polcar, D.V. Shtansky, Mechanisms of friction and wear reduction by h-BN nanosheet and spherical W nanoparticle additives to base oil: Experimental study and molecular dynamics simulation, Tribology International 151 (2020) 106493, https://doi.org/10.1016/j.triboint.2020.106493.
[151] C.M. Taylor, Engine tribology.(Vol. 26): Elsevier. (1993).
[152] C. M.C.G. Fernandes, L. Blazquez, J. Sanesteban, R. C. Martins, J. H.O. Seabra, Energy efficiency tests in a full scale wind turbine gearbox, Tribology International 101 (2016) 375-382, https://doi.org/10.1016/j.triboint.2016.05.001.
[153] R. Monge, R. González, A. Hernández Battez, A. Fernández González, J. Viesca, A. García, M. Hadfield, Ionic liquids as an additive in fully formulated wind turbine gearbox oils, Wear 328 (2015) 50-63, https://doi.org/10.1016/j.wear.2015.01.041.
[154] B.R. Höhn, K. Michaelis, M. Hinterstoißer, Influence factors on gearbox power loss, 3rd International Conference on Integrity, Reliability and Failure, 2009, pp. 1-17.
[155] M. J. G. Guimarey, M. J. P. Comuñas, E. R. López, A. Amigo, J. Fernández, Thermophysical properties of polyalphaolefin oil modified with nanoadditives, The Journal of Chemical Thermodynamics 131 (2019) 192-205, https://doi.org/10.1016/j.jct.2018.10.035.
[156] X. Liu, F. Zhou, Y. Liang, W. Liu, Tribological performance of phosphonium based ionic liquids for an aluminum-on-steel system and opinions on lubrication mechanism, Wear 261 (2006) 1174-1179, https://doi.org/10.1016/j.wear.2006.03.018.
[157] S. Cowie, P. K.Cooper, R. Atkin, H. Li, Nanotribology of Ionic Liquids as Lubricant Additives for Alumina Surfaces, The Journal of Physical Chemistry C 121 (2017) 28348-28353, https://doi.org/10.1021/acs.jpcc.7b09879.
[158] P. K. Cooper, J. Staddon, S. Zhang, Z. M. Aman, R. Atkin, H. Li, Nano- and Macroscale Study of the Lubrication of Titania Using Pure and Diluted Ionic Liquids, Front Chem 7 (2019) 287-287, https://doi.org/10.3389/fchem.2019.00287.
[159] R. González, J.L. Viesca, A. Hernández Battez, M. Hadfield, A. Fernández-González, M. Bartolomé, Two phosphonium cation-based ionic liquids as lubricant additive to a polyalphaolefin base oil, Journal of Molecular Liquids 293 (2019) 111536, https://doi.org/10.1016/j.molliq.2019.111536.
[160] B.C. Smith, Fundamentals of Fourier transform infrared spectroscopy. CRC press. (2011).
[161] D. Kumar Devendiran, V. Arasu Amirtham, A review on preparation, characterization, properties and applications of nanofluids, Renewable and Sustainable Energy Reviews 60 (2016) 21-40, https://doi.org/10.1016/j.rser.2016.01.055.

[162] W. Yu, H. Xie, A Review on Nanofluids: Preparation, Stability Mechanisms, and Applications, Journal of Nanomaterials 2012 (2012) 435873, https://doi.org/10.1155/2012/435873.
[163] S. Chakraborty, P.K. Panigrahi, Stability of nanofluid: A review, Applied Thermal Engineering 174 (2020) 115259, https://doi.org/10.1016/j.applthermaleng.2020.115259.
[164] S. Umer Ilyas, R. Pendyala, N. Marneni, Stability and Agglomeration of Alumina Nanoparticles in Ethanol-Water Mixtures, Procedia Engineering 148 (2016) 290-297, https://doi.org/10.1016/j.proeng.2016.06.616.
[165] S. Mukherjee, P. Chandra Mishra, P. Chaudhuri, Stability of Heat Transfer Nanofluids – A Review, ChemBioEng Reviews 5 (2018) 312-333, https://doi.org/10.1002/cben.201800008.
[166] A. Ghadimi, R. Saidur, H.S.C. Metselaar, A review of nanofluid stability properties and characterization in stationary conditions, International Journal of Heat and Mass Transfer 54 (2011) 4051-4068, https://doi.org/10.1016/j.ijheatmasstransfer.2011.04.014.
[167] H. P. Mungse, O. P. Khatri, Chemically Functionalized Reduced Graphene Oxide as a Novel Material for Reduction of Friction and Wear, The Journal of Physical Chemistry C 118 (2014) 14394-14402, https://doi.org/10.1021/jp5033614.
[168] F. M. Gaciño, T. Regueira, L. Lugo, M. J. P. Comuñas, J. Fernández, Influence of molecular structure on densities and viscosities of several ionic liquids, Journal of Chemical Engineering Data 56 (2011) 4984-4999, https://doi.org/10.1021/je200883w.
[169] P. Heyer, J. Läuger, Correlation between friction and flow of lubricating greases in a new tribometer device, Lubrication Science 21 (2009) 253-268, https://doi.org/10.1002/ls.88.
[170] F. Moreira-Izurieta, A. Jabbarzadeh, Tribological Studies in Cartilaginous Tissue of Lamb Synovial Joints Lubricated by Distilled Water and Interstitial-Fluid-Like Solution, Tribology in Industry 39 (2017) 319–328, http://dx.doi.org/10.24874/ti.2017.39.03.06.
[171] C. Verma, E. E. Ebenso, M.A. Quraishi, Ionic liquids as green and sustainable corrosion inhibitors for metals and alloys: An overview, Journal of Molecular Liquids 233 (2017) 403-414, https://doi.org/10.1016/j.molliq.2017.02.111.
[172] A. Hernández Battez, M. Bartolomé, D. Blanco, J.L. Viesca, A. Fernández González, R. González, Phosphonium cation-based ionic liquids as neat lubricants: Physicochemical and tribological performance, Tribology International 95 (2016) 118-131, https://doi.org/10.1016/j.triboint.2015.11.015.
[173] P. Kumar, M.F. Wani, Effect of temperature on the friction and wear properties of graphene nano-platelets as lubricant additive on Al-25Si alloy, Materials Research Express 6 (2019) 046513, http://10.1088/2053-1591/aafb46.
[174] Arcelor Mittal Prijedor, https://prijedor.arcelormittal.com/en/who-we-are/arcelormmittal-prijedor, 2021.
[175] T. Đukić, D. Stević, R. Kukobat, Y. Hattori, K. Sagisaka, M. Pisaturo, A. Senatore, S.G. Atlagić, Remediated Waste Iron-Based Nanomaghemite as Friction Modifier for Lubricants, V International Congress: Engineering, Environment and Materials In Processing Industry, Jahorina, Bosnia and Herzegovina, (2017), http://dx.doi.org/10.13140/RG.2.2.28278.06724.
[176] J. He, J. Sun, Y. Meng, H. Tang, P. Wu, Improved lubrication performance of MoS_2-Al_2O_3 nanofluid through interfacial tribochemistry, Colloids and Surfaces A: Physicochemical and Engineering Aspects 618 (2021) 126428, https://doi.org/10.1016/j.colsurfa.2021.126428.
[177] A.V. Sidashov, A.T. Kozakov, S.I. Yares'ko, N.G. Kakovkina, D.S. Manturov, Study of the phase composition and tribological properties of carbon tool steels after laser surface hardening by quasi - CW fiber laser, Surface and Coatings Technology 385 (2020) 125427, https://doi.org/10.1016/j.surfcoat.2020.125427.

[178] M. Khoshnam, H. Salimijazi, Synthesis and characterization of magnetic-photocatalytic Fe_3O_4/SiO_2/a-Fe_2O_3 nano core-shell, Surfaces and Interfaces 26 (2021) 101322, https://doi.org/10.1016/j.surfin.2021.101322.
[179] M.A. Hassaan, A. El Nemr, M.R. Elkatory, S. Ragab, M.A. El-Nemr, A. Pantaleo, Synthesis, Characterization, and Synergistic Effects of Modified Biochar in Combination with α-Fe_2O_3 NPs on Biogas Production from Red Algae Pterocladia capillacea, Sustainability 13 (2021) 9275, https://doi.org/10.3390/su13169275.
[180] N.A. Wójcik, N.S. Tagiara, S. Ali, K. Górnicka, H. Segawa, T. Klimczuk, B. Jonson, D. Möncke, E.I. Kamitsos, Structure and magnetic properties of BeO-Fe_2O_3-Al_2O_3-TeO_2 glass-ceramic composites, Journal of the European Ceramic Society 41 (2021) 5214-5222, https://doi.org/10.1016/j.jeurceramsoc.2021.04.005.
[181] M. Doig, P. Camp, The structures of hexadecylamine films adsorbed on iron-oxide surfaces in dodecane and hexadecane, Journal Physical Chemistry Chemical Physics 17 (2015) 5248-5255, https://doi.org/10.1039/C4CP05837B.
[182] R. González, A. Hernández Battez , J.L. Viesca, A. Higuera Garrido, A. Fernández González, Lubrication of DLC Coatings with Two Tris(pentafluoroethyl)trifluorophosphate Anion-Based Ionic Liquids, Tribology Transactions 56 (2013) 887-895, https://doi.org/10.1080/10402004.2013.810319.
[183] A. Ramírez Hernández, C. Aguilar Flores, A. Aparicio Saguilán, Fingerprint analysis of FTIR spectra of polymers containing vinyl acetate, Dyna 86 (2019) 198-205, https://doi.org/10.15446/dyna.v86n209.77513.
[184] J.M. Liñeira del Río, E.R. López, J. Fernández, F. García, Tribological properties of dispersions based on reduced graphene oxide sheets and trimethylolpropane trioleate or PAO 40 oils, Journal of Molecular Liquids 274 (2019) 568-576, https://doi.org/10.1016/j.molliq.2018.10.107.
[185] H. Danjo, W. Sasaki, T. Miyazaki, T. Imamoto, P-Chirogenic phosphonium salts: preparation and use in Rh-catalyzed asymmetric hydrogenation of enamides, Tetrahedron Letters 44 (2003) 3467-3469, https://doi.org/10.1016/S0040-4039(03)00668-3.
[186] M. Praveena, K. Guha, A. Ravishankar, S.K. Biswas, C.D. Bain, V. Jayaram, Total internal reflection Raman spectroscopy of poly(alpha-olefin) oils in a lubricated contact, RSC Advances 4 (2014) 22205-22213, https://doi.org/10.1039/C4RA02261K.
[187] H. Okubo, C. Tadokoro, Y. Hirata, S. Sasaki, In Situ Raman Observation of the Graphitization Process of Tetrahedral Amorphous Carbon Diamond-Like Carbon under Boundary Lubrication in Poly-Alpha-Olefin with an Organic Friction Modifier, Tribology Online 12 (2017) 229-237, https://doi.org/10.2474/trol.12.229.
[188] D. Coronado, J. Wenske, Monitoring the Oil of Wind-Turbine Gearboxes: Main Degradation Indicators and Detection Methods, 6 (2018) 25, https://doi.org/10.3390/machines6020025.
[189] C. Sequeira, A. Pacheco, P. Galego, E. Gorbeña, Analysis of the efficiency of wind turbine gearboxes using the temperature variable, Renewable Energy 135 (2019) 465-472, https://doi.org/10.1016/j.renene.2018.12.040.
[190] B. Gupta, N. Kumar, K. Panda, S. Dash, A.K. Tyagi, Energy efficient reduced graphene oxide additives: Mechanism of effective lubrication and antiwear properties, Scientific Reports 6 (2016) 18372, https://doi.org/10.1038/srep18372.
[191] B. Schlüter, R. Mülhaupt, A. Kailer, Synthesis and Tribological Characterization of Stable Dispersions of Thermally Reduced Graphite Oxide, Tribology Letters 53 (2014) 353-363, https://doi.org/10.1007/s11249-013-0275-y.

[192] V. Zin, S. Barison, F. Agresti, L. Colla, C. Pagura, M. Fabrizio, Improved tribological and thermal properties of lubricants by graphene based nano-additives, RSC Advances 6 (2016) 59477-59486, https://doi.org/10.1039/C6RA12029F.
[193] Y.B. Guo, S.W. Zhang, The tribological properties of multi-layered graphene as additives of PAO2 oil in steel–steel contacts, Lubricants 4 (2016) 30, https://doi.org/10.3390/lubricants4030030.
[194] X. Dou, A.R. Koltonow, X. He, H.D. Jang, Q. Wang, Y.W. Chung, J. Huang, Self-dispersed crumpled graphene balls in oil for friction and wear reduction, Proceedings of the National Academy of Sciences 113 (2016) 1528, https://doi.org/10.1073/pnas.1520994113.

APPENDIX

RESUMO

A Triboloxía, a ciencia que estuda o desgaste, a fricción e a lubricación, ten unha historia tan longa como a da humanidade, einflúe significativamente no aforro enerxético, na atenuación de perdas de materiais e, en consecuencia, na economía. Por este motivo, inténtase reducir substancialmente as perdas por rozamento e desgaste en sistemas lubricados mediante novas solucións tribolóxicas.

Os lubricantes son substancias que axudan a reducir o rozamento entre dúas superficies en contacto directo, o que finalmente tamén pode reducir o desgaste xerado cando estas superficies se moven unha respecto da outra. Un dos criterios máis eficaces para acadar melloras triboloxicas é deseñar novos lubricantes que funcionen como axentes antifricción e antidesgaste. Para tal fin, diminúen a interacción entre as superficies que lubrican, optimizando o rendemento tribolóxico dos lubricantes.

Os lubricantes poden ser de catro tipos diferentes: aceites, graxas, lubricantes penetrantes e lubricantes secos. Os tipos máis utilizados son os aceites e as graxas. Os aceites lubricantes son substancias constituídas por un aceite base (dálle as propiedades físicas) e unha pequena porcentaxe de aditivos (adaptan as propiedades físicas aos requirimentos específicos da aplicación e facilitan as interaccións coas superficies). Os aceites lubricantes, ademais de lubricar, teñen diversas funcións como, arrefriar, evitar a corrosión ou controlar a contaminación, entre outras. Nas aplicacións industriais, a selección de calquera lubricante debe fundamentarse en varios factores, incluíndo función, temperaturas de funcionamento, capacidade mínima e máxima de soporte de carga da película lubricante, tipo de materiais das superficies en contacto, velocidade de funcionamento, estrutura e deseño da máquina operativa, e outros aspectos relacionados co custo, durabilidade e vida útil dos propios lubricantes e da máquina lubricada.

As bases lubricantes pódense clasificar en tres tipos principais: *aceites minerais* que son refinados a partir de petróleo cru por destilación fraccionada e compostos químicamente por hidrocarburos, podendo ser parafínicos, nafténicos ou aromáticos; *aceites sintéticos* que son obtidos mediante síntese química polo que poden ser deseñados para cumprir os requisitos dunha aplicación específica; e *aceites vexetais* que consisten basicamente en triglicéridos que se extraen de plantas (xirasol, coco, colza, palma,...) e teñen un alto índice de lubricidade, alto índice de viscosidade, alto punto de inflamación, baixa volatilidade e altas propiedades dispersantes, aínda que baixo punto de vertedura (*pour point*). Outra clasificación amplamente estendida é a do *American Petroleum Institute* onde as bases lubricantes están agrupadas en cinco categorías: os aceites base dos grupos I–III son refinados a partir de petróleo cru; os aceites base do grupo IV son as polialfaolefinas (PAO, aceites totalmente sintéticos); os aceites base do grupo V son aqueles que non se atopan nas categorías dos grupos I–IV. Este grupo inclúe outros aceites base como siliconas, organofosforados, polialquilenglicoles (PAG), poliolésteres e biolubricantes.

Os aditivos son compostos orgánicos ou inorgánicos que se disolven ou suspenden nos aceites base cando se lles engaden. A maioría dos aditivos clasifícanse segundo a súa función principal para as aplicacións nas que se utiliza o lubricante. Algunhas funcións destes aditivos

inclúen antifricción, antidesgaste, anticorrosión, antioxidantes, melloradores do índice de viscosidade, etc. O lubricante final debe de ser formulado especificamente para cada aplicación.

Para mellorar as propiedades antifricción e antidesgaste, os potenciais lubricantes están en constante evolución tecnolóxica debido aos continuos desenrolos dos compoñentes mecánicos. Por isto, considérase clave mellorar os procesos tribolóxicos o que potenciará o aforro enerxético, ao reducir as perdas económicas e aumentar a durabilidade da máquina.

Por outra banda, considérase que a Nanotecnoloxía terá un papel protagonista nos avances tecnolóxicos do século XXI, e a Triboloxía non é unha excepción. Así, os nanoaditivos son nanomateriais con funcións específicas, e poden reducir a fricción e/ou o desgaste nos sistemas mecánicos. Os nanomateriais son materiais que conteñen partículas nun rango de tamaño, polo menos unha das súas dimensións, entre 1 nm e 100 nm. Poden estar formados por óxidos metálicos (TiO_2, CuO, ZnO, Fe_2O_3, Fe_3O_4,…), metais (Cu, Bi, Fe,…), nitruros e sulfuros (BN, MoS_2, WS_2,…), ou nanopartículas de carbono (diamante, grafeno, nanoplaquetas de grafeno, ou grafito), entre outros. Os nanolubricantes son lubricantes formulados a partir da dispersión de nanoaditivos en aceites base. Dende o punto de vista tribolóxico, o uso de nanomateriais como aditivos antifricción e antidesgaste atraeu a atención de investigadores co fin de deseñar nanolubricantes con mellor rendemento. Varias vantaxes levaron a utilizar estes nanomateriais como nanoaditivos para aceites base, como a) a súa baixa interacción química con outros aditivos necesarios na formulación do produto final, b) a súa capacidade de adherirse ás superficies e, en consecuencia, de formar películas protectoras, c) poden introducir terceiros corpos directamente no contacto, d) a súa capacidade para reparar calquera defecto de desgaste na superficie penetrando en pequenas fendas, e) a súa capacidade de resistir altas temperaturas ou f) a súa alta condutividade térmica.

Os líquidos iónicos (ILs) son compostos completamente formados por ións (anións e catións) cun punto de fusión inferior a 373,15 K. Os ILs presentan, en xeral interesantes propiedades como que son non volátiles, non inflamables ou térmicamente estables. No campo da Triboloxía, os ILs propuxéronse primeiro como lubricantes pero, debido ao seu alto custo, especialmente en comparación cos aceites base minerais e sintéticos convencionais, o seu potencial uso foi relegado a aplicacións críticas, propoñéndose entón o seu uso como aditivos de lubricantes. Os ILs clasifícanse en catro categorías principais en función da súa estrutura catiónica: imidazolio, alquil-amonio, piridinio e fosfonio. Os ILs baseados en fosfonio teñen unha mellor miscibilidade e rendemento tribolóxico cando se usan como aditivos lubricantes en comparación coa maioría dos outros ILs.

Así pois, tanto nanomateriais coma ILs poden presentar características desexables para ser utilizados como aditivos de lubricantes e diferentes estudos no campo puxeron de manifesto prometedores resultados. É mais, a combinación de ILs con nanofases de carbono como aditivos, os chamados *lubricantes ionanocarbonados*, revelou interesantes sinerxías. Xorde entón a idea de si estas sinerxías poden estar presentes tamén ao combinar nanomateriais e ILs como aditivos híbridos aos aceites.

Unha propiedade importante dos lubricantes é a viscosidade debido ao seu papel durante o comportamento do lubricante en réximes de lubricación elastohidrodinámicos e mixtos. É desexable que a adición de aditivos non modifique substancialmente esta propiedade xa que podería empeorar as prestacións do lubricante. O parámetro que da conta de como a viscosidade varía coa temperatura, o que está relativamente relacionado co rango de temperatura de funcionamento do sistema mecánico, é o índice de viscosidade dun lubricante. Ademais, para manter o rendemento do nanolubricante deseñado ao longo do tempo, é fundamental a estabilidade dos aceites base con aditivos. En xeral, e ademais destes factores, o principal factor que se considera crítico é a capacidade deste nanolubricante para mellorar as propiedades

tribolóxicas do aceite base e, en consecuencia, para funcionar como un axente antifricción e antidesgaste e ser de feito un potencial substituto do lubricante convencional.

Por outra banda, a remediación parcial ou total das minas de ferro aínda non está totalmente controlada hoxe en día. Os lodos acumulados no lago dunha mina son os residuos recollidos nos procesos extractivos. Unha forma de remediación é reciclar os lodos e producir a partir deles materiais reutilizables en aplicacións convencionais. Nestes lodos pódense atopar residuos de ferro mesturados con outros materiais, residuos que son potencial, económica e ecolóxicamente aceptables para ser reutilizados. Así, destes residuos pódense sintetizar nanopartículas de óxido de ferro, e usalas como potenciais nanoaditivos para lubricantes.

Esta Tese de Doutoramento ten como obxectivo deseñar novos nanolubricantes formados pola adición de nanoaditivos, aditivos híbridos NP/IL ou NP1/NP2, ou aditivos dobremente híbridos NP1/NP2/IL. PAO32 e PAO10 son os dous aceites base seleccionados neste estudo. Segundo a clasificación API, as PAO pertencen ao grupo IV. As PAO son as bases lubricantes máis utilizadas nos sistemas de caixas de engrenaxes de aeroxeradores e adoitan denominarse pola súa viscosidade cinemática en centistokes (cSt) a 373,15 K. Para as caixas de engrenaxes de aeroxeradores a PAO máis utilizado é a PAO32 mentres que a PAO10 utilízase nos motores de automoción. Un aceite base PAO32 foi fornecido por Repsol e outro PAO32, xunto co PAO10, polo grupo Tehnosint. Nesta Tese de Doutoramento utilizáronse tres nanomateriais diferentes. Dous deles foron subministrados por Iolitec (nanopartículas de nitruro de boro hexagonal, h-BN, e nanoplaquetas de grafeno, GnP) mentres o terceiro foi sintetizado no Departamento de Química da Universidade de Banja Luka en Bosnia e Hercegovina (nanopartículas de óxido de ferro). As h-BN NPs (materiais ecolóxicos) teñen un diámetro medio duns 70 nm e unha densidade aparente de 2,29 g cm^{-3}, as GnP (dispoñibles comercialmente con prezos baixos) teñen un tamaño lateral medio de 11 a 15 nm e unha densidade aparente de 2,25 g cm^{-3} e as NPs de óxido de ferro sintetizadas (relativamente non tóxicas) teñen un tamaño entre 5 e 30 nm. Ademais, seleccionáronse tres ILs de fosfonio como aditivos neste estudo. Bis(2-etilhexil)fosfato de trihexiltetradecilfosfonio, IL1, dietilfosfato de tributiletilfosfonio, IL2, e bis(2,4,4-trimetilpentil)fosfinato de trihexiltetradecilfosfonio, IL3, tamén foron proporcionados por Iolitec.

O aceite base PAO32 fornecido por Repsol, os tres ILs e as NPs de óxido de ferro sintetizadas foron caracterizados mediante diferentes técnicas, incluíndo espectroscopía infravermella (FTIR), espectroscopía Raman e/ou microscopía electrónica de varrido (SEM). Algunhas das análises realizáronse en colaboración co Servizo de Apoio á Investigación (RIAIDT) da Universidade de Santiago de Compostela e outras co Departamento de Química da Universidade de Banja Luka. Ademais, e para os tres ILs, realizáronse probas de corrosión para identificar si algún dos ILs produce corrosión na superficie de discos de aceiro AISI 52100. A temperatura ambiente, só o disco probado con IL2 mostrou corrosión. Para a proba realizada a 373,15 K non se detectou corrosión por causa dos ILs. Concluíuse que a temperatura ambiente o motivo da corrosión do aceiro era o contido en auga de IL2.

Para a preparación dos nanolubricantes que non conteñen IL utilizouse o método de dous pasos. Este método implica a adición do nanoaditivo ao aceite base que despois é dispersado no lubricante mediante métodos físicos como mestura, axitación ultrasónica, homoxeneización a alta presión, axitación de forza magnética intensa, etc. Os nanolubricantes híbridos prepáraronse mesturando continuamente os nanoaditivos e o IL nun morteiro de ágata durante dez minutos antes da súa completa adición ao aceite base. Durante a preparación dos nanolubricantes, as masas de h-BN, GnP e PAO32 (Repsol) determináronse cunha microbalanza de alta precisión Sartorius MC 210P cunha incerteza no rango de masas das medidas deste traballo de 0,00001 g e as masas de NPs de óxido de ferro, PAO32 (Tehnosint)

e PAO10 mediante unha balanza analítica Kern ABJ 220-4NM. No caso dos ILs calculouse o equivalente da masa requirida en volume, e succionouse dito volume mediante unha micropipeta automática. Despois da preparación dos nanolubricantes, para obter mostras homoxéneas, mantivéronse nun baño ultrasónico, cunha potencia efectiva de 180 W e unha frecuencia de axitación de 37 kHz. Todos os nanolubricantes sonicáronse continuamente durante 4 h. Preparáronse dous conxuntos de cada nanolubricante, excepto dos baseados en NPs de óxido de ferro. Un conxunto emprégase para analizar a estabilidade e o outro para estudos termofísicos e tribolóxicos. O conxunto de nanolubricantes baseados en NPs de óxido de ferro utilizáronse só para a observación da estabilidade.

Un reto crítico nesta tese de doutoramento é obter potenciais nanolubricantes estables durante longos períodos de tempo que poidan substituír aos lubricantes convencionais. Como se mencionou anteriormente, un conxunto completo de nanolubricantes preparados adicouse a ser preservado sen ningunha perturbación para o control da estabilidade. As mostras foron controladas visualmente tomando fotos de cando en vez para identificar calquera sedimentación parcial ou total nos recipientes. Algúns nanolubricantes presentaron estabilidade mínima de 240 días mentres que outros sedimentaron durante a primeira semana desde a súa preparación. En canto ás propiedades termofísicas dos nanolubricantes baseados en PAO32 (Repsol), os parámetros medidos foron a densidade, a viscosidade e o índice de viscosidade. O dispositivo utilizado foi un viscosímetro Stabinger SVM 3000 de Anton Paar, que pode funcionar a presión atmosférica no rango de temperaturas de 233,15 a 378,15 K, no rango de densidades de 0,65 a 3 g cm^{-3} e no rango de viscosidade de 0,2 a 20000 mm^2/s. As medicións tribolóxicas consistiron na determinación do coeficiente de fricción (COF) e do desgaste, para o cal empregáronse catro dispositivos diferentes. O COF mediuse mediante un tribómetro CSM estándar (CSM Instruments, actualmente Anton Paar) e mediante unha célula tribolóxica (Tribo-cell T-PTD200) montada nun reómetro Anton Paar MCR302. Para o primeiro dispositivo, utilizouse a configuración de bola sobre disco en movemento de rotación. Nesta configuración, unha bola de 6 mm de diámetro, fabricada en aceiro AISI 52100 e cunha rugosidade, Ra, de 0,05 μm e unha dureza Rockwell "C" de 58–66, está en contacto cun disco que rota, de 10 mm de diámetro tamén feito de aceiro AISI 52100, sendo o seu acabado superficial (Ra) 0,02 μm e a dureza 190–210 HV3. As condicións do sistema fixáronse en: unha carga de 20 N, correspondente a unha presión máxima de contacto de 1,79 GPa, un radio de traxectoria de 3 mm, unha velocidade de 0,10 m s^{-1}, unha distancia de esvaramento de 340 m, operando o dispositivo a temperatura ambiente (~294 K). Para o segundo dispositivo, realizáronse probas nunha configuración de bola sobre tres pins. Así, a bola de 12,7 mm de diámetro de aceiro cromado AISI 52100, é fixada no eixe axial do reómetro, verticalmente en contacto puntual cos tres pins (6 mm de diámetro e 6 mm de altura). Os experimentos realizáronse baixo unha forza axial de 42,43 N, que provoca tres forzas normais de 21,21 N actuando sobre cada pin. As outras condicións foron: velocidade angular de rotación do eixe de 213 rpm, unha distancia de esvaramento de 340 m, e temperaturas de 298,15 K ou 353,15 K. O desgaste determinouse mediante un perfilómetro óptico 3D e un microscopio electrónico de varrido (SEM). Para o primeiro dispositivo os parámetros medidos da pegada de desgaste xerada na superficie dos discos ou cilindros debido á proba tribolóxica foron: o diámetro da pegada de desgaste, o volume, a área de sección transversal, a profundidade máxima e o valor medio da rugosidade (Ra). O segundo dispositivo (SEM) utilizouse para obter imaxes de alta resolución da pegada de desgaste para caracterizar o tipo de desgaste superficial.

En total tres mesturas (PAO32/IL), oito nanodispersions (PAO32/NP ou PAO10/NP), dez nanodispersions híbridas (PAO32/NP/IL ou PAO32/NP1/NP2) e tres nanodispersions dobremente híbridas (PAO32/NP1/NP2/IL) foron preparadas. Tomando como base estudos

previos, a concentración dos ILs seleccionada foi do 1 wt%, mentres aquelas dos nanomateriais, h-BN e GnP, foron 0.1 wt% para h-BN e 0.05 wt% para GnP, concentracións óptimas obtidas en probas de fricción preliminares, nas cales tres dispersións de cada nanomaterial en PAO32 con concentracións 0,025, 0,05 ou 0,1 wt%, foron analizadas. Ademais, outras tres concentracións en masa (0,1, 0,25 e 0,5 wt%) foron seleccionadas para preparar, en PAO10 e en PAO32, as dispersións baseadas en NPs de óxido de ferro.

Os nanolubricantes menos estables foron os baseados en NPs de óxido de ferro, con estabilidades non máis aló de cinco días. Pola contra, os nanolubricantes baseados en h-BN, GnP e IL foron máis estables. Algúns dos nanolubricantes mantivéronse estables un mínimo de 240 días (tempo que durou a observación) como: PAO32/GnP, PAO32/GnP/IL1 e PAO32/GnP/IL3, mentres que outros, comezaron a mostrar unha sedimentación parcial despois de 30 días da preparación, por exemplo PAO32/h-BN, ou despois de 60 días (PAO32/h-BN/IL2). Ademais as mesturas PAO32/IL non mostraron signos de inmiscibilidade durante dous anos. Todos os aditivos (h-BN, GnP ou IL) produciron pequenos cambios tanto na densidade como na viscosidade do PAO32. O cambio relativo medio na densidade variou entre 0,053 % e 0,44 %, na viscosidade variou entre 1,8 % e 7,6 % e o cambio relativo no índice de viscosidade variou entre -1,7 % e 0,53 %, sendo a adición do aditivo IL2 o que provocou as variacións máis altas. En xeral, os nanolubricantes mostraron melloras nas propiedades tribolóxicas en comparación coas medidas ao usar PAO32 como lubricante base. Así, observouse que o COF de todos os nanolubricantes redúcese con respecto ao do PAO32 sendo a mellor redución deste coeficiente dun 40 % cando se utiliza como nanolubricante a nanodispersión dobre híbrida PAO32/IL3/GnP/h-BN a temperatura ambiente, mentres que a alta temperatura (353,15 K) a redución máxima da fricción foi dun 28 %, correspondente á nanodispersión híbrida PAO/IL2/h-BN. A mais alta redución do desgaste (99 %, en termos de volume de pegada de desgaste) obtívose cando se utilizou a nanodispersión híbrida PAO/IL2/h-BN a 353,15 K, mentres que a temperatura ambiente a maior redución do desgaste foi obtida usando como lubricante a nanodispersión híbrida PAO32/IL2/GnP (27 % en canto á profundidade máxima da pegada de desgaste). Ademais, a formación de tribopelículas protectoras polo IL e os nanoaditivos evidenciouse mediante microscopía Raman, e que o efecto reparador é o principal mecanismo polo cal estes nanomateriais actúan como aditivos modificadores da fricción e o desgaste mediante medidas de rugosidade. Finalmente, presentáronse algúns efectos sinérxicos entre os dous nanomateriais (h-BN e GnP) así como entre un deles ou os dous cun IL como aditivos híbridos ou dobres híbridos para PAO32.

En canto á síntese de NPs de óxido de ferro, utilizáronse lodos dunha mina de ferro situada en Omarska (Bosnia e Hercegovina). Estes lodos (residuos acumulados xerados a partir da extracción do mineral de ferro) foron dixeridos, tratados e despois secados para producir as NPs de óxido de ferro. A morfoloxía destes NPs caracterizouse utilizando un microscopio electrónico de transmisión de alta resolución (HRTEM, JEOL JEM-2010, Xapón) a unha tensión de aceleración de 200 kV, e a composición da mostra mediante un difractómetro de raios X (XRD, Rigaku Ultima IV, Xapón) no rango 2θ de 0°-90° con radiación Cu-Kα ($\lambda = 1{,}5418$ Å). Os resultados mostraron que as NPs de óxido de ferro sintetizadas teñen un tamaño entre 5 e 30 nm, é que as nanopartículas son de óxidos de ferro sendo o predominante Fe_2O_3, estando tamén presentes, en menor medida, nanopartículas de Fe_3O_4. Estas NPs foron utilizadas como nanoaditivos para PAO32 e PAO10. Preparáronse seis dispersións (PAO/x NPs, x=0,1, 0,25 e 0,5 % en peso). A observación visual e os espectros UV das dispersións determinados cun espectrómetro UV/VIS de Perkin Elmer lambda 25 a unha lonxitude de onda de 622 nm, mostrou que estes nanolubricantes eran estables ata cinco días desde a súa

preparación. Por este motivo, non se realizaron máis estudos tribolóxicos para estes nanolubricantes deseñados.

Como conclusión, os estudos realizados acadaron os principais obxectivos desta Tese Doutoral, obténdose potenciais nanolubricantes estables ata oito meses mais eficientes coa base utilizando diferentes aditivos para o aceite base PAO32.

This Doctoral Thesis presents new designed nanolubricants as potential substitutes of conventional lubricants. Hexagonal boron nitride nanoparticles, graphene nanoplatelets, iron oxide nanoparticles (synthetized from iron mine sludge), three phosphonium ionic liquids and two polyalphaolefin base oils (PAO32 and PAO10) were the materials selected. The techniques used in the characterization of nanoparticles, base oil, ionic liquids, and the worn surfaces from the tribological tests were Raman, SEM, FTIR, HRTEM, XRD or 3D profilometry. Viscosity, density, viscosity index, stability and tribological behavior (friction and wear) of designed nanolubricants were studied. Most of them improved the overall
properties of PAO32 40 % reduction in friction and 99 % in wear being stable up to 240 days.